INVESTIGATION OF PARAMETERS FOR IMPROVING THE PERFORMANCE OF CENTRIFUGAL PUMP

A THESIS

Submitted by

ULAGANATHAN K

in partial fulfillment of the requirements for the degree of

DOCTOR OF PHILOSOPHY

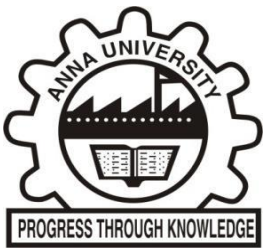

FACULTY OF MECHANICAL ENGINEERING

ANNA UNIVERSITY

CHENNAI 600 025

JUNE 2019

ANNA UNIVERSITY

CHENNAI 600 025

CERTIFICATE

The research work embodied in the present Thesis entitled "**INVESTIGATION OF PARAMETERS FOR IMPROVING THE PERFORMANCE OF CENTRIFUGAL PUMP**" has been carried out in the Department of Mechanical Engineering, Sri Ramakrishna Engineering College, Coimbatore. The work reported herein is original and does not form part of any other thesis or dissertation on the basis of which a degree or award was conferred on an earlier occasion or to any other scholar.

I understand the University's policy on plagiarism and declare that the thesis and publications are my own work, except where specifically acknowledged and has not been copied from other sources or been previously submitted for award or assessment.

ULAGANATHAN K
RESEARCH SCHOLAR

Dr. P. KARUPPUSWAMY
SUPERVISOR
Professor
Department of Mechanical Engineering
Sri Ramakrishna Engineering College
Coimbatore

ABSTRACT

To improve the efficiency of the centrifugal pump commonly used in irrigation, wastewater treatment plant, water and distribution plant, and processing industries is the objective of this research work. A centrifugal pump of duty point flow rate 0.015 m^3/s at a total head of 32 m and the speed of rotation 2900 rpm used for the agricultural purpose is selected with a support of MSME, namely M/s Coimbatore Engineering Company (CEC), Coimbatore, Tamil Nadu, India for this research work. The efficiency of the selected pump at the guaranteed duty point is 65.6 %. This efficiency value is less than the minimum efficiency required by the pump standard at the guaranteed duty point. The present efficiency level of the pump is studied and found to be in the range of 63 to 67 % and its average is 65 %. The minimum efficiency required by the Indian Standard IS 9079: 2002 corresponding to the selected the duty point of the pump is 66%. Comparing the efficiency values of present level and pump standard requirements, the current efficiency is less than the standard values, and also less than the maximum achievable efficiency level specified in the specific speed Vs Pump Efficiency chart of the Centrifugal pump hand book. Referring to the chart, the pump efficiency corresponding to the specific speed (N_S = 1363.4 US unit) is 77%. So there is a scope for increasing the pump efficiency from the present level 63 to 67 %.

The research work is divided in to five stages. In the first stage, experimental analysis of the selected pump was conducted and its performance is compared with the pump standard efficiency. In the second stage, a pump impeller is designed for the duty point based on turbo machinery theory and its performance is experimentally measured and numerical analysis is done using Computational Fluid Dynamics (CFD) tool. In the third stage, impeller geometry is optimized using Design of

Experiments combined with CFD analysis. In the fourth stage, sensitivity analyses are carried out for ranking the impeller design parameters. In the fifth stage, the effect of surface coating on the pump components are studied using experimental and numerical analysis.

The centrifugal pump selected for the study is tested as per ISO 9906: 2012 standard and its performance is measured. The efficiency of the selected pump at the duty point is 65.6% which is less than the pump standard efficiency. A centrifugal pump impeller for the duty point is designed and its performance is found 66%. The efficiency of the designed impeller is just satisfying the pump standard value and it is need to improved.

The efficiency of the pump is improved through the optimization of impeller design parameters using Design of Experiments (DOE) coupled with CFD analysis. For optimization process, five impeller design parameters such as impeller Outer diameter (D_2), inlet blade angle (β_1), outlet blade angle (β_2), number of blades (Z) and blade thickness (t) are selected. Design of Experiments (DOE) with Response Surface Methodology (RSM) Central Composite rotatable Design (CCD) is employed for design optimization of the impeller geometry. Computational Fluid Dynamics (CFD) tool is used for numerical analysis. Using RSM, the second order mathematical model is developed for responses pump total head, power input and efficiency of the pump. The optimum design parameters are found from the RSM optimizer. Finally, a new impeller is fabricated for the optimized design parameters and its performance is measured experimentally. The experimental results of the new impeller show that the efficiency and other performance characteristics have increase significantly and satisfy the requirements of pump standard and Bureau of Energy Efficiency (BEE).

The selection of geometrical parameters plays a vital role in the design of the centrifugal pump impellers. However, the compound effects of the parameters are seldom available in the open literature. The influence of five impeller design parameters is ranked by applying sensitivity analysis. The adaptation of sensitivity analysis in the pump design is a novel method and the results suggest that outer diameter, the number of blades and the blade thickness have strongly influenced the performance of the pump. Based on the requirements of head, efficiency, and power input, change in dimension of the three parameters would result in better performance.

The efficiency of the pump can be improved through the application of a surface coating on the flow passage of the pump impeller and volute casing. The material used for producing the pump impeller and volute casing is FG210 grade cast iron and is moulded through green sand casting process. The surface finish of the cast iron impeller and volute casing on the water flow passage are normally in the range from 4 to 12 μm $R_{a.}$ Due to the increase in surface roughness, the power input of the pump is increases and so pump efficiency decreases. Due to this reason, improving surface finish is one of the requirements of pump manufacturer and due to an increase of surface roughness, erosion also occurs. Erosion would reduce the life of the pump. Hence in this study, the surface coating is applied to the impeller and volute casing to improve the efficiency. Two types of coating materials (Epoxy and Polyurethane) are selected and applied on the pump components. For this analysis, six centrifugal pumps with similar design specifications are selected and their performance testing is carried out. Then the pump casing and impellers are disassembled. The epoxy coating material is applied to three pump components with different coating thicknesses and the other three pump components are coated with the polyurethane material with different coating thicknesses. Now thickness of coating and surface finish values is measured

and all the six pumps are assembled and performance test is conducted. The test results show that the performance of the coated pumps has significantly increased than the uncoated pumps. The efficiency of epoxy coated pump has improved up to 2.2% and its power input has decreased up to 0.35 kW. The efficiency of the polyurethane coated pump has improved up to 4.75 % and its power input has decreased up to 0.75 kW. The numerical simulation on the uncoated pump and coated pump also carried out using CFD. The numerical results show that the efficiency of the pump has improved due to the applications of surface coating. In addition to the efficiency of the pump, the surface coating improves the life of the pump and this helps to reduce the maintenance cost of the pump. Finally, cost analysis is performed to estimate amount of money saved when surface coating technology is implemented.

Similar work can be done in future for pumps used on domestic, chemical, oil industries to handle different types of fluids. The results would help manufacturers to produce energy efficient pump which would reduce the cost of the pump.

ACKNOWLEDGEMENT

I wish to account my deep sense of gratitude and profound thanks to my research supervisor **Dr.P.Karuppuswamy**, Professor & Head, Department of Mechanical Engineering, Sri Ramakrishna Engineering College, Coimbatore for his keen interest, inspiring guidance and constant encouragement during all stages of my work to bring this thesis into reality.

I am thankful to my Doctoral Committee members **Dr.G.Sundararaj**, Professor, Department of Mechanical Engineering, PSG College of Technology, Coimbatore and **Dr.K.Sundararaj**, Professor & Head, Department of Aeronautical Engineering, Kumaraguru College of Technology, Coimbatore for their valuable suggestions and encouragements during the entire course of my research work.

I am incredibly indebted to **Mr.Soundarajan**, Managing Director, Coimbatore Engineering Company (CEC), Coimbatore for providing the facilities and encouragement for doing this industry project. I also thank **Mr.A.M.Selvaraj** Joint Director and **Mr.D.Anguraj** Scientific and Industrial Testing and Research Centre (Si'Tarc) and management for providing the necessary supports for samples testing for this research work.

I also thank the faculty and non-teaching staff members of the Department of Mechanical Engineering, Kumaraguru College of Technology, Coimbatore, for their valuable support throughout my research work. Also my sincere thank to all others who directly or indirectly helped me to complete this work. I am indebted to my wife, **Mrs.M.Santhi** and my daughter, **Ms.U.S.Indira** whose provide complete support and encouragements have made this work possible.

ULAGANATHAN K

TABLE OF CONTENTS

CHAPTER NO. **TITLE** **PAGE NO.**

CHAPTER NO. **TITLE** **PAGE NO.**

CHAPTER NO. **TITLE** **PAGE NO.**

LIST OF TABLES

TABLE NO. **TITLE** **PAGE NO.**

LIST OF FIGURES

FIGURE NO. **TITLE** **PAGE NO.**

FIGURE NO.	TITLE	PAGE NO.

FIGURE NO.	TITLE	PAGE NO.

LIST OF SYMBOLS AND ABBREVIATIONS

BEP	-	Best Efficiency Point
X_2	-	blade angle at inlet
β_2	-	Blade angle at outlet
B_1	-	Blade height at inlet
B_2	-	blade height at outlet
Z	-	blade number
X_5	-	blade thickness
CCD	-	Central Composite Rotatable Design
CFD	-	Computational Fluid Dynamics
DOE	-	Design of Experiments
Q	-	Discharge through the pump
β_1	-	Inlet blade angle
D_1	-	Inlet diameter of the impeller
IC	-	Internal Combustion engine
k	-	kinetic energy
ε	-	kinetic energy dissipation coefficient
KRG	-	Kriging
NPV	-	Net Present Value
D_n	-	Nominal Diameter of the impeller
X_4	-	number of blades
X_1	-	outer diameter
D_2	-	outer diameter of the impeller
X_3	-	outlet blade angle
PBP	-	Pay Back Period
P	-	Power input
η	-	Pump efficiency

RBNN	-	Radial Basis Neural Network
RNG	-	Re-Normalization Group
RSA	-	Response Surface Approximation
RSM	-	Response Surface Methodology
RANS	-	Reynolds Average Navier-Stoke equation
SST	-	Shear Stress Transport
N_S	-	Specific Speed of the pump
N	-	Speed of the pump
R_a	-	Surface Roughness Value
t	-	Thickness of the vanes
H	-	Total head

CHAPTER 1

INTRODUCTION

1.1 CENTRIFUGAL PUMP AT A GLANCE

Pump is a mechanical device and it is used to handle different types of fluids from lower position to higher position. A Pump draws the fluid inside, pressurizes it and delivers it through the outlet. Generally, electric motor and Internal Combustion (IC) engines are used to drive the pumps to handle the fluids.

A centrifugal pump is a kinetic device, i.e. it adds energy to the pumped liquid by increasing its velocity. As the addition of energy depends on liquid velocity, the amount of energy added varies with the rate of flow through the pump. These are the fundamental physics behind the usual head versus capacity characteristics of the centrifugal pump. It is important to note that the distinct difference between the head (energy added) versus flow characteristics of a centrifugal pump and a displacement pump. Centrifugal pumps have low flow regulation. The flow varies widely with variations in system resistance, a characteristic that lends itself to easy flow control. Displacement pumps exhibit high flow regulations. The flow is mostly independent of variations in system resistance, making them ideal for services where a constant flow is necessary over varying system conditions. The limitations of displacement pumps are larger machine size and mechanical complexity.

A centrifugal pump is a simple mechanical machine consisting of a set of rotating blades enclosed within a volute casing. The torque applied by

the pump's driver is converted to the total head by the action of vanes on the pumped liquid, and these vanes are the only component that adds energy to the liquid. This action follows Euler's equation faithfully, provided it has recognized the effective liquid velocities, magnitude and direction cannot be determined directly from the geometry of the vanes. The determination is part of the centrifugal pump designer's "art". Stripped of all refinements, a centrifugal pump has just two main parts: (1) a rotor, made up of a series of blades component, known as an impeller and a shaft, and (2) a stator, made up of the impeller enclosure, known as a casing, some form of seal where the shaft passes through the casing and bearings to support the rotor.

1.2 CLASSIFICATION OF PUMPS

A pump is classified into two categories such as rotodynamic pumps and positive displacement pumps. The other classifications of the pumps are presented in Figure 1.1.

Today the global market is flooded with plenty of varieties, types and sizes of pumps. Inspire of its age, today the design of pumps has not attained saturation phase. The design of centrifugal pumps involves many parameters that are interdependent and in-turn iterative makes the difficulty at hand more complexity for the human brain to manipulate. Centrifugal pumps are widely used in domestic, irrigation and process industries to handle different types of fluids for a different application.

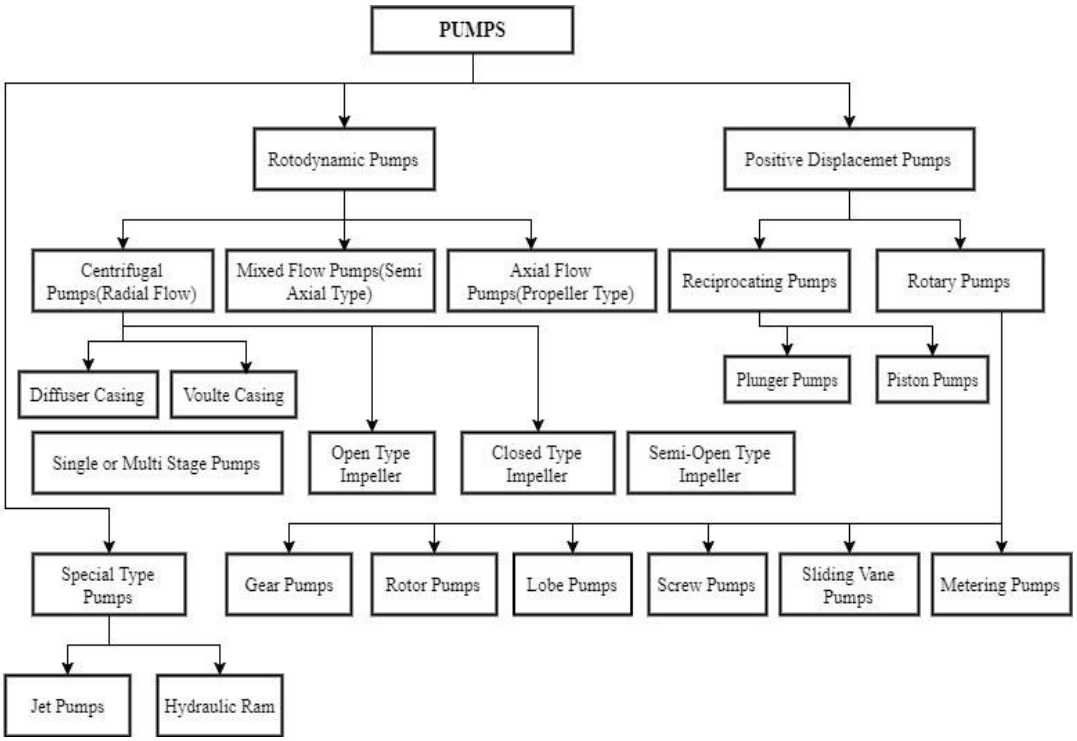

Figure 1.1 Classification of a pump

1.3 COMPONENTS OF THE CENTRIFUGAL PUMP

The centrifugal pump has two main components housing or casing and impeller. The purpose of the housing or casing is to gather and diffuse the high-velocity liquid discharged by the impeller. This process is necessary to (1) slow the liquid to a usable velocity and (2) convert the kinetic energy into pressure energy, thus recovering more of the pump's energy input.

1.3.1 Types of Centrifugal Pump Casing

The manufacturer employs different types of casings. The primary requirement of the casing is to provide adequate support to the impeller and other components of the pump and to minimize the loss of energy due to eddy formation. The pump efficiency depends on the type of casing used. Three types of casings are

- Volute type casing
- Vortex type casing
- Diffuser type casing

The volute type casings are simple in construction and provide better performance, and it is commonly used to manufacturing pumps for domestic, agriculture and other industrial applications.

1.3.2 Types of Centrifugal Pump Impeller

Impeller is a rotating element of the centrifugal pump. It is used to transfer energy from the prime mover, either an electric motor or IC engine, which drives the pump to the fluid pumped by accelerating the fluid outwards from the axis of the pump.

Impellers are classified based on four design category:

- Shaft mounting
- Inlet or suction arrangement
- Vane shape and form
- Vane closure

Vane shape and form is generally divided into three groups:

- Plain vane
- Francis vane
- Mixed flow

1.3.3 The Propeller or Axial Flow

In a plain vane impeller, the vanes are of single curvature, with all vane surfaces straight lines parallel to the axis of rotation.

The vane surfaces in a Francis-vane impeller have a double curvature. This impeller is also often called the Francis screw-vane or screw-vane impeller

For a given pump, except in very small sizes, a closed-impeller design is more economical to make for high efficiency than open or a semi-open-impeller design. The reasons for this are the sensitivity of the latter two designs to clearance at the ends of their impeller vanes and the need for clearance adjustment. Sensitivity to end clearance requires additional care in machining to achieve consistently high performance.

1.4 DESIGN OF CENTRIFUGAL PUMPS

Basically, pumps are analyzed and compared by design conditions; i.e. at the head and capacity condition at rated speed at which maximum efficiency has obtained.

The specific speed of a given pump will also undoubtedly reflect in the shape of the pump characteristic curves, whereas some variations in the shape of these curves can be obtained by changing in the design of the impeller and casing waterways. The variation can be obtained without affecting the pump efficiency.

1.5 SCOPE OF THE RESEARCH

This research work is mainly focuses on improving the centrifugal pump performances which is commonly used in the agricultural, wastewater treatment plant and water supply and distribution system applications. The type and rating of pump selected for this work is 7.5 kW / 10 HP 2900 rpm electric motor driven pump of 75 mm x 65 mm inlet and outlet pipe size,

single suction radial flow closed type impeller with volute casing pump. The scope of this research work is listed as follows:

- To select the suitable centrifugal pump to irrigate the land of 3hectre as per the requirements of Indian Standard (IS 9694 (Part1):1987 Code of practice for the Selection, Installation, Operation and Maintenance of Horizontal Centrifugal Pumps for Agricultural Applications, Part 1: Selection).

- To fabricate the pump testing set up in accordance with International Pump Standards (ISO 9906: 2012 Rotodynamic Pumps- Hydraulic Performance Acceptance Tests- Grade 1, 2).

- To conduct the performance testing of the selected pump as per pump standard and calculate the pump performance characteristics and draw the corresponding performance curves.

- To estimate the uncertainty in measurement of the pump output parameters such as flow rate (Q), head (H), power input (P) and efficiency (η).

- To design and develop a radial flow closed type impeller for the duty point conditions using the turbo machinery theory and to fabricate the new impeller for conducting the performance test.

- To predict numerically, the performance of the designed impeller using the computational fluid dynamics analysis and validate the numerical simulation through experimental study.

- To select the impeller parameters which influences the pump performance characteristics and its ranges, based on the literature. Create the design matrix for using the Design Of Experiments (DOE). Predicting the numerical performances for the pump output parameters head, power input and efficiency for the duty point flow rate.

- To develop the second order regression models for all responses using Response Surface Methodology (RSM) and validate the model developed statistically and using RSM optimizer, find out the optimum design parameters.

- To fabricate and conduct the experimental and numerical analysis on the optimized impeller.

- To rank the impeller design parameters through sensitivity analysis.

- To perform multi-objective optimization of the response functions using Genetic Algorithm (GA).

- To study the effects of surface roughness and surface coating on the pump components and its performance characteristics and compare the performance of the coated pumps with uncoated pumps through experimental and numerical analysis.

- Cost analysis of the surface coating process is performed using Pay Back Period (PBP) and Net Present Value (NPV) methods.

1.6 OBJECIVE OF THE THESIS

The main objectives of the thesis are as follows.

- To study the present level of efficiency of the selected pump for this research work.
- To estimate the measurement uncertainty of the pump performance characteristics.
- To study the performance of the developed impeller.
- To optimize the impeller geometrical parameters and to improve the pump performance using DOE.
- To rank the impeller design parameters using the sensitivity analysis.
- To study the direct effects of the impeller parameters on the pump performance characteristics.
- To find out the multiple optimum solution of the impeller parameters through Pareto front analysis.
- To improve the performance of the centrifugal pump through the application of surface coating on the pump components.
- To perform the economic analysis of the coating process and calculate the cost saving.

1.7 STRUCTURE OF THESIS

The structure of thesis is presented as per the following order.

Chapter 2 presents the detailed literature survey on the internal flow analysis of the centrifugal pump, experimental study to evaluate the pump performance characteristics, design techniques used to develop the impeller and casing, numerical models used for predicting the numerical performance of the pump, optimization techniques used for design optimization of impeller and volute casing to enhance the performance, effects of surface roughness, Reynolds number, viscosity of the fluid on the pump performance.

Chapter 3 presents the experimental analysis of the selected pump for this research work. Design and fabrication of pump testing set up and performance testing of the selected pump, pump performance calculations, and estimation of the measurement uncertainty on the pump performance characteristics are discussed.

Chapter 4 presents the design and development of centrifugal pump impeller based on the turbo machinery theory, and experimental study of the developed pump impeller.

Chapter 5 discusses about the numerical analysis of the centrifugal pump under steady-state incompressible flow. Numerical analysis of the developed impeller is carried out and their results are validated with experimental results.

Chapter 6 presents the development of a mathematical model for the pump performance characteristics using Design of Experiments, statistical

validation of the mathematical models, optimization of impeller design parameters and experimental and numerical performance analysis on the optimized impeller.

Chapter 7 presents the summary of the results finding in chapter 6, which includes the sensitivity analysis of the mathematical models developed and multi-objective optimization of the responses.

Chapter 8 presents the experimental and numerical performance study on the effects of surface roughness and surface coating on the pump components. A detailed cost analysis of the surface coating process is also discussed.

Chapter 9 presents the summary and conclusions and scope of future work followed by the cited references in the thesis.

CHAPTER 2

LITERATURE SURVEY

2.1 INTRODUCTION

This chapter presents a review of related research works took place during the past and recent years in the field of the centrifugal pumps.The existing research works are presented in the following headings.

2.2 EXPERIMENTAL AND NUMERICAL STUDY ON THE CENTRIFUGAL PUMP

During the past few years, the design and performance analysis of turbo machinery had experienced a great progress due to the joint evolution of computer power and the accuracy of numerical methods and optimization techniques. The 3D inverse design of impeller blade profile, 3D CAD modeling, automatic grid generation and CFD analysis of flow passage reduced the time and manufacturing cost of the pump and produced an efficient pump

Goto *et al.* (2002) developed an inverse design procedure for the design of the pump system. They integrated the Computational Fluid Dynamics analysis, 3D CAD modeling and automatic mesh generation of the centrifugal pump. The inverse design process was used to optimize the pump geometry of both impeller and volute casing and creating the 3D model of the pump for the optimized parameter. Goto & Zangeneh (2002) also proposed the inverse design method to optimize the diffuser blade shape of a low specific speed (N_s = 0.109 non-dimensional) centrifugal pump coupled with CFD analysis. It was found that the corner flow separation was completely

suppressed in the inverse design and the pump efficiency was significantly improved and it was validated by experimental analysis.

Cheah *et al.* (2007) performed a CFD analysis on a six twisted vane impeller pump at design and off-design conditions using the standard k-ε turbulence model. The pump domain was discretized using coarse and finer tetrahedral mesh. Mesh dependency test at the design point for the pump head coefficient (ψ) was calculated and it was found that the difference in head coefficient using coarse mesh and the finer mesh is 0.001. From the analysis, it was concluded that the effect of numerical simulation did not majorly affect the use of either coarse or finer mesh. But it was not close to the experimental total head as found by Gonz´alez *et al.* (2002). Further, they compared the experimental values of head and pump efficiency with the numerical results for the entire flow range and found only very small variation. Flow separation was developed at the leading edge at the design point flow rate due to non-tangential flow within the pump. The pressure inside the pump was increased gradually along the stream wise direction and the static pressure decreased when the impeller speed was decreased.

Gao *et al.* (2014) investigated the numerical analysis of a larger size pump with stay vanes under the steady and unsteady state conditions. The computational domain of the pump was discretized using the tetrahedral grid. The Navier- Stokes equation was solved using SST k-ω model. SIMPLEC code was used for solving the steady-state condition and the PAISO code was used for unsteady state conditions. The numerical results were compared with the experimental data. They found that in the unsteady state condition, the numerical results were closely matched with experimental results of the entire operating range.

Shigemitsu *et al.* (2011) studied the effects of various impeller outlet vane angle and vane thickness on a very small capacity pump. For numerical analysis, the standard k-ω turbulence model was used to solve the steady-state Reynolds Averaged Navier-Stokes equation (RANS). Three impellers of outlet vane angles 22.5^o, 45^o and 60^o with vane thickness 2 mm and another three impellers of same outlet vane angle with 1 mm vane thickness were analyzed through experimental and numerical simulations. From the analysis they found that the total head of the pump improved when the outlet vane angle increased and vane thickness decreased.

Chakraborty & Pandey had performed the CFD analysis on a high-speed centrifugal pump run at 4000 rpm with different vane numbers. The geometry of the pump impeller had very complex and different dimensional parameters such as outer and inner diameter, outlet and inlet vane angle, number of vanes, vane thickness and so on. The authors fixed all the other parameter except number vanes on the impeller. Different vane numbers 4, 5, 6, 7, 8, 9, 10 and 12 were selected for their study and other parameters were fixed. The FLUENT software was used to simulate the internal flow pattern of the pump under the steady state condition. SIMPLEC codes were used to solve RANS equations. It was found that the head of the pump increased continuously when the impeller vanes were increased. But, the increase in pump efficiency was very small. They found the optimum efficiency of the pump corresponding to the vane number 10.

Luo *et al.* (2008) studied the effects of impeller inlet geometry on the performance of the centrifugal pump with rotational speed of 1480 rpm. Extending vane leading edge and inlet vane angles were selected for the study. Three impellers were fabricated with extending leading edge at the inlet and two impellers were prepared with larger vane inlet angle. Pump

performances including cavitation parameter of the impellers with a common volute casing were found by numerical and experimental analysis. RANS and RNG k-ε model were used for pump performance and Rayleigh-Plesset equation used for cavitation analysis. The experimental results were well matched with numerical results at the design flow rate. From the study, the authors found that pump performance including cavitation were much improved due to the extended inlet vane leading edge and larger vane angle at the inlet.

Tan Lei *et al.* (2014) investigated the effects of blade wrap angle on the centrifugal pump performance through experimental and numerical simulations. Three impellers were modeled and fabricated with a wrap angle of 100^{o}, 110^{o} and 120^{o} and other dimensions of the impeller were fixed. For numerical analysis, the RNG k-ε turbulence model was used to investigate the hydraulic performance of the pump. The numerical results showed that at the inlet of the impeller, the relative velocity was less and it increased and reached the maximum value at the impeller outlet. Comparatively the velocity gradient was more at the vane surface. Among the various turbulence model available in commercial CFD packages, k-ε, k-ω, and SST models are commonly used.

Kaewnai *et al.* (2009) performed the numerical analysis on the radial flow impeller to calculate the performance of the pump and validate the results with experimental results which were carried out by Guelich (2004). ANSYS CFX 5.5 package was used to simulate the 3D incompressible unsteady flow through the impeller. The hexahedral structured grid with inlet total pressure and outlet mass flow rate with no slip wall were selected as the boundary conditions. k-ε, k-ω and RNG k-ε were used to predict the impeller performance. Results of the total head found from these three models were

compared and the deviation was 0.3%. Different turbulence intensity was used (ε = 1%, 5% and 10%). Among these, the k-ε model with 5% turbulence intensity was selected for the entire simulation work. From the CFD analysis the head coefficient and the static pressure coefficient were calculated and compared with the experimental results and the results was found good agreement. The effects of surface roughness of the impeller surface was also studied and found that the increase in head losses was due to increase in surface roughness values.

Cai *et al.* (2014) investigated the effects of impeller tongue-gap in the un-shrouded impeller with five backswept vanes. The experimental performance was measured at a different rotational speed of the pump (900 to 1700 rpm) and the results followed the affinity law i.e. flow rate of the pump was increased linearly with speed and pump head increased square of the speed. Numerical analysis of the impeller was performed to solve the unsteady RANS equation using hexahedral unstructured mesh. ANSYS CFX tool was used and the boundary conditions were selected as per the solver guidelines. The numerical results were good agreement with the experimental results.

Wang & Wang (2013) performed the numerical and experimental study of low specific speed pump under the unsteady state condition. The standard k-ε, SST k–ω and RNG k-ε turbulence models with unstructured grids were employed and the results were compared with experimental values. They found that the RNG k-ε models was efficient than the SST k-ω and k-ε models. The deviations between the experimental values with these three models were 2.6%, 3.65%, and 4.78%.

2.3 DESIGN OPTIMIZATION OF CENTRIFUGAL PUMP

Kim *et al.* (2015) performed the design optimization using Design of Experiments (DOE) for centrifugal pump handling multiphase flow which was applicable in crude oil wells. The authors employed the experimental study on the prototype pump to evaluate the performance of the actual pump. Since the actual geometrical configuration of the pump was larger, the prototype was used. RANS equation solved the steady state incompressible turbulent flow through the pump. Impeller hub angle and impeller shroud angle at inlet and outlet and volute hub angle and volute shroud angle at inlet and outlet were selected as design parameters and their working ranges were selected. 2k full factorial design was employed for optimizing these parameters and a new impeller and volute was developed for the optimum parameters and results was compared with a prototype model. It was found that the total head and pump efficiency of the optimized pump was increased by 30.9 kPa and 1.9%.

Heo *et al.* (2015) performed the design optimization of a backward curved vane pump with a specific speed of 150. Three surrogate models Response Surface Approximation (RSA), Kriging (KRG) and Radial Basis Neural Network (RBNN) were used to optimize the impeller design parameters. Four input parameters such as inlet and outlet vane hub angles, hub profile and vane angle profile were selected for the optimization process and pump efficiency at the design flow has the objective function. 36 design locations were selected by using Latin Hypercube technique and evaluate the pump efficiency at each location using the three surrogate models. Optimum pump efficiency of these models was compared with the CFD results of RANS model. It was found that the increase in pump efficiency between RANS and surrogate models were 1.58%, 1.72%, and 2.01%. Among the three models, RBNN model was efficient one and the results of this model

were further validated with the experimental values and found the deviations were 4.4% and 2.9% on total head and efficiency.

Pei *et al.* (2016) performed the optimization of the meridional profile of the centrifugal pump impeller using Latin Hypercube (LHS) method. The impeller parameters controlling the pump head and efficiency shroud diameter (D_1), hub diameter (D_2), shroud angle (a_1) and hub angle (a_2) were selected for optimization. LHS was used to locate thirty-five design points and pump efficiency was found numerically to solve RANS equation by SST k-ε model utilized by Mentor (1994) corresponding to the design points at 0.6, 1.0 and 1.62 times of the design flow rate. The Response Surface Methodology (RSM) was employed to derive a second-order regression model for the pump efficiency and this model was optimized using the NSGA –II algorithm. Optimum impeller parameters were found and the results of the optimized impeller were compared by experimental results and showed the increase in pump efficiency by 3.9%, 6.1% and 2.6% at the design flow rate. From the analysis it was found that the RSM has one of the good and accurate methods for pump optimization process.

Kim *et al.* (2009) optimized the meridional shape of the centrifugal pump impeller using 2^k factorial design and RSM. 3D model of the impeller was generated using ANSYS BladeGen tool and structural meshes were created by ANSYS CFX TurboGrid tool.Numerical performance of the impeller was analyzed using ANSYS CFX 10.0 which solves the RANS equation for a viscous incompressible flow through the pump.2k factorial design coupled with the RSM method was used for the numerical optimization process. The impeller hub and shroud sweep angle, hub, midspan and shroud incidence angles, exit vane angle, vane leading edge angles at the hub and shroud were selected as the process variables for

optimization. Out of these variables, the hub and shroud incidence angle and exit vane angle had more influence on the pump total head and efficiency.

Jung *et al.* (2016) performed the design optimization of a high-speed centrifugal fan diffuser using 2^{k-1} fractional factorial design and RSM. The advantage of the fractional design was to reduce the number of experiments by half. Authors had selected six independent variables number of guide blades, length of the meridional plane, leading edge area, trailing edge angle, airfoil thickness and position of the airfoil. Numerical analysis of the computational domain was performed which solved the 3D steady-state compressible RANS equation using ANSYS CFX 15.0 code with the hexahedral grid system. The objective function vacuum and fan efficiency were optimized using RSM with Central Composite Design (CCD).

Weidong *et al.* (2013) performed the optimization of centrifugal pump design parameters through the orthogonal array and CFD analysis. The orthogonal test had one of the popular optimization techniques were used to optimize centrifugal pump design parameters and to reduce the number of experiments and time. The process parameters selected were impeller outer diameter, inlet and outlet vane angles, vane width at the outlet, the inlet guide blade width, number of guide vanes and number of impeller vanes. To reduce the number of experiments the authors selected L_{18} $(3)^7$ orthogonal array. Experiments were conducted at the eighteen set parameters and values of the objective function were found numerically. For CFD analysis the standard k-ε turbulent model with SIMPLEC code was used. The optimum set parameters were found from the numerical study and new model pump was developed for the optimum parameters and performance test was conducted. The numerical results were in good agreement with the experimental results at the design point.

Senthilkumar *et al.* (2016) used the RSM technique with the central composite rotatable design for optimization of Flux Cored Arc Welding process (FCAW) parameters. The same technique was employed by Sahu *et al.* (2013), Tanco *et al.* (2009), Datta *et al.* (2014), Periyanan & Natarajan (2013) for optimization of the various welding process.

Gundale & Joshi (2013) developed the procedure for construction of radial flow impeller blade profile. The authors presented the procedure based on the existing theory.

Singh & Nataraj (2014) performed modeling and simulation of the low capacity centrifugal pump for domestic applications. The impeller blade profile was created using the commercial CAD tool. Backward and forward blade shapes were constructed using tangent circular arc and point-to-point methods. Performances of both blade shapes were found by numerical analysis using the modified k-ε turbulence model with the structural grid. It was found that the tangent circular arc profile with backward curved shape have better efficiency than the forward blade shape.

Cheah *et al.* (2011) study the steady and unsteady state flow simulation on a centrifugal pump. The standard k-ε, RNG k-ε, k-ω, and SST turbulence model were used to solve the RANS equation using the commercial CFD code. It was found that the deviation between the head coefficient calculated from the above four models was very small. The predicted value of head coefficient by the k-ω model was more than the other three models, however considering the convergence speed and overall efficiency, the k-ε model had more efficient than other models.

Kim & Kim (2012) performed the optimization of mixed flow pump diffuser to enhance the efficiency of the pump. The numerical

performance was found by solving the 3D RANS equation using the SST turbulence model with ANSYS CFX 11.0 software. Design parameters, straight blade length ratio, diffuser area ratio, diffuser vane angle at the tip and the distance ratio of the impeller blade and diffuse blade leading edge were selected for the optimization process. LHS technique was used to select the design space and values of the objective function were found corresponding to these points. The surrogate RBNN algorithm was used to optimize the objective function. The optimized results showed that the efficiency of the mixed flow pump was increased by 9.75% at the design point.

Nataraj & Singh (2014) investigated the internal flow analysis of a small capacity pump run at 2880 rpm with a specific speed of 6 rpm using FLUENT code. The steady state N-S equation was solved using the k-ε turbulence model and the results were compared with experimental results and they found the deviation from 3.5 to 4.9%. The RSM with CCD was used to optimize the impeller design parameters. From the study it was found that decrease of impeller eye diameter and exit blade angle with an increase of exit vane width, pump total head were improved by 2.06 m and power input decreased by 0.065 kW.

Li (2011) studied the effects of exit vane angle on the performance of a centrifugal pump used in the oil industry to handle different viscosities. Experimental performance of the centrifugal pump with the standard fluid (water) of kinematic viscosity 1 mm^2/s and china 100# machine oil of kinematic viscosities 29, 45, 75, 98, 134, 188 and 255 mm^2/s were measured with exit vane angle of 15^o, 25^o, 45^o and 60^o. They found that the exit vane angle had more influence on the head, shaft power and efficiency of the pump

at different viscosities. The pump head and efficiency were rapidly decreased with the increase in fluid viscosity and increase the shaft power.

Fan *et al.* (2011) performed the CFD and design optimization of a centrifugal jet pump used in power plant and refrigeration applications. Standard k-ε turbulence model was employed for the CFD analysis. Initially, the authors validated the CFD results with the analytical solutions and it was found that there is a significant variation between CFD and analytical results. Optimization of the objective function using surrogate genetic algorithm was performed using DOE with Latin Hypercube Sampling technique. They found that the pump efficiency was improved by 4% and the power consumption was reduced by 20% for the optimum design.

Korkmaz *et al.* (2017) studied the effects of vane exit angle (β2), a number of vanes (Z) and the length of the splitter vanes through experimental analysis. The values of these parameters selected were $\beta_2 = 25^o$ and 35^o, Z = 5, 6 and 7 and splitter vane length = 40%, 55%, 70% and 85% of the actual vane length. The other impeller parameter was chosen based on the empirical equation found by (Stepanoff, 1957; Dicmas, 1987; Lobanoff and Ross, 1992; Tuzson, 2000; Karassik *et al.*) Authors designed and fabricated the impellers with and without splitter vanes and measured the pump performance. It was found that the total head, power input, and efficiency were increased due to the addition of splitter vane length. The authors concluded that proper selection methodology was developed to optimize these parameters.

Yang *et al.* (2012) investigate the effect of impeller trimming on the pump performance characteristics and changes of other impeller dimensions through numerical and experimental analysis. Initially, the experimental performance was measured with impeller diameter 0.255 m and validates the CFD results. CFD analysis was done using ANSYS CFX to

solve k-ε turbulence two-equation models. The computational domain of the pump was discretized with hexahedral structural mesh using ICEM-CFD. From the experimental and numerical analysis, it was found that by decreasing the outer diameter (D_2), inlet blade angle (β_2) increased from 20^o to 35^o; blade wrap angle (ϕ) decreased from 130^o to 90^o and inlet width (b_2) increased from 11 mm to 17 mm. When the outer diameter decreased, the pump performances flow rate, head, power, and efficiency also decreased at the Best Efficiency Point (BEP) and due to decreasing the wrap angle all performances were increased at BEP. Also, it was found that due to increase in inlet blade angle and the impeller inlet width all characteristics of the pump were increased at BEP. From the study it was concluded that the impeller dimensions D_2, β_2, ϕ and b_2 had more influencing parameters on the pump performance.

Bing *et al.* (2013) investigated the effects of impeller meridional shape on a mixed flow pump performance. Two input parameters impeller Hub to Shroud Radius Ratio (HSRR) and Diffusion Outlet Angle (ODA) were selected for the internal flow analysis. Twenty-five impellers of specific speed 496 rpm with different design combinations were modeled and their performances were measured by numerical simulation. Among these combinations, one impeller with HSRR = 1.94 and ODA = 90^o was fabricated and conduct the experiment at the standard test rig. For numerical simulation, SIMPLEC code with k-ε turbulence model was used to solve the 3D steady incompressible RANS equation. The numerical results were well matched with the experimental results at the design point flow rate.

Alemi *et al.* (2015) investigate the effects of volute cross-section and diffuser shape on the centrifugal pump performance at off-design conditions. Three volute casings of rectangular, circular and trapezoidal cross

section were analyzed numerically using the standard k-ε, low Reynolds k-ω and shear stress transport models. The numerical results were compared with the work performed by Kelder *et al.* (2001). At the design flow rate, numerical results were compared with the experimental results. Among the three volute sections, it was found that the circular cross-section with radial diffuser gives the better efficiency and pump head.

Grapsas *et al.* (2010) performed the design optimization of radial flow centrifugal pump impeller through numerical simulation and Evolutionary Algorithm System (EASY) tool developed by Kampolis *et al.* (2008) Length of the blade, blade height at the inlet, leading edge angle, camber and mean line radius were selected as design variables. The numerical analyses were performed using the standard k-ε model which solved the N-S equation for 3D flow inside the pump. Numerical results were in good agreement with the experimental data at the design point. It was found that the optimum values of the parameters had given the maximum hydraulic efficiency of the pump.

Barrio *et al.* (2010) investigated the unsteady state flow analysis in near tongue area of volute type low specific speed (0.47) centrifugal pump at various operating locations. The test pump was analyzed numerically from 20% to 160% of nominal (Q_n) flow rate using commercial CFD codes which solve the 3D URANS equation. This study revealed that the leakage between the impeller- tongue clearances increased by 160 % Q_n.

Mortazavi *et al.* (2017) studied the effect of impeller back blades on the performance of the centrifugal pump using CFD. Seven impeller back vanes were added into the regular standard impeller and its performance was measured numerically using the shear stress transport turbulence model which solved the steady state RANS equation. Results of the back vane impeller

were compared with an impeller having without back vanes. Design variables considered for the back vanes are outlet diameter, vane width, the thickness of vane, axial clearance, number of vane and vane root angle. Among these variables, vane outer diameters had a significant effect on head, power, efficiency and axial thrust. The axial thrust load of the pump can be controlled considerably by back vanes.

SHI Weidong *et al.* (2013) studied the effects of impeller outlet width on deep-well pump using experimental and numerical analysis. Four impellers of outlet width 9 mm, 10 mm, 11mm and 12 mm were studied numerically using 3D steady-state RANS equation solved by standard k-ε, RNG k-ε, realizable k-ε, and SST k-ω turbulence models. The numerical results were compared with experimental results and it was found that the numerical values were higher than the tested values among that result of the standard k-ε model which was very close to the tested data. From the analysis it was found that an increase in impeller outlet width which increased the total head, power consumption and flow rate at the best efficiency point. Due to the increase in power, the pump efficiency has to reduced.

Taylor *et al.* (2005) performed the numerical simulation to investigate the effects of inlet blade angle (β_1) and impeller gap (δ) on the performance of a centrifugal fan. The FLUENT code was used to analyze the steady-state RANS equation. The standard k-ε turbulence model logarithmic-law wall function was used. From the study they found that due to an increase in β_1, remarkable changes in total pressure and fan efficiency and increase on impeller gap the air leakage increased and thus reduce the fan efficiency.

Shojaeefard *et al.* (2012) studied the effects of outlet blade angle (β_2) and outlet impeller width(b_2) on centrifugal pump performance handling water and oil numerically. Six impellers were prepared with different

combinations of outlet blade angle and width. Numerical simulation on this impeller was performed under steady-state incompressible flow condition. SST turbulence model was used for flow simulation inside the pump. Numerical results were compared with experimental results and found in good agreement at BEP. From the analysis it was found that due to an increase in outlet angle and width, head and power increased and the efficiency decreased due to overloading of the pump. At the BEP, comparing the performance of pump handled water and oil, due to increasing the viscosity of the oil, head, efficiency were decreased by 1.4 m and 20.5% and power consumption had increased by 1.03 kW compared with water.

PEI Ji *et al.* (2016) performed optimization of a low specific speed (N_s = 46.5) centrifugal pump impeller surrogate models and Particle Swarm Optimization (PSO). Three impeller design variables outlet vane angle (β_2), outlet vane width (b_2) and vane wrap angle (ϕ) were selected. Twenty impeller design points were located using LHS and pump head and hydraulic efficiency was calculated through CFD analysis at 100% and 140% of the design flow rate (Q_d). For numerical simulation, a 3D RANS equation was solved with SST turbulence model using ANSYS CFX 14.5. Numerical results were validated with the experimental data and it was found that the deviation on the total head was 3.2% and 4.3% at 100% and 140% Q_d respectively. At the design points, the hydraulic efficiency (ηh) were calculated numerically. Two surrogate models RSM and KRG were used to develop the mathematical models of the objective function. Since the modeling accuracy of KRG was better than RSM, the mathematical model obtained by KRG was coupled with PSO for the optimization of the objective function. Optimum impeller design variables were found and calculated the η_h corresponding to 100% and 140% Q_d. It was found that the η_h were improved by 4.18% and 0.62% under the two operating conditions.

Nataraj & Arunachalam (2006) performed design optimization of centrifugal pump impeller through Taguchi quality analysis. Four control parameters, impeller width (b), eye diameter (d), outlet blade angle (β_2) and a number of blades (Z) and three noise parameters, shaft speed, current, and supply frequency were selected. Eight experiments were conducted on the selected parameters based on L_8 orthogonal array. 3D CAD model was developed for setting parameters and its performance was measured using CFD analysis. From the study they concluded that pump performances, total head, efficiency increased and power consumption decreased significantly for optimum impeller that reduced the design and manufacturing cost.

Abdalla *et al.* (2015) investigated the effect of impeller side gap on centrifugal pump performance in a semi-open type impeller. Experimental and numerical analysis on semi-open impeller with different side gap (e) were measured. Shear stress transport turbulence model available in ANSYS CFX 14.5 were used to solve the governing equations. It was found that impeller side clearance was more effect on the pump performance. Due to the increase in gap, head and efficiency was reduced and secondary flow also happened which reduced the flow rate and head. Power consumption was reduced due to a drop in impeller blade loading.

Wang *et al.* (2016) has use RSM, KRG and RBNN surrogate models for optimizing the efficiency of the centrifugal pump. The impeller design parameters inlet incident angle, outlet vane angle and blade wrap angle were selected for the optimization process. The design matrix was developed using LHS techniques. From the study the authors found that among these three models RSM improves the better efficiency up to 8.34% and RBNN had good prediction capabilities of the mathematical models

PEI Ji *et al.* (2016) studied the cavitation performance of the centrifugal pump using $L_9(3^3)$ Orthogonal array coupled with CFD analysis. The impeller geometrical parameters inlet diameter, inlet incident angle, and blade wrap angle was selected as the optimization parameters. They found that the impeller inlet diameter had more influence on the cavitation performance.

Kim *et al.* (2015) performed the optimization of centrifugal pump impeller diffuser using RSM technique coupled with CFD analysis. Four impeller geometrical parameters such as inlet and outlet angles of hub and shroud were selected.RSM analysis using Minitab statistical software was used to optimize the design parameters. Optimal set design parameters with optimum performance values were found from RSM plot and it was tested numerically. The error between the RSM results and numerical results were in good agreement.

Bellary *et al.* (2014) proposed the global optimization Pareto front through RANS analysis with the Multi Objective Evolutionary Algorithm (MOEA). Impeller inlet vane angle, outlet blade angle, and a number of blades were selected as design variables and RSA and KRG meta-models were used for optimization of total head and pump efficiency. The MATLAB code was used to optimize the multi-objective function. From the study, the authors found that the total head and efficiency were increased by 9.52 m and 2.37% and the Pareto optimal points provided the wide range of optimum set parameters and reduced the time and expenses.

Heo *et al.* (2016) performed the optimization of mixed flow centrifugal pump using RSA surrogate model. The steady-state incompressible RANS equation solved the SST turbulence model using ANSYS 14.5. Eight diffuser geometrical parameters were selected and the

experimental design was fixed by using 2^k factorial design. The efficiency of the pump was improved by 1.36% and the error between the RSA predicted model and RANS calculation was found by 0.001%.

Zhang Lei, *et al.* (2013) performed the optimization of centrifugal fan performance using MOGA. L49 (7^3) Orthogonal array was used to design the experimental matrix and function value was estimated using the own numerical code. Optimal fan design parameter was found and it was tested experimentally and found the total pressure was significantly increased.

Derakhshan *et al.* (2013) used Artificial Neural Network (ANN) and Artificial Bee Colony (ABC) algorithm coupled with CFD analysis for the geometrical shape optimization of the centrifugal pump impeller. Impeller hub diameter, inlet and outlet diameter, inlet and outlet vane angles and outlet width were selected as a design parameter. Optimum design parameter was found from the multi-objective optimization process and it was tested numerically. The numerical results show that the pump total head and efficiency was improved by 6.89 m and 3.59 % respectively.

Son *et al.* (2014) studied the effects of varying the cross-sectional area of the spiral casing of the centrifugal pump using ANSYS CFX. Five different cross - section of the pump casing (a standard cross section and +10% and +30% increasing and -10% and -30% decreasing of the standard the cross section) was selected and its performance was evaluated numerically at the entire flow range of the pump. The authors found that the total head of the pump was optimum at low flow range for a +10% cross section casing and at higher flow range for a +30% cross-section of the casing.

Kim *et al.* (2009) carried the design optimization of impeller geometry through RSM coupled with commercial CFD code ANSYS CFX

10.0. Impeller meridional angles were selected as the design parameters and 2^k factorial design was used to set the experimental design. ANSYS BladeGen was used to generate a 3D model of the impeller for set points and analyzed its performance numerically. Optimum impeller parameter was obtained from RSM optimum plot and evaluated the model numerically. The optimum impeller improved the total head by 10.46 % and efficiency by 0.26% when compared with the original model.

Cao Lei *et al.* (2015) studied the effects of axial clearance of the shrouded centrifugal pump using CFD analysis. Different axial clearance of the pump model has developed and numerical simulation was performed using RANS equation solved the SST turbulence model. From the study the authors found that the pump head and efficiency has dropped due to an increase in axial clearance and the shaft power remained unchanged.

Baun & Flack (2003) studied the effects of volute casing design and the number of impeller vanes on the performance of the pump. Three types of the volute casing with an impeller having four vanes and five vanes were tested experimentally. They found that at the best efficiency point, the five vane impeller gave higher head and efficiency over the four vane impeller.

Afzal Husain *et al.* (2016) performed the design optimization of the jet pump using the multi-objective genetic algorithm through CFD analysis. Three design parameters were selected for optimization of pump head and efficiency. Design space was created using LHS and evaluated the objective function numerically. Four surrogate models RSA, KRG, RBNN and PRESS based Weighted averaged surrogate (PWS) were formulated and they found that the RSA model had better prediction capability. The Pareto

front optimal points were created through MATLAB and this gave a wide range of optimum points for the objective function.

Heinrich & Schwarze (2016) performed the optimization of centrifugal compressor volute shape using single objective GA coupled with CFD analysis. Cross section parameter of the volute casing was selected as a design parameter and the optimum cross-section was found from GA. The optimization results showed that the total pressure ratio and the isentropic efficiency of the compressor increased significantly.

Sayed Ahmed Imran Bellary & Abdus Samad (2016) used RSA, RBNN and KRG models for shape optimization of centrifugal pump impeller coupled with CFD analysis. Three impeller parameters inlet and outlet blade angles and a number of blades were selected as a design variable. The standard k-ε turbulence model with hexahedral structural grid was used to study the internal flow of the pump with water; crude oil and gasoline as fluids. Optimal impeller design was found from the three surrogate model and RSA had the best efficient model when compare with the other two models.

Yang & Xiao (2014) performed the design optimization of pump-turbine impeller using multi-objective GA. 3D Inverse design method was used for the parameterization of the vane profile. CFD analysis coupled with RSM and Orthogonal array was used to evaluate the responses and developed the second order mathematical model for the objective functions. Then the objective functions were optimized using GA.

Murugesan & Rudramoorthy (2016) has studied the numerical and experimental analysis of a single and multistage mixed flow bore-well pump. Different turbulent models were studied and the k-ω SST turbulence model was selected for further analysis. The numerical results of the single stage and

three stage submersible pumps were compared with experimental results and they found that the numerical results were in good agreement with the experimental result.

Bellary & Samad (2016b) studied the effects of viscosity of fluid on the centrifugal pump performance by CFD analysis at various speeds. The RANS equation was solved and the numerical performance of the pump was found for the different fluid with different viscosities. The standard k-ε turbulence model was used for 3D incompressible steady state analysis. The efficiency of the pump was decreased when the fluid viscosity increased and large recirculation also occurred at high viscosity fluids. At the low pump speed, inlet recirculation and reverse flow were also developed.

Gao *et al.* (2014) performed the experimental and numerical performance of the larger size centrifugal pump with stay blades. For numerical analysis RANS equations with k-ω SST turbulence model was used to simulate the flow inside the pump. The steady and unsteady state CFD results were compared with the experimental results. The error in the predicted performance of the steady-state simulation was more than the unsteady state simulation with the experimental data.

Zhou *et al.* (2012) performed the numerical and experimental study on the deep-well pump with a different type of diffuser. ANSYS code was used to solve N-S equation for 3D steady state incompressible flow. Numerical results were compared with experimental results and results showed the 3D return surface diffuser had performed better than the traditional cylindrical type diffuser.

Olivier Petit & Håkan Nilsson (2013) performed the numerical simulation of a centrifugal pump with a vaned diffuser at steady and unsteady

state using OpenForm CFD open source code. CFD results were compared with experimental results. The unsteady state results were closely matched with the experimental results.

Kim & Kim (2011) performed the design optimization of the mixed flow pump vane diffuser using RSA, KRG and RBNN weighted surrogate models. Two design parameters diffuser area ratio and straight blade length ratio were selected and nine design points were created using three-level full factorial design. Numerical performance at the design points was found using ANSYS CFX11.0 code which solved RANS equation with the SST turbulence model. The authors found that the RSA model had less prediction error and RBNN had more prediction error. The CFD results were in good agreement with the experimental results and efficiency of the pump was increased by 7.05%.

Bonaiuti *et al.* (2010) performed the parametric design of a water jet pump using inverse design and CFD and experimental analysis.

Choi *et al.* (2006) studied the experimental and internal flow analysis of a very small specific speed pump (N_s = 0.24). The closed type and semi-open type impeller with different impeller design combinations were tested on a standard test bench. The internal flow characteristics were measured by the Particle Imaginary Viscometry (PIV) method. It was found that a large head difference between the closed and semi-open type impeller and strong reversible occurred on the semi-open impeller.

Das *et al.* (2010) predicted the performance of the vertical borehole pump with water and slurry concentration at 5 to 18 %. Energy losses in the pump handling water and slurry concentration were presented

and it was found that the total head of the pump was decreased due to increase in slurry concentration.

Yang *et al.* (2011) investigated the numerical performance of the centrifugal pump volute of different geometry. RNG k-ε turbulence model was used to predict the numerical performance of the pump. The authors were found that the volute casing of circular cross-section gave more head and efficiency than the Trapezoid, Horseshoe shaped and Rectangular cross-section.

Friedrichs & Gu¨nter Kosyna measured the cavitation of the two different impellers of the low specific speed centrifugal pump by experimental analysis. The pump performance characteristics curves with Net Positive Suction Head (NPSH) curve were presented.

Behzadmehr *et al.* (2006) performed the sensitivity analysis of a centrifugal fan to study the effects of entrance geometry of a backward-inclined centrifugal fan on efficiency parameters. The numerical simulation was coupled with DOE. The design matrix was formulated using DOE 24 full factorial design and DOE Central Composite Design (CCD) and the optimized set parameters were found. It was found that the efficiency of the fan was improved by 5%.

Kang & Kim (2016) performed the multi-objective design optimization of the centrifugal compressor using MOGA. Four design parameters which affected its performance were selected and 25 design points were created using Box-Behnken Design (BBD). Numerical performance of the objective functions isentropic efficiency and pressure ratio at the design points were evaluated and the second order regression equation was developed using RSM. These objective functions were optimized using

MOGA and the efficiency of the compressor was improved by 1% and the sensitivity of the design parameters on the response functions was also studied.

Rameez Badhurshah & Abdus Samad (2014) performed the optimization of air turbine RSA and three Kiring variant models such as Universal Kiring (UKR), Ordinary Kiring (OKR) and Blind Kiring (BKR) were used. Three level full factorial design was used to create the design points and the functions values were found numerically using solving RANS equation. It was found that the relative efficiency of the air turbine was improved by 13% at the optimum design point.

Samad & Kim (2009) performed the multi-objective optimization of turbo machinery using MOGA. Four surrogate models RSA, KRG, RBNN, and PRESS Based Averaging (PBA) were used to optimize the objective functions. It was found that the multiple objective optimizations gave different optimum points from the Pareto front analysis.

Rouhollah Torabi & Seyyed Ahmad Nourbakhsh studied the effects of viscosity of fluid on the very low capacity pumps of specific speed (N_s = 12.8). Numerical performance of the pump at different viscosity was estimated using the k-ω SST turbulence model which solved the 3D N-S equation. The numerical results are compared with the experimental results and it was found in good agreement with the experimental results. It was also found that the shaft power increased when the viscosity of fluid was increased.

Zhou *et al.* (2014) performed the design optimization of the pump impeller by combining 2D hydraulic design, vortex flow analysis and GA. An optimum impeller was developed after the number of iteration of this

procedure. The authors have also developed five impellers with same design variable using single arc, two arc, three arc, logarithmic spiral and linear variable angle spiral methods. The numerical performances of these six impellers were calculated by solving RANS equation with RNG k-ε turbulence model. It was found that the hydraulic performance of the optimum impeller was better than the other five impellers.

Goto & Zangeneh (2002) proposed the inverse design method to optimize the diffuser blade shape of a low specific speed (N_s = 0.109 non-dimensional) centrifugal pump coupled with CFD analysis. It was found that the corner flow separation was completely suppressed in the inverse design and the pump efficiency was significantly improved and it was validated by experimental analysis.

Allali *et al.* (2015) studied the effects of different volute shape on the pump performance using the numerical approach. The pump flow variables such as velocity, total pressure, and shear stress were evaluated for different volutes configurations with Newtonian and non-Newtonian fluids. The pump impeller meshed with structured grid and volute meshed with unstructured grids and k-ε turbulence model was used for the simulation. It was found that a significant effect on the flow parameter was observed using the different shape of the volute casings.

Mohammadi & Fakharzadeh (2017) studied the effects of different outlet blade angle on the centrifugal pump performance using CFD analysis. The k-ε turbulence model with unstructured mesh was used. It was found that the optimum pump head and efficiency were obtained when the outlet blade angle was at 30^o.

Cao *et al.* (2005) performed the numerical simulation with inverse design procedure for developing high specific speed helical axial flow pump. The two-phase gas-liquid mixture as the fluid through the pump. A steady-state RANS equation for the incompressible flow was employed and the numerical results were compared with experimental results. It was found that the numerical results were well matched with the experimental results.

Ding *et al.* (2011) has predicted the pump performance of an industrial pump including the cavitation using 3D CFD analysis. The numerical performance was evaluated at the different flow rate and it was validated with experimental results. It was found that CFD results were closely matched with experimental results.

2.4 EFFECTS OF SURFACE ROUGHNES AND SURFACE COATING

Gulich (2003) studied the effects of Reynolds number and wall roughness on the efficiency of a centrifugal pump. Local heating was produced near the boundary layer if the kinematic viscosity of the fluid were in the range of 1000 to 2000 cSt. The efficiency of the pump was improved with the improvement of wall surface roughness.

Aldaş & Yapıcı (2014) studied the effects of wall surface roughness on water jet pump using ANSYS Fluent solver. The k-ω SST turbulence model was used for the transient flow analysis. The efficiency of the pump was predicted at different roughness scale between ¼ to 20/1 and a wide range of area ratio using the CFD analysis. The optimum efficiency of 60% was found for the area ratio 5.92 at the roughness scale of 0.05.

Limbach & Romuald (2017) investigated the effects of wall surface roughness on the pump performance including the cavitation through

the numerical and experimental study in a small centrifugal pump of specific speed N_s = 12. The numerical and experimental performance was measured at a different flow rate and different wall roughness values. It was found that the pump head was slightly decreased with increase in wall roughness and the cavitation effects, at low and nominal flow rate it was minimum and it was more at the overload condition.

Bellary & Samad (2016a) has study the effects of surface roughness, viscosity and outlet blade angle on the performance characteristics using CFD analysis. A 3D steady-state RANS equation was solved using the standard k-ε turbulence model. From the study the authors found that the influence of outlet blade angle on pump head and efficiency were more and dropped in efficiency due to the increase in surface roughness. It was also found that the increase in outlet angle and increase in surface finish, improved the pump head and negligible amount of increasing the pump efficiency.

Murugesan & Rudramoorthy (2016) investigated the effects of surface roughness and application of surface coating on the pump components on submersible pump. It was found that the surface roughness of the impeller and casing before coating was 2.5 μm and after coating was 0.2 μm (polymer coated) and 0.8 μm (ceramic coated). The efficiency of the polymer coated pump was improved by 4.25 % and power input was decreased by 0.3 kW to 0.5 kW when compared with the uncoated pump. On the other hand, there was no significant change on the flow rate and pump head values due to the improvement of surface finish.

Zhou *et al.* (2013) performed the design optimization of centrifugal pump impeller geometry parameters through orthogonal test coupled with CFD analysis. Five impeller parameters inlet and outlet vane angles, impeller inlet diameter, impeller outlet width and wrap angle are selected and sixteen design points were created using orthogonal test. CFD analysis was

performed on these impeller design points ANSYS- CFX and the same volute casing was used for entire analysis and optimum combination was found through variance analysis. Optimized impeller was tested with the same volute casing and the result was compared with the experimental results of the original impeller. It was found that efficiency of the pump was improved significantly.

Safikhani *et al.* (2014) performed the optimization of centrifugal pump efficiency and NPSHr using CFD analysis coupled with GA and Neural Network. For numerical simulation NUMECA code was used and the mathematical model was developed. Results showed that the efficiency of the pump improved and the Pareto front gave the wide range of optimal solution for the objective functions.

2.5 CONCLUSION

In past, the centrifugal pump performance was improved by optimization of impeller or volute casing geometry parameters (two or three parameters were considered). Selecting five impeller parameters for improving pump performance was not studied yet and performance improvement through improving the surface finish of the impeller and volute casing of the centrifugal pump also not carried out. For the requirement of the pump standard and BEE, the efficiency of the pump needs to be improved by the manufacturer. Therefore, in this research work, performance of the centrifugal pump is improved through optimization of impeller parameters (five geometrical parameters are considered) and improving the surface finish of the impeller and volute casing.

CHAPTER 3

EXPERIMENTAL ANALYSIS OF A CENTRIFUGAL PUMP

3.1 INTRODUCTION

The objective of the experimental analysis is to calculate the actual performance of the selected pump at the duty point and understand the variation of different performance characteristics under the various operating conditions. The construction and fabrication of the pump test setup and various measuring instruments used for testing are discussed in this chapter. Measurement uncertainty analysis is carried out to estimate the uncertainty in various pump performance parameters.

3.2 RADIAL FLOW CENTRIFUGAL PUMP

Agriculture irrigation pumps are provided with maximum area coverage (IS 9694(Part 1): 1987). Since India has a large number of small farmers having a cultivated land of 2 to 3 hectares and the Tamil Nadu State Government provides a free power supply for the irrigation sector, and it is essential to develop energy efficient pumps to save electric energy. The duty point discharge and total head were derived from IS 9694(Part1):1987 standard to cover 3 hectares and the details are shown in Table 3.1. A centrifugal pump of duty point flow rate of 0.015 m^3/s at a total head of 32 m and the speed of rotation 2900 rpm are selected from MSME, M/s Coimbatore Engineering Company (CEC), Coimbatore, Tamil Nadu, India for this research work. The design specification of the selected pump at the guaranteed duty point is presented in Table 3.1. The guaranteed duty point is the point at which the pump designer or the manufacturer shall declare or guaranteed the performance of the pump.

Table 3.1 Pump design specifications at guaranteed duty point

Parameters		Value	Unit	Nomenclature
Flow Rate		0.015	m^3/s	Q_G
Total Head		32	m	H_G
Speed of Rotation		2900	rpm	N
Pump Specific Speed	metric unit	96.35	(rpm, m^3/s, m)	$N_S = \frac{3.65N\sqrt{Q}}{H^{\frac{3}{4}}}$
	US unit	1363.4	(rpm, US gpm, ft)	$N_S = \frac{N\sqrt{Q}}{H^{\frac{3}{4}}}$
Prime Mover Rating		7.5 / 10	kW/ HP	P

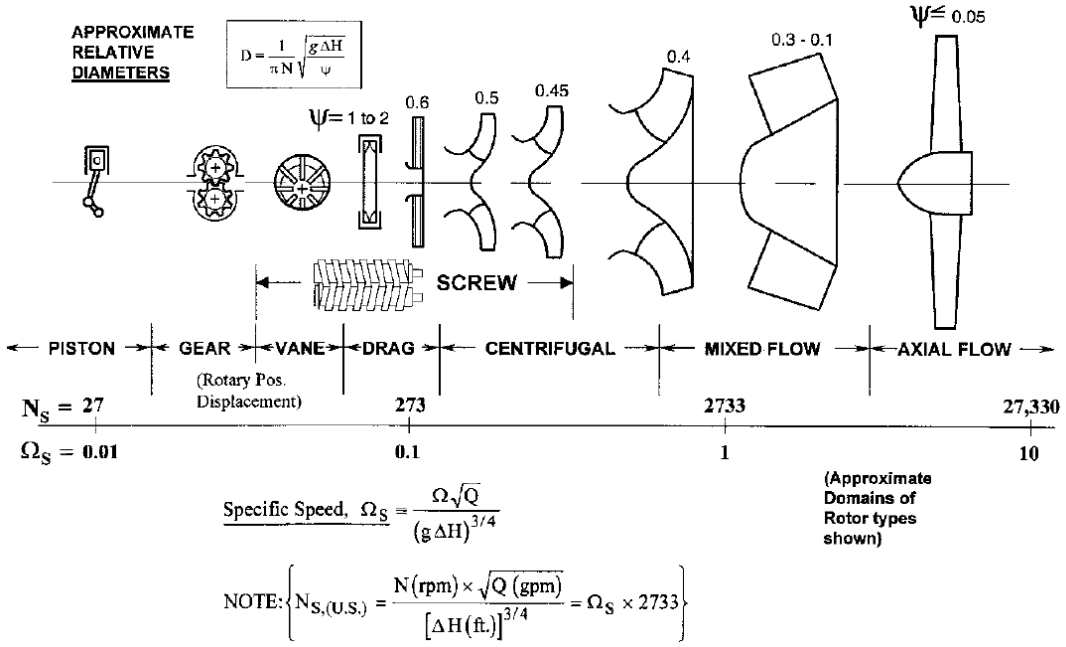

(Source: Karassik *et al.* 2001)

Figure 3.1 Pump classification Vs Specific speed

The pump specific speed calculated to the corresponding duty point specifications is 1363.4 rpm in US unit. Referring the Figure 3.1, it is concluded that the pump model corresponding to this specific speed is purely radial flow centrifugal pump.

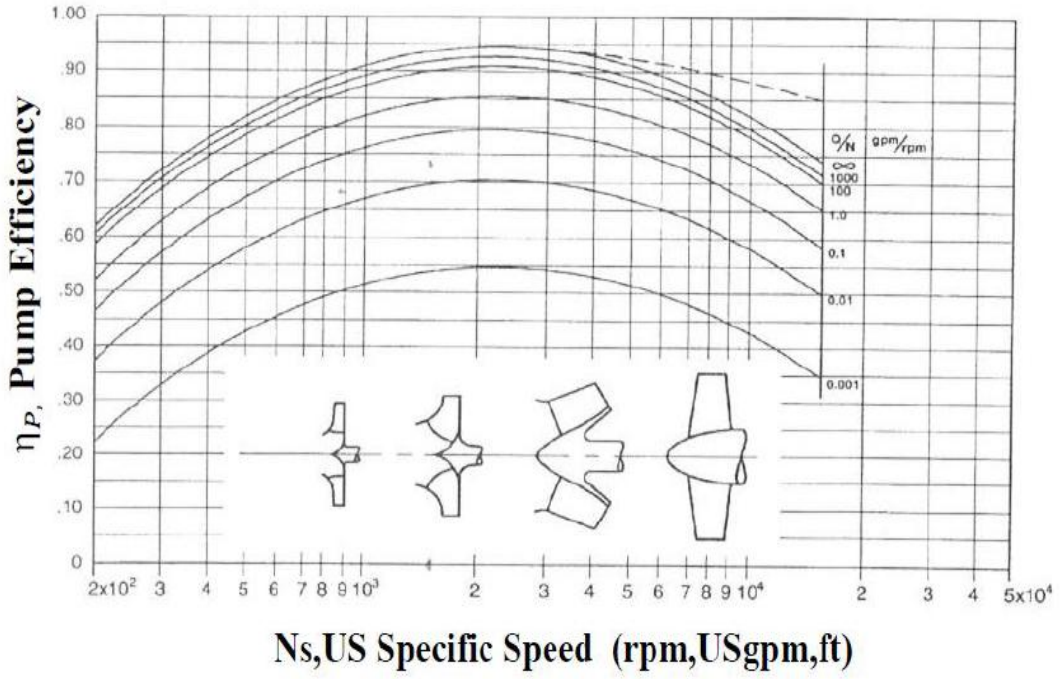

(Source: Karassik *et al.* 2001)

Figure 3.2 Specific speed Vs Pump efficiency chart of a centrifugal pump

This pump model is required for the agricultural applications throughout India in larger quantity. The efficiency of the pump at present condition for this model is studied and found in the range of 63 to 67 % and its average is 65 %. The minimum efficiency required by the Indian Standard IS 9079: 2002 for the duty point of the pump is 66%. Comparing the efficiency values of present level and standard requirements, the current efficiency level is less than the standard values, and also found it was less than the maximum achievable efficiency level specified in the specific speed Vs Pump Efficiency chart available in the Centrifugal pump handbook as shown in Figure 3.2 and it is referred as a benchmark value globally by the pump manufacturer. Referring to the chart, the pump efficiency corresponding to the specific speed (N_S = 1363.4 US unit) is 77%. Hence it is concluded that there is a scope for increasing the pump efficiency from the present level of 63 to 67 %. By satisfying the requirements of the Bureau of

Indian Standards (BIS) and Bureau of Energy Efficiency (BEE) the pump manufacturer need to improve the efficiency of the pump. The increase of efficiency saves significant electricity in the agricultural sector.

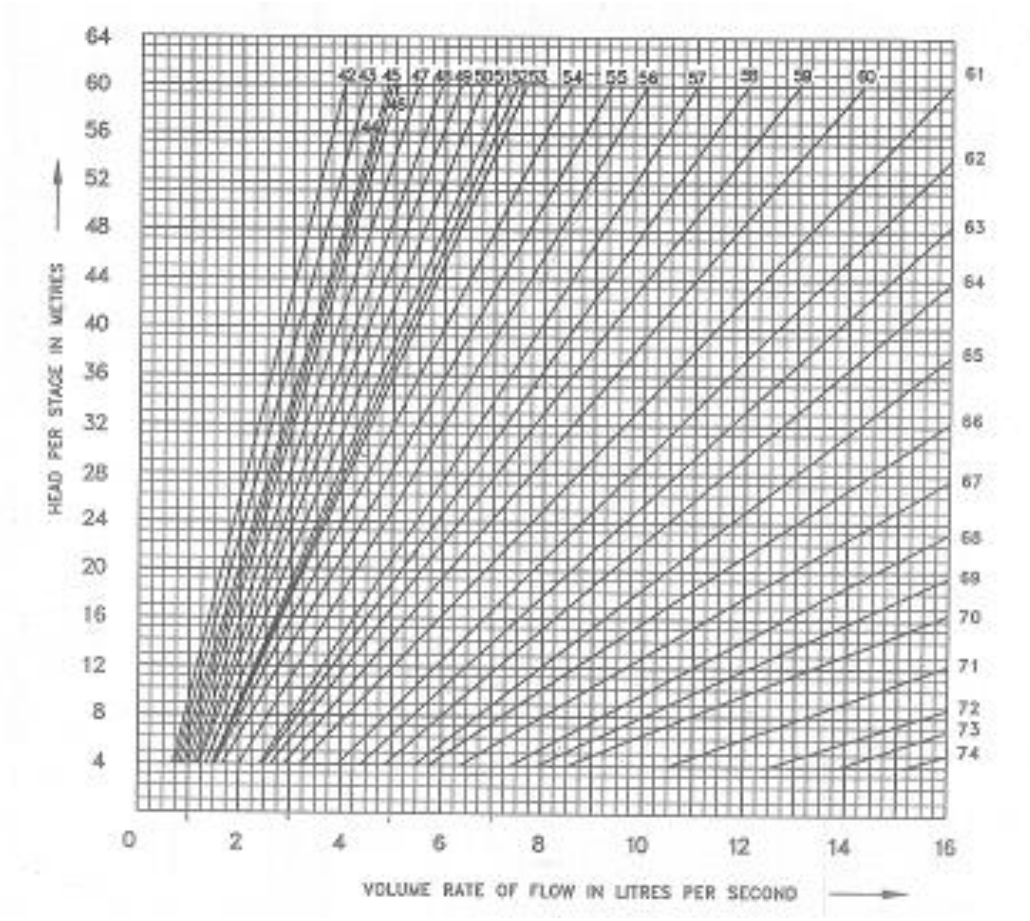

(Source: Indian Standard IS 9079: 2002)

Figure 3.3 Centrifugal pump efficiency chart

3.3 EXPERIMENTS ON RADIAL FLOW CENTRIFUGAL PUMP

Experiments on a selected centrifugal pump are carried out to study the actual performance of the pump. The testing setup for conducting the performance test on the selected pump is fabricated in accordance with ISO 9906:2012 and IS 11346:2002 Standard. Figure 3.4 shows the general

layout and Figure 3.5 shows the experimental test set up to carry out performance testing of the selected pump. The pump test setup consists of the test pump coupled with a three-phase induction motor, inlet and outlet pipelines with control valves, foot valve at inlet pipe, sump and volumetric tank for the required capacity as specified in IS 11346: 2002. Vacuum and Pressure transducers are mounted at the inlet and outlet pipes in order to measure the inlet and the outlet pressure. An electromagnetic flow meter and three phase power meters are connected to measure the amount of fluid through the pump and input power taken by the prime mover.

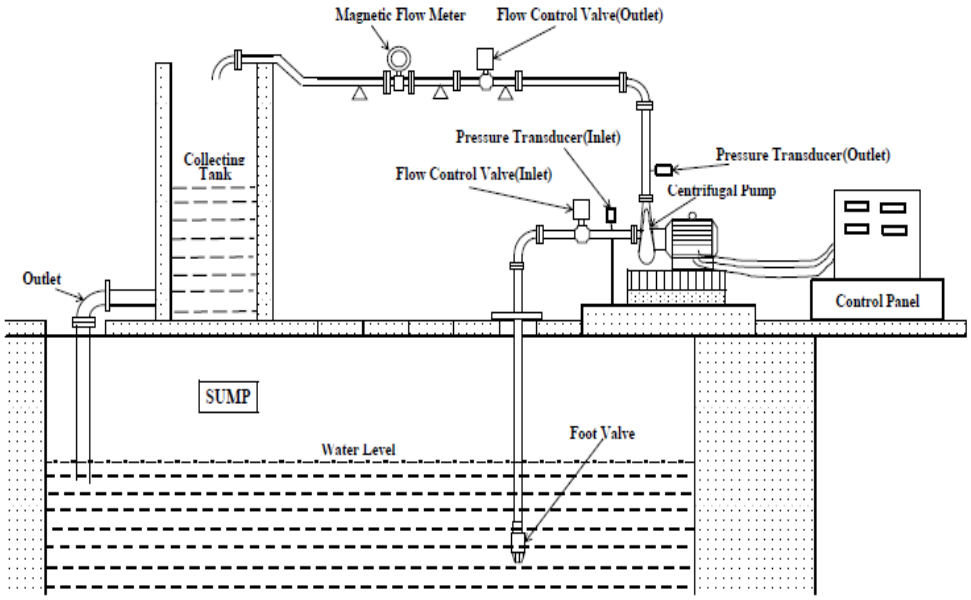

Figure 3.4 General test layout of a centrifugal pump as per ISO 9906 and IS 11346

Figure 3.5 (a) Laboratory test setup as per ISO 9906 and IS 11346

Figure 3.5(b) Three phase AC control panel for power measurement

3.3.1 Testing Instruments and its Technical Specifications

To reduce the uncertainty in the measurement, the measuring devices with the Best Measurement Capability (BMC) are used. Table 3.2 to 3.7 present the detailed specifications of the various measuring instruments used for measuring the various parameters during the performance testing of the centrifugal pump.

Table 3.2 presents the specifications of a vacuum transmitter used to measure the pump suction head, is connected to the inlet pipeline. The 4-20 mA input signal is converted by the transducer in to pressure values and they are displayed in pressure units. In order to reduce the uncertainty in suction head measurement, the transmitter with better accuracy is used.

Table 3.2 YOKOGAWA make pressure transmitter used for measuring suction pressure

Model	EJA130A
Pressure Range	0 – 760 mmHg
Output	4 – 20 mA
Accuracy (% of Full-Scale Reading)	± 0.2
Stability	± 0.5 % for 10 years
Response Time	90 ms
Measurement Uncertainty at 95% Confidence Level(% of Full-Scale Readings)	± 1.65

Table 3.3 presents the specifications of a pressure transmitter used to measure the pump delivery head, is connected to the outlet pipeline. The 4-20 mA input signal is converted by the transducer in to pressure values

and they are displayed in pressure units. In order to reduce the uncertainty in delivery head measurement, the transmitter with better accuracy is used.

Table 3.3 YOKOGAWA make pressure transmitter used for measuring delivery pressure

Model	EJA530A
Pressure Range	0 – 10 bar
Output	4 – 10 mA
Accuracy (% of Full-Scale Reading)	± 0.2
Stability	± 0.5 % for 10 years
Response Time	90 ms
Measurement Uncertainty at 95% Confidence Level(% of Full-Scale Readings)	± 1.65

Table 3.4 presents the technical specifications of the electromagnetic flow meter. The flow meters have an indicating device and a flow tube. The indicating device displays the volume of fluid through the flow line and flow sensor in the flow tube senses the amount of fluid. The flow meter have flanged/screwed/ or OEM welded ends and it is easily connected to the outlet pipeline. The velocity of the fluid through the meter is in the range of 0 to 10 m/s and the volume of flow through the meter is depend on the nominal diameter of the flow meter.

The YOKOGAWA makes three-phase power meter (Table 3.5) which is used for measuring power input parameters such as current, voltage, input power and supply frequency to the AC induction motor. The accuracy of the power meter for all these parameters is 0.2%. If the current and power

rating values exceed 20A and 2.4 kW, then a current transformer is used. Table 3.5 presents the detailed specification of the power meter.

Table 3.4 YOKOGAWA make magnetic flow meter used for measuring flow rate

Model	SE 208 MJ
Nominal Diameter	80 mm
Flow Rate Range	0.0 – 0.628 m^3 /s
Velocity of Flow	0 - 10 m/s
Output	4 – 20 mA
Accuracy (% of Full-Scale Readings)	± 0.5
Stability	± 0.5 % for 10 years
Response Time	30 s
Measurement Uncertainty at 95% Confidence Level(% of Full Scale Readings)	± 0.23

A contact / noncontact type tachometer is used to measure the speed of rotation of the shaft either in contact or in non-contact mode. In case of contact mode, the tachometer is directly contacted with the shaft and so the speed is measured. In the case of non- contact mode, a reflective sticker is fixed on the shaft and an LED transmitter is used to locate the spot of RED light which is emitted on the shaft. The reflective sticker reflects the beam of light and they are connected in to pulses, which indicate the speed of the shaft. Table 3.6 presents the technical specification of a LINESEKI make tachometer.

Table 3.5 YOKOGAWA make 3 phase digital power meter used for measuring current, voltage, power input, and frequency

Model		WT 230
Measurement Range	Current	0 – 20 A
	Voltage	0 – 600 V
	Power Input	0 – 2.4 kW
	Current Transformer	0 – 100 A
	Frequency	0.5 – 100 kHz
Accuracy (% of Full Scale Readings)	Current	± 0.2
	Voltage	± 0.2
	Power Input	± 0.2
	Current Transformer	± 0.2
	Frequency	± 0.2
Stability		± 0.2% for 10 years
Response Time		0.1 s
Measurement Uncertainty at 95% Confidence Level(% of Full-Scale Readings)	Current	±0.40
	Voltage	± 0.075
	Power Input	±0.53
	Current Transformer	± 0.5
	Frequency	±0.60

Table 3.6 LINESEKI make tachometer used for measuring the speed of the pump

Model		TM 4000
Speed Range	Contact Mode	6 – 99999.9 rpm
	Noncontact Mode	6 – 99999.9 rpm
The accuracy of the Full-Scale Reading		± 1 rpm
Resolution		0.1 rpm
Stability		±0.2% for 10 years
Response Time		1.0 – 10.0 s
Measurement Uncertainty at 95% Confidence Level(% of Full Scale Readings)		± 0.15

3.3.2 Pump Performance Testing

Performance testing of the pump is conducted from fully open to shutoff condition of the outlet control valve at an equal interval. Test readings of all the measuring instruments are recorded simultaneously to reduce the error. The output power of the pump is calculated using the total head and flow rate of the pump for all sets of readings and input power is directly measured using a power meter and finally, the efficiency of the pump is calculated. For ease of comparison, the performance results are converted into the rated speed of the pump at 2900 rpm.

Rated discharge,

$$Q = Q_a \cdot \left(\frac{N_r}{N_a} \right) \tag{3.1}$$

Where,

Q_a – actual flow rate through the flow meter in m^3/s

N_r – rated speed (2900 rpm)

N_a – actual pump speed in rpm

Rated total head,

$$H = \left(H_s + H_d + k.Q_a + Z\right).\left[\frac{N_r}{N_a}\right]^2 \tag{3.2}$$

Where,

H_s – suction head form vacuum transmitter in m

H_d - delivery head from pressure transmitter in m

Z – datum head in m

k – a constant

Rated power input,

$$P = P_a.\left[\frac{N_r}{N_a}\right]^3 \tag{3.3}$$

Where,

P_a - input power of the prime mover from power meter in kW

Pump output,

$$P_o = \frac{Q.H}{102} \tag{3.4}$$

Pump efficiency,

$$\eta = \frac{P_o}{P.\eta_m} \tag{3.5}$$

Where, η_m – efficiency of the prime mover and it is equal to 81% which is taken from IS 9079:2002 standard.

The performance values of each set point are calculated and are presented in Table 3.7. The pump performance curves are shown in Figure 3.6.

Table 3.7 Experimental performance of a selected pump

Discharge (Q) x 10^{-3}, m^3/s	Head(H), m	Power Input(P), kW	Efficiency (η), %
22.00	10.69	9.20	31.31
21.95	15.89	10.02	42.98
21.50	20.59	10.73	50.55
21.20	25.22	11.13	58.86
19.75	29.45	11.11	64.13
16.50	33.75	10.41	65.57
13.65	35.88	9.72	61.74
9.85	38.00	8.64	53.06
6.50	39.15	7.65	40.74
0.00	41.25	5.72	0.00

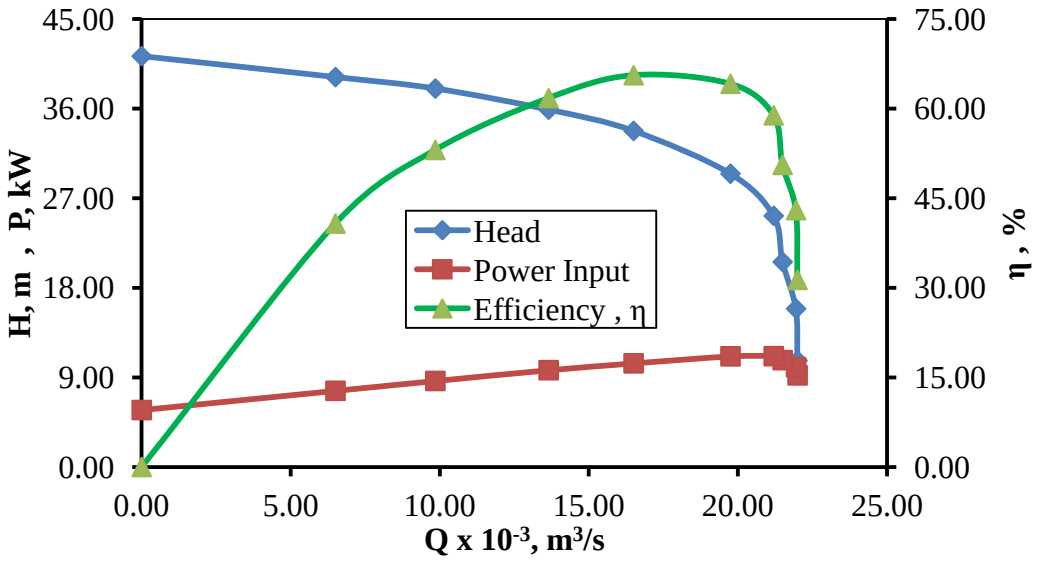

Figure 3.6 Performance characteristics of a selected pump

At the duty point, the experimental performance values are 34.8 m, 65.6% and 10.05 kW respectively. The experimental results confirm the increase of power input and pump efficiency when the discharge and total head increases and satisfies the requirements of the pump standard (IS 9079:2002). However, the performance characteristic of the selected impeller has to improve for maximizing the efficiency as required by BEE and Hydraulic Institute. So the dimension of the selected impeller needs some modifications for further improvement.

3.4 ESTIMATION OF MEASUREMENT UNCERTAINTY IN PUMP TESTING

A quality measurement is one of the main requirements of all measuring system. Measuring the TRUE value in any process is practically not possible. The measured quantity obtained from the process is an estimate or the approximate quantity of the true value. Even an appropriate error can be applied to the measured quantity the system itself have some uncertainty. The measurement results are completed only if the statement of measured values is reported along with the uncertainty which is associated with those results. Without uncertainty of the measured values, the results are not compared with any other measured values or the reference or standard values.

Random and systematic error components may affect the measured values and contribute to the uncertainty. The contribution of the random error component is called random uncertainty and the systematic error components are called system uncertainty.

The random errors occur due to the selection of measurement procedure, influence of environmental climate, instability of the measuring instruments and equipments used, judgment of person involved in the

measurements, etc. The random error does not eliminate completely but it can be minimized by implementing the suitable control system.

The other source of error is called systematic errors reported in the calibration certificates of the measuring instruments, equipment, accuracy, resolution of the instruments, etc.

3.4.1 Measurement Uncertainty of Flow Rate (Q)

In centrifugal pump testing, various instruments are used to measure the flow rate, suction and delivery pressure, datum height, input power, voltage, the speed of rotation and supply frequency. The various parameters are measured simultaneously from the delivery valve in full open to full closed conditions. Estimating the uncertainty due to the random and systematic errors is mandatory requirement of a pump manufacturer, customers, third-party independent testing laboratories and other statutory governing bodies for comparing the results with specified/ standard values.

Measurand or the output parameter is a particular item which is subject to measurement. In pump testing, the flow rate Q is the one of the output parameter which depends on many numbers of input quantities $A_i, [i = 1, 2, 3, ..., N]$.

The functional relationships between Q and A_i are given in Equation (3.6)

$$Q = f\left[A_1, A_2, A_3, ..., A_N\right] \tag{3.6}$$

The estimate of the output parameter is denoted by A and the value is obtained from Equation (3.6) using the input estimates a_i for all the input quantities A_i

$$q = f\left[a_1, a_2, a_3, ..., a_n\right] \tag{3.7}$$

From Equations (3.6) and (3.7) it is clearly understood that the input quantities are the best estimates of the output parameter Q.

The standard uncertainty associated with estimate q is denoted by u (q) and is equal to the standard deviation of the true values of Q corresponding to the estimate q. It is to be calculated from the model Equation (3.6) using the estimates a_i of the input quantities A_i and their associated standard uncertainties u (a_i).

The unit of dimensions for the estimate q is the same as that of standard uncertainty u(q) associated with the estimate. In certain cases, the unit of the estimate may differ with the unit of standard uncertainty. In that case, the sensitivity coefficient of each input quantities is used. The sensitivity coefficient is the partial derivative of the output parameter with respect to each input quantities.

The collections of standard uncertainty of all input quantities are combined and it is called combined standard uncertainty of the output parameter Q. Finally, the expanded uncertainty of the output can be calculated by multiplying the coverage factor (k). The coverage factor is the multiplication factor which is taken from the student t - statistics table corresponding to the effective degree of freedom and confidence interval of the measurement.

3.4.1.1 Estimation of Random or Type A Uncertainty of Flow Rate

The repeated measurement at the duty point flow rate is taken for ‘n’ of the times and these values are used for the estimation of type A

uncertainty. The type A uncertainty can be reduced by increasing the value of 'n'. Therefore, the number observation is taken as 20.

Standard deviation,

$$\sigma = \sqrt{\frac{\left(a - \bar{a}\right)^2}{n-1}} \tag{3.8}$$

Standard uncertainty (in random measurements),

$$u_A(Q) = \frac{\sigma}{\sqrt{n}} \tag{3.9}$$

Degree of freedom, υ_1 = (n-1) (3.10)

3.4.1.2 Estimation of Systematic or Type B Uncertainty of Flow Rate

Rated discharge,

$$Q = Q_a . \left(\frac{N_r}{N_a}\right) \tag{3.11}$$

$$Q = f\left(Q_a, N_a\right) \tag{3.12}$$

The contributory variances are

$$u_c^2\left(Q\right) = C_{Q_a}{}^2 . u_c^2\left(Q_a\right) + C_{N_a}{}^2 . u_c^2\left(N_a\right) \tag{3.13}$$

Where,

C_{Q_a} - Sensitivity Coefficient of flow rate

C_{N_a} - Sensitivity Coefficient of speed

The sensitivity coefficients are

$$C_{Q_a} = \frac{\partial Q}{\partial Q_a} = \left[\frac{N_r}{N_a} \right] \tag{3.14}$$

$$C_{N_a} = \frac{\partial Q}{\partial N_a} = (-1).(Q_a).\left[\frac{N_r}{N_a^{\,2}} \right] \tag{3.15}$$

Combined Type B Uncertainty,

$$u(Q) = \sqrt{\left(C_{Q_a}{}^2 . u_c{}^2 (Q_a) + C_{N_a}{}^2 . u_c{}^2 (N_a) \right)} \tag{3.16}$$

Combined Uncertainty,

$$u_C (Q) = \sqrt{\left(u_A{}^2 (Q) + u_B{}^2 (Q) \right)} \tag{3.17}$$

Effective degree of freedom,

$$\upsilon_{eff} = \frac{u_C{}^4 (Q)}{\left(\frac{u_A{}^4 (Q)}{\upsilon_1} + \frac{u_{Q_a}{}^4 (Q)}{\upsilon_2} + \frac{u_{N_a}{}^4 (Q)}{\upsilon_3} \right)} \tag{3.18}$$

Expanded Uncertainty,

$$u(Q) = k . u_C (Q) \tag{3.19}$$

Where, k is the coverage factor

Equations (3.8) to (3.19) are used to estimate the uncertainty of the flow rate and their budget is given in Table 3.8.

Table 3.8 Uncertainty budget for flow rate

Uncertainty sources A_i	Estimate a_i	Limits $\pm a_i$	Types of probability distribution and divisor	Standard uncertainty $u(A_i)$	Sensitivity coefficient C_i	Uncertainty contribution $u_i(q)$, lps	Degree of freedom
Repeated measurement, u1	16.53 lps		Normal Type A $\sqrt{10}$	0.0093 lps	1.0	0.0093	$\upsilon_1 = 9$
Calibration uncertainty of flow meter, u2		0.23 %	Normal Type B 2	0.115%	C_{Q_a} = 1.002	0.1152	$\upsilon_2 = \infty$
Calibration uncertainty of tachometer, u3		0.3 rpm	Normal Type B 2	0.15 rpm	C_{f_a} = -0.3319	0.0498	$\upsilon_3 = \infty$
Error due to variation in speed measurement, u4		0.05 rpm	Rectangular Type B $\sqrt{3}$	0.0289 rpm	C_{f_a} = -0.3319	0.0096	$\upsilon_4 = \infty$
Combined Uncertainty, $u_c(Q)$						0.1287	$\upsilon_{eff} = \infty$
Expanded Uncertainty, u(Q)			k = 2			0.2524	∞

Reporting of the Result:

The measured flow rate Q at the duty point is

$$16.53 \pm 0.25 \text{ lps}$$

with k = 2 for a confidence interval of 95% and the $\upsilon_{eff} = \infty$

A similar procedure discussed in the section 3.4.1 which is used for estimating the uncertainty of total head, power input and efficiency.

3.4.2 Estimation of Uncertainty of Head (H)

3.4.2.1 Estimation of random or type A uncertainty of head

Standard deviation,

$$\sigma = \sqrt{\frac{\left(a - \bar{a}\right)^2}{n-1}} \tag{3.20}$$

Standard uncertainty (in random measurements),

$$u_A(H) = \frac{\sigma}{\sqrt{n}} \tag{3.21}$$

The degree of freedom $\upsilon_1 = (n-1)$ (3.22)

3.4.2.2 Estimation of systematic or type B uncertainty of head

The rated head of the pump,

$$H = \left(H_s + H_d + k.Q_a + Z\right).\left[\frac{N_r}{N_a}\right]^2 \tag{3.23}$$

The contributory Variances on head measurement are

$$u_c^2(H) = C_{H_s}^2.u_c^2(H_s) + C_{H_d}^2.u_c^2(H_d) + C_{Q_a}^2.u_c^2(Q_a) + C_z^2.u_c^2(Z) + C_{N_a}^2.u_c^2(N_a) \quad (3.24)$$

Where, C_{H_s} - Sensitivity Coefficient of suction head

C_{H_d} - Sensitivity Coefficient of the delivery head

C_{Q_a} - Sensitivity Coefficient of flow rate

C_z - Sensitivity Coefficient of datum head

C_{N_a} - Sensitivity Coefficient of speed

The sensitivity coefficients are

$$C_{H_s} = \frac{\partial H}{\partial H_s} = \left[\frac{N_r}{N_a}\right]^2 \quad (3.25)$$

$$C_{H_d} = \frac{\partial H}{\partial H_d} = \left[\frac{N_r}{N_a}\right]^2 \quad (3.26)$$

$$C_{Q_a} = \frac{\partial H}{\partial H_{Q_a}} = \left[\frac{N_r}{N_a}\right]^2 \quad (3.27)$$

$$C_z = \frac{\partial H}{\partial H_z} = \left[\frac{N_r}{N_a}\right]^2 \quad (3.28)$$

$$C_{N_a} = \frac{\partial H}{\partial N_a} = (-2).(H_s + H_d + k.Q_a + Z).\left[\frac{N_r^2}{N_a^3}\right] \quad (3.29)$$

The combined type B uncertainty of head,

$$u_B(H) = \sqrt{\left(C_{H_s}^2.u_c^2(H_s) + C_{H_d}^2.u_c^2(H_d) + C_{Q_a}^2.u_c^2(Q_a) + C_z^2.u_c^2(Z) + C_{N_a}^2.u_c^2(N_a)\right)} \quad (3.30)$$

Combined uncertainty,

$$u_C(H) = \sqrt{\left(u_A{}^2(H) + u_B{}^2(H)\right)} \tag{3.31}$$

Effective Degree of Freedom,

$$\upsilon_{eff} = \frac{u_C{}^4(H)}{\left(\frac{u_A{}^4(H)}{\upsilon_1} + \frac{u_{H_s}{}^4(H)}{\upsilon_2} + \frac{u_{H_d}{}^4(H)}{\upsilon_3} + \frac{u_{Q_a}{}^4(H)}{\upsilon_4} + \frac{u_z{}^4(H)}{\upsilon_5} + \frac{u_{N_a}{}^4(H)}{\upsilon_6}\right)} \tag{3.32}$$

Expanded Uncertainty,

$$u(H) = k.u_C(H) \tag{3.33}$$

Where k is the coverage factor

Equations (3.20) to (3.33) are used to estimate the uncertainty of the total head and its budget is given in Table 3.9

Table 3.9 Uncertainty budget for total head

Uncertainty sources Ai	Estimate ai	Limits ± ai	Types of probability distribution and divisor	Standard uncertainty u(ai)	Sensitivity coefficient Ci	Uncertainty contribution Ui(h), m	Degree of freedom
Repeated measurement, u1	33.64 m		Normal Type A $\sqrt{10}$	0.0211 m	1.0	0.0211	$\upsilon_1 = 9$
Calibration uncertainty of suction pressure transmitter, u2		0.54 %	Normal Type B 2	0.27 %	C_{H_s} =1.004	0.2721	$\upsilon_2 = \infty$
Calibration uncertainty of delivery pressure transmitter, u3		0.56 %	Normal Type B 2	0.28 %	C_{H_d} =1.004	0.2781	$\upsilon_3 = \infty$
Uncertainty due to flow rate measurement, u4		0.2524 lps	Normal Type B 2	0.1262 lps	C_{Q_a} = 1.004	0.1269	$\upsilon_4 = \infty$
Uncertainty due to datum head measurement,u5		0.005 m	Rectangular Type B $\sqrt{3}$	0.0029 m	C_z =1.004	0.0029	$\upsilon_5 = \infty$
Calibration uncertainty of tachometer,u6		0.3rpm	Normal Type B 2	0.15 rpm	C_{f_a} = -1.6303	0.2445	$\upsilon_6 = \infty$
Error due to variation in speed measurement, u7		0.05 rpm	Rectangular Type B $\sqrt{3}$	0.0289 rpm	C_{f_a} = -1.6303	0.0471	$\upsilon_7 = \infty$
Combined Uncertainty, uc(H)						0.4795	$\upsilon_{eff} = \infty$
Expanded Uncertainty, u(H)			k = 2			0.9590	∞

Reporting of the result:

The measured total head at the duty point is

$$33.64 \pm 0.96 \text{ m}$$

With k = 2 for a confidence interval of 95% and the $\upsilon_{eff} = \infty$

3.4.3 Estimation of Uncertainty of Power Input (P)

3.4.3.1 Estimation of random or type A uncertainty of power input

Standard deviation,

$$\sigma = \sqrt{\frac{\left(a - \bar{a}\right)^2}{n-1}} \tag{3.34}$$

Standard uncertainty (in random measurements),

$$u_A(P) = \frac{\sigma}{\sqrt{n}} \tag{3.35}$$

Degree of freedom $\upsilon_1 = (n-1)$ (3.36)

3.4.3.2 Estimation of systematic or type B uncertainty of power input

Rated power input,

$$P = P_a . \left[\frac{N_r}{N_a}\right]^3 \tag{3.37}$$

The contributing variances are

$$u_c^{\,2}(P) = C_W{}^2 . u_c{}^2(P_a) + C_{N_a}{}^2 . u_c{}^2(N_a) \tag{3.38}$$

Where,

C_{P_a} - Sensitivity coefficient of power input

C_{N_a} – Sensitivity coefficient of frequency

$$C_{P_a} = \frac{\partial P}{\partial P_a} = \left[\frac{N_r}{N_a}\right]^3 \tag{3.39}$$

$$C_{N_a} = (-3) P_a . \left[\frac{N_r{}^3}{N_a{}^4}\right] \tag{3.40}$$

Combined Type B uncertainty,

$$u_B(P) = \sqrt{\left(C_{P_a}{}^2 . u_c{}^2(P_a) + C_{N_a}{}^2 . u_c{}^2(N_a)\right)} \tag{3.41}$$

Combined Uncertainty,

$$u_C(P) = \sqrt{\left(u_A{}^2(P) + u_B{}^2(P)\right)} \tag{3.42}$$

Effective Degree of Freedom,

$$\upsilon_{eff} = \frac{u_C{}^4(P)}{\left(\frac{u_A{}^4(P)}{\upsilon_1} + \frac{u_{P_a}{}^4(P)}{\upsilon_2} + \frac{u_{N_a}{}^4(P)}{\upsilon_3}\right)} \tag{3.43}$$

Expanded Uncertainty,

$$u(P) = k . u_c(P) \tag{3.44}$$

Where k is the coverage factor

Equations (3.34) to (3.44) are used to estimate the uncertainty of the power input and its budget is given in Table 3.10.

Table 3.10 Uncertainty budget for power input

Uncertainty sources Ai	Estimate ai	Limits ± ai	Types of probability distribution and divisor	Standard uncertainty u(ai)	Sensitivity coefficient Ci	Uncertainty contribution ui(p), kW	Degree of freedom
Repeated measurement, u1	10.17 kW		Normal Type A $\sqrt{10}$	0.0115 kW	1.0	0.0115	$\upsilon_1 = 9$
Calibration uncertainty of the power meter,u2		0.008 kW	Normal Type B 2	0.004 kW	C_w =1.006	0.004	$\upsilon_2 = \infty$
Calibration uncertainty of tachometer,u3		0.3 rpm	Normal Type B 2	0.15 rpm	C_{f_a} = -0.6209	0.0931	$\upsilon_3 = \infty$
Error due to variation in speed measurement, u4		0.05 rpm	Rectangular Type B $\sqrt{3}$	0.0289 rpm	C_{f_a} = -0.6209	0.0179	$\upsilon_4 = \infty$
Combined Uncertainty, uc(P)						0.0956	$\upsilon_{eff} = \infty$
Expanded Uncertainty, u(P)			k = 2			0.1911	∞

Reporting of the result:

The measured power input at the duty point is

$$10.17 \pm 0.191 \text{ kW}$$

With k = 2 for a confidence interval of 95% and the $\upsilon_{eff} = \infty$

3.4.4 Estimation of Uncertainty of Efficiency (η)

3.4.4.1 Estimation of random or type A uncertainty of efficiency

Standard deviation,

$$\sigma = \sqrt{\frac{\left(a - \bar{a}\right)^2}{n-1}} \tag{3.45}$$

Standard uncertainty (in random measurements),

$$u_A(\eta) = \frac{\sigma}{\sqrt{n}} \tag{3.46}$$

Degree of freedom $\upsilon_1 = (n-1)$

(3.47)

3.4.4.2 Estimation of systematic or type B uncertainty of efficiency

Pump efficiency,

$$\eta = \frac{Q.H}{102P} \tag{3.48}$$

The contributing variances are

$$u_c^{\,2}(\eta) = C_Q{}^2.u_c{}^2(Q) + C_H{}^2.u_c{}^2(H) + C_P{}^2.u_c{}^2(P) \tag{3.49}$$

Where,

C_Q - Sensitivity coefficient of flow rate

C_H - Sensitivity coefficient of head

C_P - Sensitivity coefficient of power input

$$C_Q = \frac{\partial \eta}{\partial Q} = K.\frac{H}{P} \tag{3.50}$$

$$C_H = \frac{\partial \eta}{\partial H} = K.\frac{Q}{P} \tag{3.51}$$

$$C_P = \frac{\partial \eta}{\partial P} = (-1).K.\frac{QH}{P^2} \tag{3.52}$$

where K – is a constant = 100/102 =0.980392

Combined type B uncertainty,

$$u_B(\eta) = \sqrt{\left(C_Q{}^2.u_c{}^2(Q) + C_H{}^2.u_c{}^2(H) + C_P{}^2.u_c{}^2(P)\right)} \tag{3.53}$$

Combined uncertainty,

$$u_C(\eta) = \sqrt{\left(u_A{}^2(\eta) + u_B{}^2(\eta)\right)} \tag{3.54}$$

Effective degree of freedom,

$$\upsilon_{eff} = \frac{u_C{}^4(\eta)}{\left(\frac{u_A{}^4(\eta)}{\upsilon_1} + \frac{u_Q{}^4(\eta)}{\upsilon_2} + \frac{u_H{}^4(\eta)}{\upsilon_3} + \frac{u_P{}^4(\eta)}{\upsilon_4}\right)} \tag{3.55}$$

Expanded uncertainty,

$$u(\eta) = k.u_c(\eta) \tag{3.56}$$

Where k is the coverage factor

Equations (3.45) to (3.56) are used to estimate the uncertainty of the efficiency and its budget is given in Table 3.11

Table 3.11 Uncertainty budget for efficiency

Uncertainty Sources Ai	Estimate ai	Limits ± ai	Types of probability and divisor	Standard Uncertainty u(ai)	Sensitivity Coefficient Ci	Uncertainty Contribution ui(η), %	Degree of freedom
Repeated measurement, u1	65.57 %		Normal Type A $\sqrt{10}$	0.0287	1.0	0.0287	$\upsilon_1 = 9$
Uncertainty due to flow rate measurement,u2		0.2524 lps	Normal Type B 2	0.1262	C_Q =3.212	0.4053	$\upsilon_2 = \infty$
Uncertainty due to total head measurement,u3		0.9590 m	Normal Type B 2	0.4795	C_H =1.578	0.7566	$\upsilon_3 = \infty$
Uncertainty due to power input measurement,u4		0.1911 kW	Rectangular Type B 2	0.0956	C_P =-5.169	0.4942	$\upsilon_4 = \infty$
Combined Uncertainty, uc(η)						0.9908	$\upsilon_{eff} = \infty$
Expanded Uncertainty, u(η)			k = 2			1.9816	∞

Reporting of the result:

The measured efficiency at the duty point is

$$65.57 \pm 1.98\ \%$$

With k = 2 for a confidence interval of 95% and the $\upsilon_{eff} = \infty$

Table 3.12 Summary of uncertainty measurement of pump performance characteristics

Pump Performance Characteristics	Experimental Performance at the Duty Point	Uncertainty Measurement at 95% Confidence Level with k=2	
		In terms of values	In terms of %
Flow rate, Q	16.53 lps	± 0.25 lps	± 1.51
Head, H	33.64 m	± 0.96 m	± 2.85
Power input, P	10.17 kW	± 0 .191 kW	± 1.87
Efficiency, η	65.57 %	± 1.98 %	± 3.02

3.5 CONCLUSION

The experiment is conducted on the selected pump and its performance values are calculated. Comparing the efficiency of the selected pump with standard values at the duty point, it is found that the efficiency level is 0.5% less than the standard value. So the efficiency level has to be improved. The uncertainty of flow rate, head, and power input and efficiency values are estimated. Flow physics of fluid inside the impeller and volute casing cannot be studied experimentally.

CHAPTER 4

DESIGN OF A CENTRIFUGAL PUMP IMPELLER

4.1 INTRODUCTION

The efficiency of the existing pump is less than the required efficiency level of the pump standard (IS 9079: 2002). The performance of a centrifugal pump is mainly depends on the impeller. For which, new impeller is designed and developed based on the turbo machinery theory (Srinivasan. 2008) for the duty point of the pump and its experimental performance are measured. This chapter details the design procedure for developing the centrifugal pump impeller and its performance results.

4.2 DESIGN PROCEDURE FOR CLOSED TYPE IMPELLER

A closed type impeller has two walls or shrouds on both side and the plain or curved blades are fixed. If the shroud of the impeller is normal to the pump axis then the pump is called radial flow pump. An impeller is mounted on a shaft and is enclosed by a pump casing. Pump casing supports the bearing and other parts of the pump. It has a provision to mount the inlet and outlet pipelines to handle fluid from sump or well to the required level.

4.2.1 Impeller Design Calculations

The pump impeller is designed and developed for the duty point flow rate (Q) = 0.015 m^3/s , head (H) = 32 m, speed of rotation (N) = 2900 rpm, and pump inlet and outlet pipe sizes are 0.075 m and 0.065 m respectively. The pump impeller has many numbers of deign parameters and

these parameters are calculated using turbo machinery equations (K.M.Srinivasan. 2008) and are presented in Table 4.1.

Table 4.1 Impeller design parameters

Impeller Design Parameters	Equations	Values	Unit
Specific Speed of the Pump, N_S	$\frac{3.65N\sqrt{Q}}{H^{\frac{3}{4}}}$	96.35	rpm
Nominal Diameter of the Impeller , D_n	$\sqrt[3]{\frac{91.125Q}{N}}$	77.82	mm
Hydraulic Efficiency, η_h	$1-\frac{0.42}{(\log D_n - 0.172)^2}$	85.79	%
Volumetric Efficiency, η_v	$\frac{1}{1+0.68N_s^{\frac{-2}{3}}}$	96.85	%
Taking Mechanical Efficiency, η_m =0.96,	-	96	%
Overall Efficiency, η_o	$\eta_h.\eta_v.\eta_m$	79.76	%
Pump Output Power, P_o	$\frac{\rho QH}{1000}$	4.71	kW
Pump Input Power, P_i	$\frac{\rho QH}{1000\eta_o}$	5.90	kW
Torque, T	$\frac{1.15P_i}{2\pi N}$	0.0224	KN-m
Working Stress, f_s	$\frac{Ultimate\ Stress, f_m}{FOS}$	17500	KN/m^2
Shaft Diameter, d_s	$\sqrt[3]{\frac{16T}{\pi f_s}}$	19	mm
Theoretical Flow rate, Q_t	$\frac{Q}{\eta_v}$	0.0155	m^3/s
Axial velocity of Impeller, C_o	$\frac{4Q_t}{\pi D_s^2}$	3.376	m/s
Velocity of flow at inlet, C_i	$0.06\sqrt[3]{Q_t N^2}$	3.041	m/s
Blade height at Inlet,B_1	$\frac{Q_t}{\pi D_1 C_i}$	18	mm
Meridional flow velocity,Cm_1 Taking K_1 = 1.4	$K_1 C_i$	4.26	m/s

Blade Velocity at Inlet, u_1	$\frac{\pi D_1 N}{60}$	13.67	m/s
Blade angle at Inlet,β_1	$\tan^{-1}\left(\frac{C_{m1}}{u_1}\right)$	18	o
Manometric Head, H_m	$\frac{H}{\eta_h}$	37.3	m
Blade Velocity at Inlet, u_2	$\sqrt{\frac{gH_m}{C_2}}$	27.05	m/s
Outer Diameter of the Impeller, D_2	$\frac{60u_2}{\pi N}$	178.1	mm
Blade angle at Outlet,β_2 Taking $\frac{K_2}{K_1}$ =0.86, $\frac{w_1}{w_2}$ = 1.2, $\frac{C_2}{C_m} = 0.80$	$\sin^{-1}\left[\sin\beta_1.\frac{K_2}{K_1}.\frac{w_1}{w_2}.\frac{C_2}{C_m}\right]$	15	o
Number of Blades, Z	$\frac{6.5(D_2+D_1)}{(D_2-D_1)}.\sin\left(\frac{\beta_1+\beta_2}{2}\right)$	6	-

4.3 3D MODELING OF PUMP IMPELLER

The various design parameters of a centrifugal pump for the duty point are presented in Table 4.1. It is believed that the backward curved blade design provides superior efficiency as compared with the forward curved design. Therefore, in this work, a backward curved design is adopted and the 3D model is developed using standard CAD package which is shown in Figure 4.1 to 4.3. Figure 4.1 shows the backward curved profile of the impeller blade. Figure 4.2 shows the wireframe model and Figure 4.3 shows the 3D CAD model of the designed impeller. This model is used for developing a numerical model for CFD analysis and also used for fabrication and experimental investigation of the pump. It is noteworthy to mention that the casing is not designed but the existing volute casing is used.

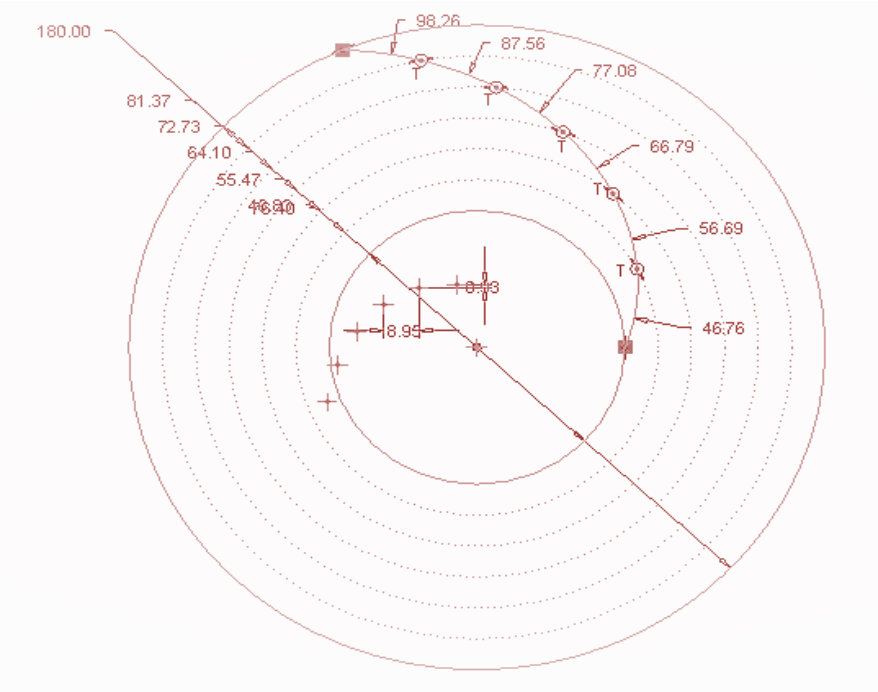

Figure 4.1 Backward curved profile of the impeller blade

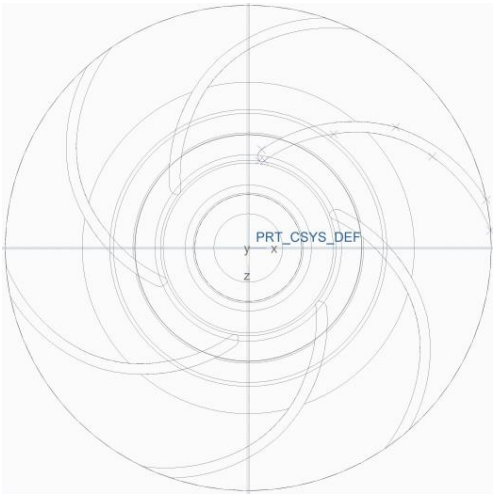

Figure 4.2 Wireframe model of the impeller

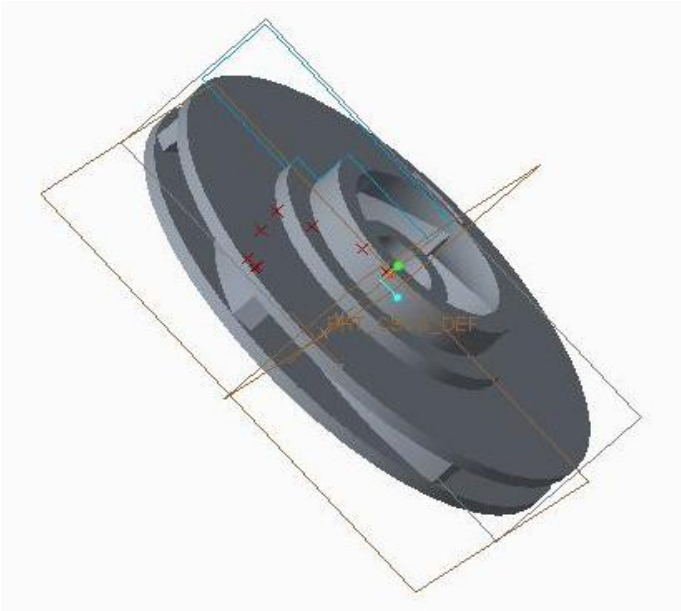

Figure 4.3 3D Model of the impeller

4.4 EXPERIMENTATION WITH PUMP

The pump impeller developed in this work is produced using FG 210 grade Cast Iron material recommended by the pump standard (IS 9079: 2002). The impeller is assembled with the same volute casing and its performance is tested through test setup discussed in section 3.3. The experimental performance of the designed impeller is presented in Table 4.2 and the corresponding performance curves are shown in Figure 4.4. From the performance curves, the performance values corresponding to the duty point is observed as head (H) = 34.8 m, power input (P) = 10.02 kW and efficiency (η) = 66.0 %.The efficiency of the pump is now improved that meets the standard (IS 9079: 2002) value.

Table 4.2 Experimental results of the designed impeller

$Q \times 10^{-3}$, m^3/s	Experimental Result		
	H, m	P, kW	η ,%
22.03	10.75	9.12	31.82
21.98	15.95	10.10	42.54
21.59	20.68	10.72	51.04
21.32	25.32	11.10	59.60
19.85	29.62	10.95	65.80
16.56	33.84	10.29	66.74
13.85	35.92	9.60	63.51
9.92	38.12	8.54	54.26
6.70	39.21	7.68	41.92
0.00	41.32	5.56	0.00

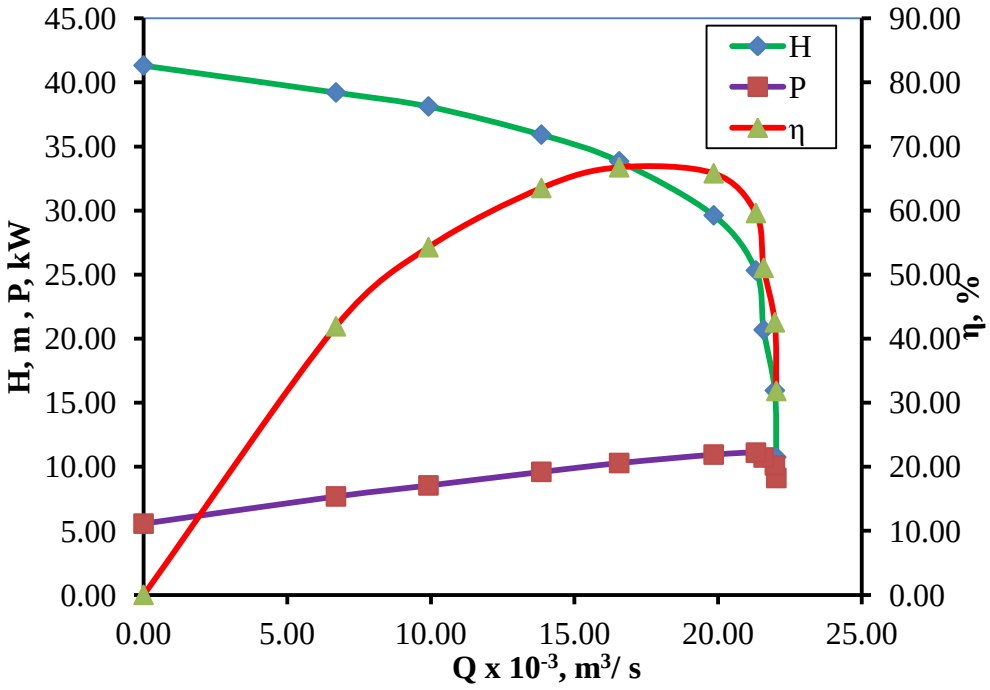

Figure 4.4 Experimental performance curves of the designed pump

4.5 CONCLUSION

In this chapter, a detailed discussion is made to develop a centrifugal pump impeller for the selected duty point condition. The impeller is modelled and fabricated and its performance test is conducted through the test setup. The pump efficiency of the designed impeller has improved, and satisfying the pump standard (IS 9079: 2002). Further improvement of the pump efficiency is necessary and possible by optimizing the impeller design parameters.

CHAPTER 5

NUMERICAL ANALYSIS IN CENTRIFUGAL PUMP

5.1 INTRODUCTION

It is very important step for understanding the flow field inside the simulation region. Flow inside the centrifugal pump is quite complex and three dimensional which involves flow separation, turbulence, cavitations and recirculation. Finding the performance through experiment for the existing pump model and new model consumes more time and cost. The best alternate way to overcome these difficulties is numerical simulation. There is a tremendous growth in the field of turbo machineries due to the evolution of numerical methods and computational fluid dynamics is one of them.

Computational Fluid Dynamics (CFD) is mainly used for solving complex flow field and also helps the researcher to visualize the flow field inside the impeller and volute. This helps the researcher to understand the flow phenomenon clearly. In this chapter the CFD analyses of an impeller developed in chapter 4 was discussed and validate the simulation through the experimental results.

5.2 MESHING OF COMPUTATIONAL DOMAIN

Discretization of the given geometrical domain into a number of cells or elements on which flow is considered is called as meshing. The domain discretization /mesh generation for the pump models were carried out using Ansys Workbench. Unstructured mesh was generated for the computational pump model. For achieving reliable results, mesh quality

parameters like skewness, smoothness and aspect ratio of the elements were considered and kept well within the range.

5.3 BOUNDARY CONDITIONS

To define the flow simulation fully, boundary condition has to be imposed to the computational model. We have to properly define where fluid enters and leave our computational domain. Also we have to define the impeller rotation. The relative motion between impeller and volute is specified as mesh interface and mesh motion was selected. Dirichlet type boundary conditions involving total pressure at inlet and mass flow rate at outlet have been imposed for all the simulations involved.

5.4 NUMERICAL STUDY OF THE IMPELLER

Numerical studies of the impeller with volute casing were performed by using ANSYS 15.0 code that solves the basic governing equations. The fluid domains of the baseline impeller with volute casing were modelled. Various turbulence models available on commercial CFD code were studied. The standard k-ε, k-ω and Shear Stress Transport (SST) turbulence model are used to simulate the fluid domain. Among these three models, the standard k-ε model offers a good relationship between numerical effort and computational accuracy when compared to the other two models. Hence the standard k-ε model was selected for further analysis. Unstructured grids with the tetrahedral element are generated for the computation domain of the impeller and volute casing and it is shown in Figure 5.1. The results of the numerical study were validated with work performed by (Cheah *et al*. 2011) Table 5.1 present the boundary conditions for numerical simulation.

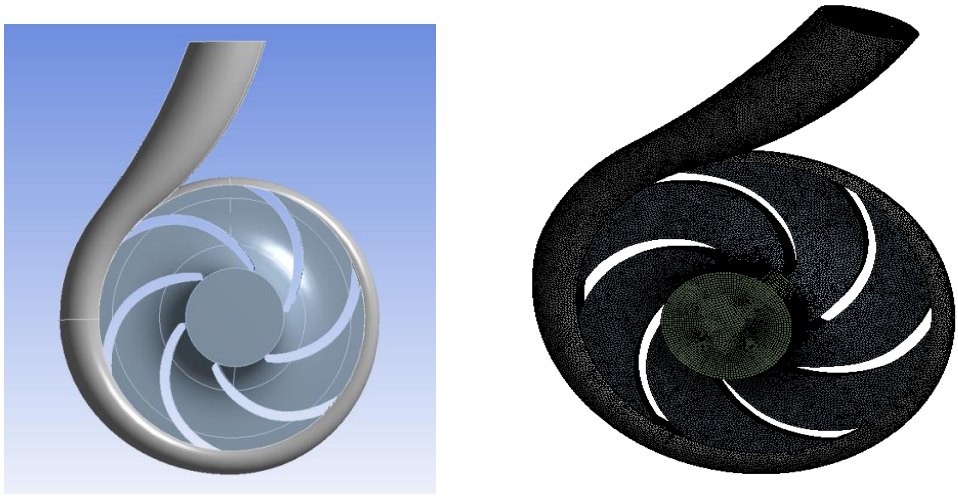

Figure 5.1 Computational domain of the impeller

Table 5.1 Boundary conditions for numerical simulation

Analysis type	Steady state incompressible
Fluid	Clear cold water
CFD Model	k –ε Turbulence model
Turbulence Intensity	5% (medium intensity)
Inlet	Total pressure(10^5 Pa)
Outlet	Mass flow rate
Rotational Speed	2900 rpm

5.4.1 Grid Dependency Test

The number of grids and selection of suitable turbulence model plays a vital role in having close matching with experimental data. An investigation is required before carrying out the rest of the simulations. Grids dependency test of the impeller and volute casing was performed for pump

total head at a different number of grids ranging from 0.151 to 5.67 million for the duty point discharge 0.015 m^3/s and are shown in Figure 5.2. From the figure, it was observed that the total head values are increases when the number of grids increase up to the grids values of 1.69 million and a further increase of the grids, there is no significant improvement on pump total head values. Hence the grid value of 1.69 million was used for the entire simulation work. The selected convergence criteria are the maximum residual of 10^{-4} and the mass imbalance of less than 10^{-2}. The performance values of the baseline impeller were confirmed by numerical analysis and it was compared with the experimental results.

Table 5.2 Grid information

Gird Size	No of Gird (x 10^5)	Total Head, m
3.5	1.51	18.81
3.0	2.21	24.57
2.5	3.81	27.12
2.0	7.25	28.41
1.5	16.95	33.11
1.0	56.70	33.13

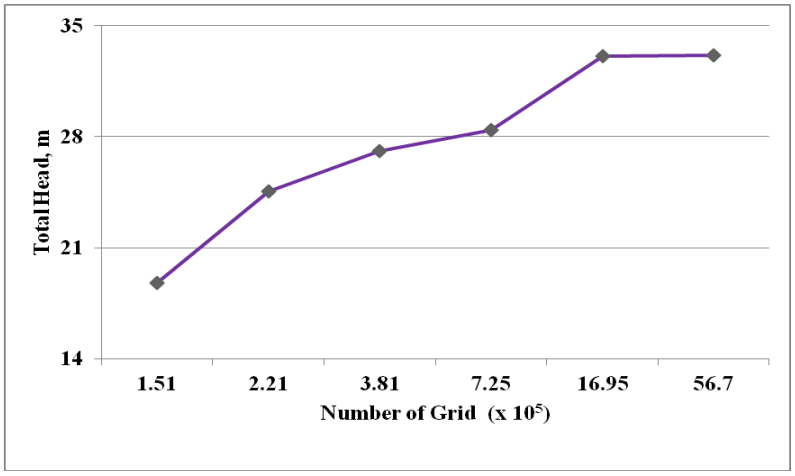

Figure 5.2 Grid dependency test

5.4.2 Numerical Simulation of the Impeller

The numerical analysis of the impeller developed in chapter 4 with volute casing was performed using k-ε, k-ω and SST turbulence models. Figure 5.3 shows the pressure (Pa) and velocity (m/s) distribution of baseline impeller with the volute casing.

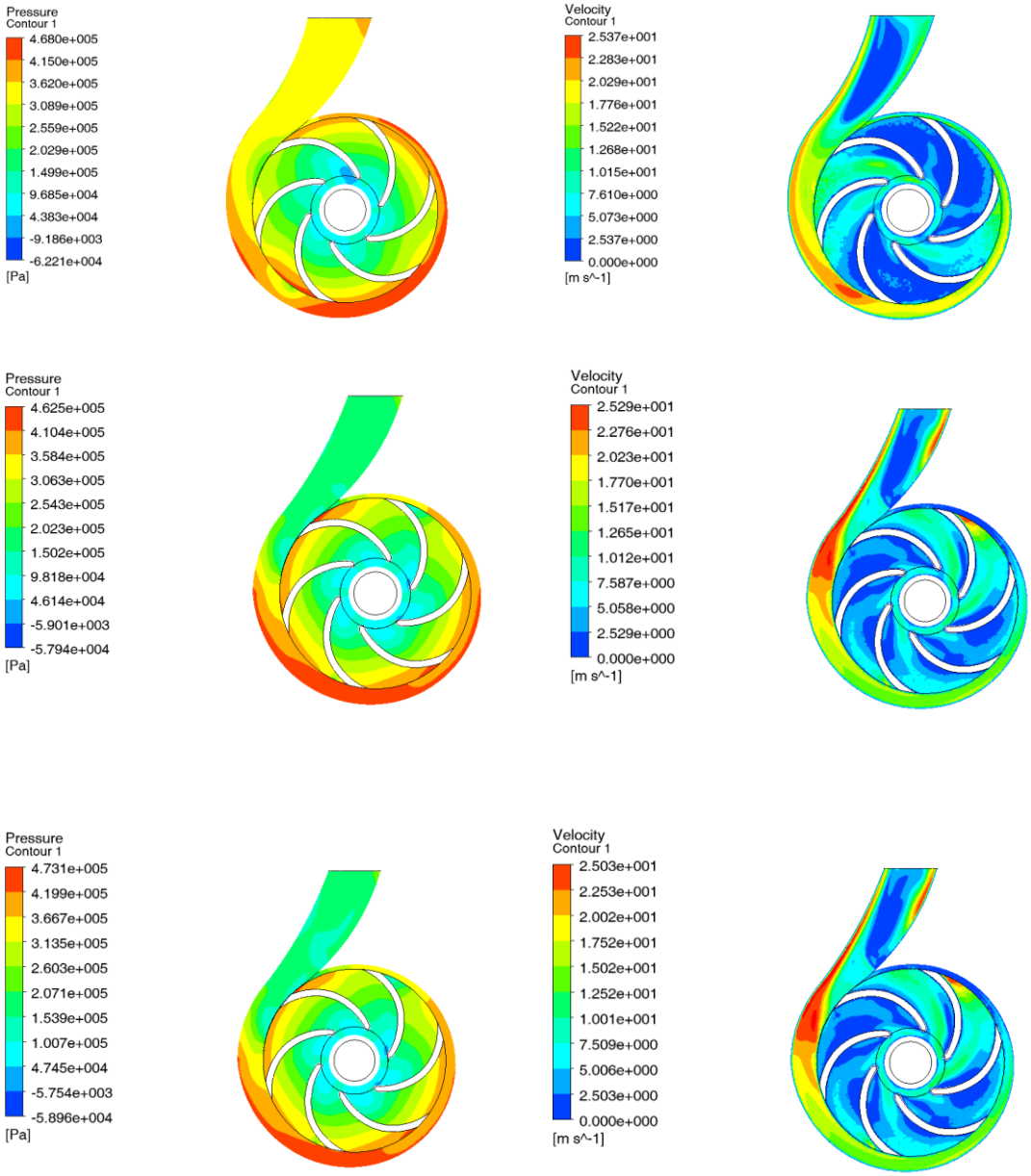

Figure 5.3 Pressure (Pa) and velocity (m/s) distribution of a k – ε, k – ω and SST models

5.4.3 COMPARATION OF EXPERIMENTAL AND NUMERICAL PERFORMANCE OF THE IMPELLER

The comparative study of experimental and numerical performance characteristics was done for the developed impeller and is shown in Figure 5.4. Numerical results are matching closely with experimental results. At the duty point, the numerical performance values are the head (H) = 35.8 m, pump efficiency (η) = 68.1% and power input (P) = 9.65 kW and the corresponding experimental performance values are 35.3 m, 66 % and 9.83 kW respectively. Table 5.3 presents the CFD simulation and experimental results of the developed impeller. The experimental results confirm the increase of power input and pump efficiency when the discharge and total head increase and satisfied the requirements of the pump standard IS 9079:2002. However, the performance characteristic of the developed impeller needs to improve for maximizing the efficiency as the requirements of BEE. Hence the dimensions of the developed impeller required to modify.

Table 5.3 Experimental and CFD results of the developed impeller

Q x 10^{-3}, m^3/s	Experimental Result			CFD Result			The deviation between Experimental and Numerical Results, %		
	H, m	P, kW	η ,%	H, m	P, kW	η, %	H	P	η
22.03	10.75	9.12	31.82	11.01	8.93	33.29	2.42	-2.10	4.62
21.98	15.95	10.10	42.54	16.25	9.86	44.38	1.88	-2.34	4.32
21.59	20.68	10.72	51.04	21.19	10.47	53.56	2.47	-2.35	4.93
21.32	25.32	11.10	59.60	25.95	10.84	62.55	2.49	-2.34	4.95
19.85	29.62	10.95	65.80	30.35	10.70	69.03	2.46	-2.32	4.90
16.56	33.84	10.29	66.74	34.65	10.05	69.98	2.39	-2.34	4.85
13.85	35.92	9.60	63.51	36.80	9.38	66.62	2.45	-2.34	4.91
9.92	38.12	8.54	54.26	39.02	8.34	56.88	2.36	-2.35	4.82
6.70	39.21	7.68	41.92	40.18	7.50	43.99	2.47	-2.34	4.93
0.00	41.32	5.56	0.00	-	-	-	-	-	-

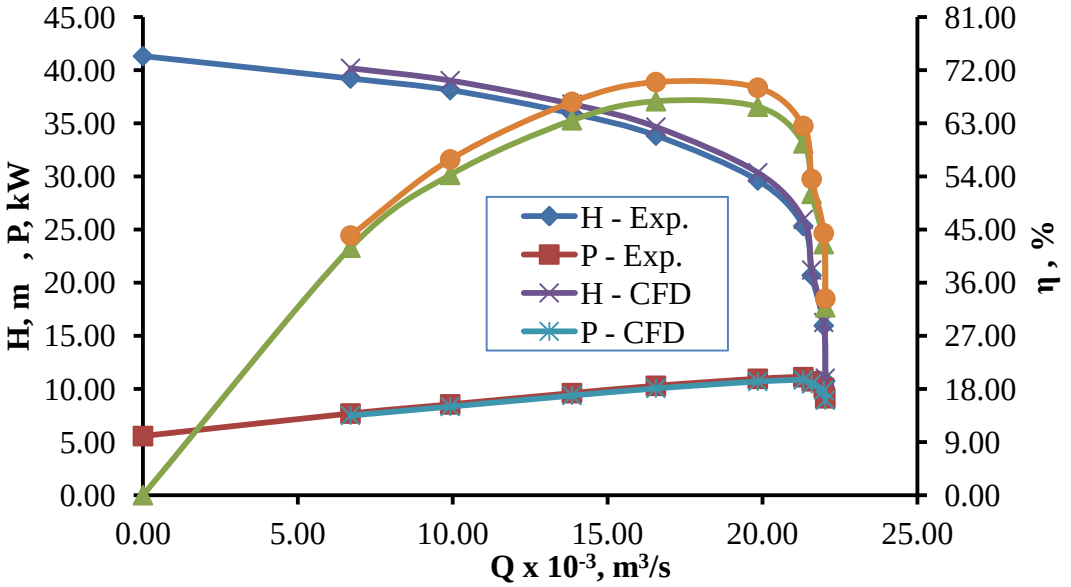

Figure 5.4 Experimental and CFD performance curves of the developed impeller

5.5 CONCLUSION

The numerical simulation of the developed impeller based on the turbo machinery theory was performed using ANSYS CFX 15.0 and the results are compared with the experimental results. The percentage of error found between the experimental and numerical results are 2 to 3% in head and power values and 4 to 5% in the efficiency values for the entire operating range of the pump.

CHAPTER 6

OPTIMIZATION OF IMPELLER DESIGN PARAMETERS

6.1 INTRODUCTION

In this chapter, the various steps involved in optimization of a centrifugal pump impeller design parameters are discussed. Selection of impeller design parameters for creating the design matrix for DOE, evaluating the numerical performance and develop mathematical model for the responses, statistical validation of the model and optimization of impeller design variable using response surface methodology (RSM) are described in detail. Finally, the performance analysis for optimum impeller geometry found from RSM optimizer is verified through experiments and CFD analysis.

6.2 OPTIMIZATION OF THE PUMP IMPELLER

In order to maximize the efficiency of the impeller, an optimization process is combined with response surface methodology and numerical analysis is performed. From the RSM, an optimum set of impeller parameter is found. Finally, an optimized impeller is fabricated for the optimum parameters and an experiment is conducted. The general optimization process is shown in the flowchart of Figure 6.1

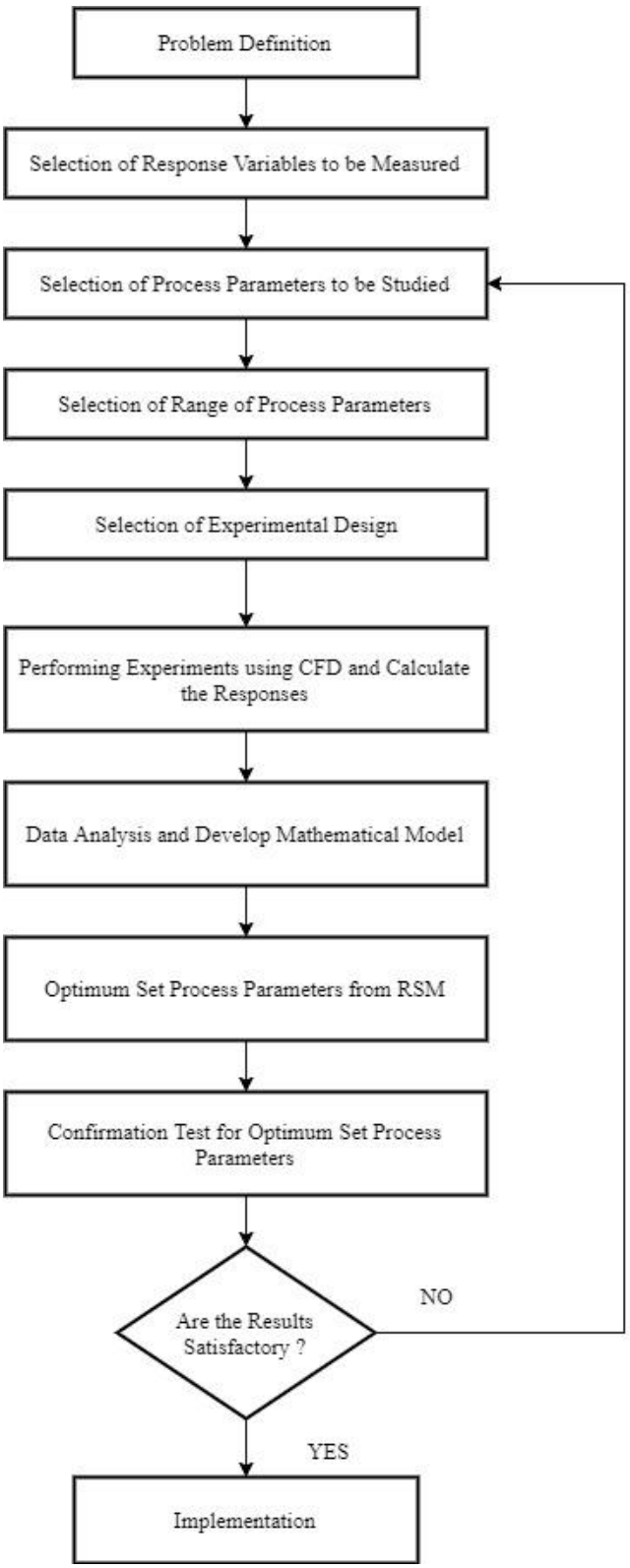

Figure 6.1 Optimization process flowchart

6.3 DEVELOPMENT OF MATHEMATICAL MODEL USING DOE

Design of Experiments (DOE) technique is used to develop a second order regression model for assessing the pump performance characteristics. Since the pump has a considerable amount of randomness due to ambient temperature and pressure, density and viscosity of fluid and voltage and frequency of the input supply to the prime mover (three phase AC induction motor is used as a prime mover), rotational speed, Central Composite Rotatable Design (CCD) are also adopted in this work (Yang & Xiao, 2014). This work is limited to five factors and five levels to reduce the computational complexity. The DOE involves following five key steps to developing and statistical testing of the mathematical model.

6.3.1 Selection of Impeller Design Parameters

Based on the influence on performance characteristics, five design parameters are selected: 1) Outer diameter of the impeller (X_1), 2) Inlet blade angle (X_2) 3) Outlet blade angle (X_3) 4) Number of blades (X_4) and 5) Blade thickness (X_5). Each parameter will be tested for the output parameters such as the total head (H), input power (P) and pump efficiency (η).

6.3.1.1 Working ranges of impeller design parameters and coding

The working ranges of impeller parameters are defined based on the data used by the pump manufacturer and pump designer (Srinivasan, 2008). The maximum and minimum levels are coded as +2 and –2 respectively and the intermediate levels were calculated using the Equation (6.1). Table 6.1 presents the details of impeller geometry parameters, their levels, and coding.

$$X_i = \frac{2[2X - [X_{max} + X_{min}]]}{[X_{max} - X_{min}]} \quad (6.1)$$

Where, X_i is the coded value of impeller design parameter (X) between X_{max} and X_{min}.

Table 6.1 Impeller design parameters and their levels and coding

Impeller Design Parameters	Units	Symbols	Levels				
			(-2)	(-1)	(0)	(+1)	(+2)
Outer Diameter	mm	X_1	176	178	180	182	184
Inlet Blade Angle	^{o}	X_2	18	20	22	24	26
Outlet Blade Angle	^{o}	X_3	22	24	26	28	30
No of Blades	-	X_4	4	5	6	7	8
Blade Thickness	mm	X_5	2	3	4	5	6

6.3.2 Development of Design Matrix and Data Collection

The design matrix used for conducting experiments is formulated by using five factors with five levels of central composite rotatable design. It consists of 16(2^4) factorial combinations, ten-star points and six centre points (Senthilkumar & Kannan 2015). Table 6.2 represents the impeller design parameter combinations for each experiment in coded form and its actual values for numerical simulation. The CFD analyses for all 32 combinations are performed in a similar procedure discussed earlier in chapter 4. Table 6.3 presents the numerical results of the responses head, power and efficiency.

Table 6.2 Design matrix with coded and its actual values

Exp. No.	Impeller Design Parameters									
	Outer Diameter(X_1)		Inlet Blade Angle(X_2)		Outlet Blade Angle(X_3)		No of Blades(X_4)		Blade Thickness(X_5)	
Units	Coded	Actual, mm	Coded	Actual, ^{o}	Coded	Actual, ^{o}	Coded	Actual	Coded	Actual, mm
1	1	182	1	24	-1	24	1	7	-1	3
2	-1	178	1	24	1	28	1	7	-1	3
3	-1	178	-1	20	1	28	1	7	1	5
4	0	180	0	22	0	26	0	6	0	4
5	-2	176	0	22	0	26	0	6	0	4
6	0	180	0	22	0	26	-2	4	0	4
7	1	182	-1	20	1	28	-1	5	1	5
8	0	180	0	22	0	26	0	6	2	6
9	-1	178	-1	20	-1	24	1	7	-1	3
10	1	182	1	24	1	28	1	7	1	5
11	0	180	-2	18	0	26	0	6	0	4
12	2	184	0	22	0	26	0	6	0	4
13	-1	178	-1	20	1	28	-1	5	-1	3
14	1	182	-1	20	-1	24	-1	5	-1	3
15	0	180	0	22	0	26	0	6	0	4
16	0	180	0	22	0	26	0	6	0	4
17	1	182	-1	20	-1	24	1	7	1	5
18	0	180	0	22	0	26	2	8	0	4
19	0	180	0	22	2	30	0	6	0	4
20	0	180	0	22	0	26	0	6	0	4
21	0	180	0	22	0	26	0	6	-2	2
22	-1	178	1	24	-1	24	1	7	1	5
23	1	182	-1	20	1	28	1	7	-1	3
24	0	180	0	22	-2	22	0	6	0	4
25	0	180	0	22	0	26	0	6	0	4
26	0	180	2	26	0	26	0	6	0	4
27	-1	178	-1	20	-1	24	-1	5	1	5
28	1	182	1	24	1	28	-1	5	-1	3
29	-1	178	1	24	1	28	-1	5	1	5
30	-1	178	1	24	-1	24	-1	5	-1	3
31	1	182	1	24	-1	24	-1	5	1	5
32	0	180	0	22	0	26	0	6	0	4

Table 6.3 Numerical results of responses head, power and efficiency

Experiment No.	Head, H	Power Input, P	Pump Efficiency, η
Units	m	kW	%
1	34.53	9.95	63.79
2	32.40	9.48	62.83
3	32.90	9.19	65.81
4	31.70	9.14	64.18
5	30.78	9.09	62.25
6	31.62	8.78	66.20
7	33.27	9.49	64.44
8	31.65	8.92	65.22
9	31.83	9.34	62.65
10	32.79	9.48	63.58
11	32.39	9.39	63.41
12	34.20	9.98	61.15
13	31.18	8.92	64.26
14	33.23	9.95	60.84
15	31.70	9.14	64.18
16	31.70	9.14	64.18
17	34.18	9.43	66.63
18	33.73	9.03	68.66
19	31.89	9.02	64.99
20	31.70	9.14	64.18
21	32.21	9.38	63.12
22	31.11	8.34	68.57
23	32.68	9.26	64.87
24	31.56	9.15	63.40
25	31.70	9.14	64.18
26	31.37	9.12	63.79
27	30.94	8.99	63.26
28	32.93	9.18	65.94
29	30.68	8.69	64.90
30	30.53	8.71	64.43
31	31.19	9.45	60.67
32	31.70	9.14	64.18

6.3.3 Development of a Mathematical Model

The second order mathematical model for the output responses head, power input and efficiency are developed.

The relationships between the impeller design parameters in coded form and output responses of DOE is given in Equation (6.2)

$$Y = f\left(X_1, X_2, X_3, X_4, X_5\right) \tag{6.2}$$

Where,

Y – Response variable

X_1 - Outer diameter (coded)

X_2 - Inlet blade angle (coded)

X_3 - Outlet blade angle (coded)

X_4 - No of blades (coded)

X_5 - Blade thickness (coded)

The statistical software Minitab® 16 is used to calculate the coefficients of linear, quadratic and interactive terms.

The second order mathematical equations from response surface methodology are present in Equation (6.3)

$$Y = \beta_0 + \sum_{i=1}^{5} \beta_i X_i + \sum_{i=1}^{5} \beta_{ii} X_i^2 + \sum_{\substack{i=1 \\ i<j}}^{5} \beta_{ij} X_i X_j \tag{6.3}$$

Where, Y is the response parameter, X_i is the independent variables, β_i, and $\beta_{i,j}$ refers to the regression coefficients.

The Equation (6.3) is expanded with all the coefficient of the developed model (Montgomery, 1997) and is given in Equation (6.4).

$$Y = \beta_0 + \beta_1 X_1 + \beta_2 X_2 + \beta_3 X_3 + \beta_4 X_4 + \beta_5 X_5 + \beta_{11} X_1^2 + \beta_{22} X_2^2 + \beta_{33} X_3^2 + \beta_{44} X_4^2 + \beta_{55} X_5^2 + \beta_{12} X_1 X_2 + \beta_{13} X_1 X_3 + \beta_{14} X_1 X_4 + \beta_{15} X_1 X_5 + \beta_{23} X_2 X_3 + \beta_{24} X_2 X_4 + \beta_{25} X_2 X_5 + \beta_{34} X_3 X_4 + \beta_{35} X_3 X_5 + \beta_{45} X_4 X_5 \quad (6.4)$$

The full model equation for the responses head, power input and efficiency is given in the Equations (6.5), (6.6) and (6.7) respectively.

$$H = 31.6926 + 0.8363 X_1 - 0.2538 X_2 + 0.0813 X_3 + 0.5287 X_4 - 0.1404 X_5 + 0.2024 X_1^2 + 0.0499 X_2^2 + 0.0111 X_3^2 + 0.2486 X_4^2 + 0.0624 X_5^2 + 0.0131 X_1 X_2 - 0.2631 X_1 X_3 - 0.0844 X_1 X_4 - 0.01019 X_1 X_5 + 0.0994 X_2 X_3 + 0.1581 X_2 X_4 - 0.4369 X_2 X_5 - 0.1906 X_3 X_4 + 0.1969 X_3 X_5 + 0.0831 X_4 X_5 \quad (6.5)$$

$$P = 9.13216 + 0.26292 X_1 - 0.07625 X_2 - 0.03042 X_3 + 0.06625 X_4 - 0.11042 X_5 + 0.10659 X_1^2 + 0.03659 X_2^2 - 0.00591 X_3^2 - 0.05091 X_4^2 + 0.01034 X_5^2 + 0.07187 X_1 X_2 - 0.14187 X_1 X_3 - 0.06187 X_1 X_4 + 0.04688 X_1 X_5 + 0.07687 X_2 X_3 + 0.08438 X_2 X_4 - 0.06188 X_2 X_5 + 0.07313 X_3 X_4 + 0.10938 X_3 X_5 - 0.09062 X_4 X_5 \quad (6.6)$$

$$\eta = 64.1822 - 0.3396 X_1 + 0.1129 X_2 + 0.3738 X_3 + 0.6212 X_4 + 0.5187 X_5 - 0.6222 X_1^2 - 0.1472 X_2^2 + 0.0016 X_3^2 + 0.8103 X_4^2 - 0.0047 X_5^2 - 0.4719 X_1 X_2 + 0.5006 X_1 X_3 + 0.2481 X_1 X_4 - 0.5306 X_1 X_5 - 0.3881 X_2 X_3 - 0.2706 X_2 X_4 - 0.4244 X_2 X_5 - 0.9306 X_3 X_4 - 0.4119 X_3 X_5 + 0.7906 X_4 X_5 \quad (6.7)$$

The reduced model is derived from the full model of all the responses using backward elimination method which removes the insignificant factors less than 5%. Then the models with significant influence of the output responses head, power and efficiency are presented in Equations (6.8), (6.9) and (6.10).

$$H = 31.6926 + 0.8363X_1 - 0.2538X_2 + 0.0813X_3 + 0.5287X_4 - 0.1404X_5 + 0.2024X_1^2 + 0.0499X_2^2 + 0.2486X_4^2 + 0.0624X_5^2 - 0.2631X_1X_3 - 0.0844X_1X_4 - 0.01019X_1X_5 + 0.0994X_2X_3 + 0.1581X_2X_4 - 0.4369X_2X_5 - 0.1906X_3X_4 + 0.1969X_3X_5 + 0.0831X_4X_5$$

(6.8)

$$P = 9.13216 + 0.26292X_1 - 0.07625X_2 - 0.03042X_3 + 0.06625X_4 - 0.11042X_5 + 0.10659X_1^2 + 0.03659X_2^2 - 0.05091X_4^2 + 0.07187X_1X_2 - 0.14187X_1X_3 - 0.06187X_1X_4 + 0.04688X_1X_5 + 0.07687X_2X_3 + 0.08438X_2X_4 - 0.06188X_2X_5 + 0.07313X_3X_4 + 0.10938X_3X_5 - 0.09062X_4X_5$$

(6.9)

$$\eta = 64.1822 - 0.3396X_1 + 0.1129X_2 + 0.3738X_3 + 0.6212X_4 + 0.5187X_5 - 0.6222X_1^2 - 0.1472X_2^2 + 0.8103X_4^2 - 0.4719X_1X_2 + 0.5006X_1X_3 + 0.2481X_1X_4 - 0.5306X_1X_5 - 0.3881X_2X_3 - 0.2706X_2X_4 - 0.4244X_2X_5 - 0.9306X_3X_4 - 0.4119X_3X_5 + 0.7906X_4X_5$$

(6.10)

The scatter diagram is constructed between the actual values and predicted values of head, power input and efficiency which are presented in the Figure 6.2, 6.3 and 6.4. The prediction capability of the model developed is evaluated using the R^2-value. The R^2 -value of predicted and actual value for the head, power and efficiency is 0.9912, 0.9891 and 0.9885 respectively. If the value is more than 0.9, then the model has good prediction capability (Wang *et al*, 2016).

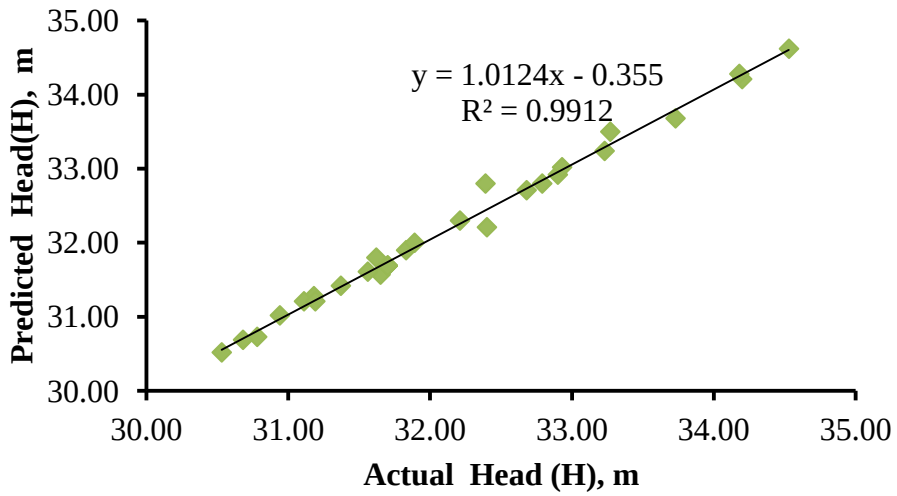

Figure 6.2 Scatter plot for the actual and predicted values of head

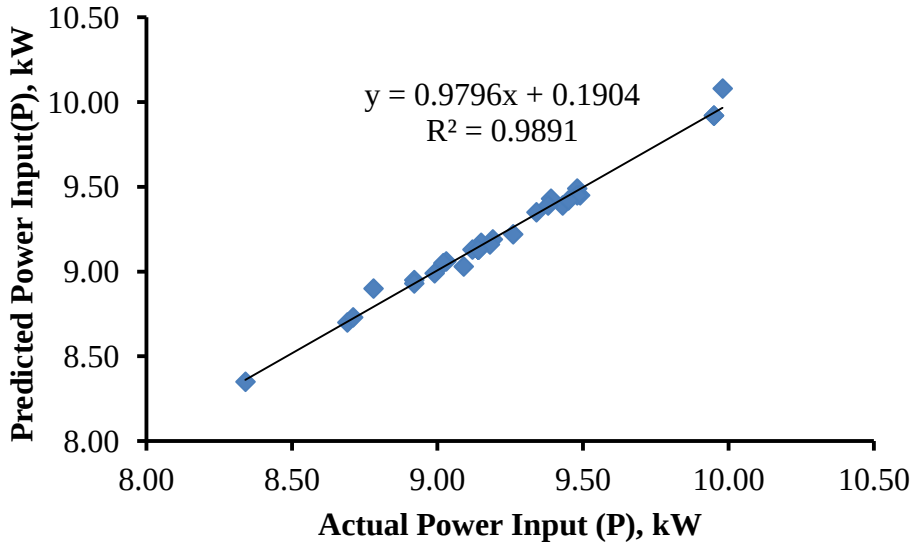

Figure 6.3 Scatter plot for the actual and predicted values of power input

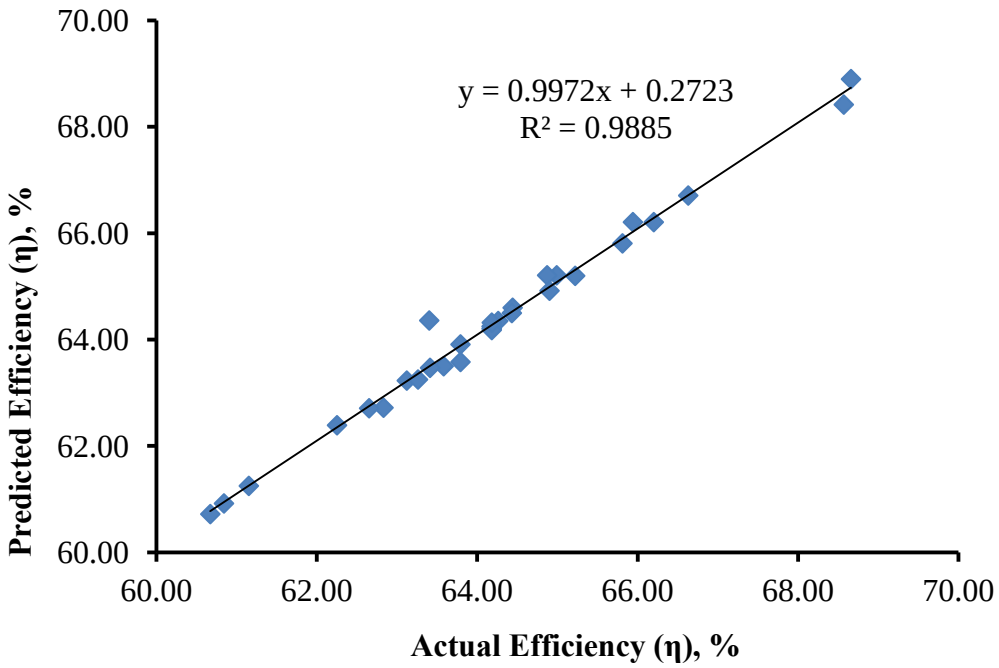

Figure 6.4 Scatter plot for the actual and predicted values of efficiency

6.3.4 Statistical Validation of the Developed Mathematical Models

The results of DOE are validated through two criterion:1) using R^2- value of the full and reduced models and 2) applying model adequacy test using the F-ratio and R-ratio. Table 6.4 presents the comparisons of R^2 -value and Adj.R^2-values of full and reduced models for all the responses. The R^2-values of full model and adj.R^2-values of the reduced model have more than 95% confidence level and are adequate (Palani & Murugan, 2006). Adequacy of the model is also confirmed based on F-ratio and R-ratio. The calculated F-ratio of the responses is less than the critical value of 95% confidence level and the calculated R-ratio of the responses is over the critical value of 95% confidence level and hence the models are adequate (Senthilkumar and Kannan, 2015). Details of the model adequacy test are presented in Table 6.5.

Table 6.4 R^2 and Adj.R^2 values of full and reduced models

Responses	R^2 - value		Adj. R^2 -value	
	Full model	Reduced model	Full model	Reduced model
Head(H), m	0.9998	0.9759	0.9995	0.9689
Power Input(P), kW	0.9925	0.9784	0.9790	0.9541
Efficiency (η), %	0.9994	0.9712	0.9983	0.9672

Table 6.5 Model adequacy test

Responses	First order terms		Second order terms		Lack of fit		Error term		F – ratio*	R – ratio**	Adequacy of the model
	SS	DF	SS	DF	SS	DF	SS	DF			
Head, H	25.67	5	2.83	15	0.01	6	0.01	5	0.83	71.25	Adequate
Power Input, P	2.21	5	0.47	15	0.03	6	0.03	5	0.83	22.33	Adequate
Efficiency, η	22.14	5	34.09	15	0.06	6	0.06	5	0.83	23.42	Adequate

Notes:

SS – Sum of Squares, DF – Degree of Freedom, F-ratio = MS of lack of fit / MS of the error term.

R-ratio = (MS of first-order +MS of second order term) / MS of error terms.

*Critical value of F-ratio F (6, 5, 0.05) = 4.95, **Critical value of R-ratio (20, 5, 0.05) = 4.56

6.3.5 Analysis of Experimental Results

Table 6.6 presents the estimated regression coefficients and p-values for response parameters. The linear effects, squared effects and interaction effects between parameters of p-values less than 0.05($\alpha = 0.05$) are significant contribution to the model. If p-values are more than 0.05, then impeller parameters have no significant contribution to the model.

Table 6.6 Estimated regression coefficients and p-values of responses

Variables Terms	Head (H)		Power Input (P)		Efficiency (η)	
	coefficients	p – values	coefficients	p – values	coefficients	p – values
constant	31.692	0.000	9.1321	0.000	64.182	0.000
X_1	0.8363	0.000	0.2629	0.000	-0.3396	0.000
X_2	-0.2538	0.000	-0.0762	0.000	0.1129	0.000
X_3	0.0813	0.000	-0.0304	0.015	0.3738	0.000
X_4	0.5287	0.000	0.0662	0.000	0.6212	0.000
X_5	-0.1404	0.000	-0.1104	0.000	0.5187	0.000
X_1*X_1	0.2024	0.000	0.1065	0.000	-0.6222	0.000
X_2*X_2	0.0499	0.000	0.0365	0.003	-0.1472	0.000
X_3*X_3	0.0111	0.033	-0.0059	0.547	0.0016	0.911
X_4*X_4	0.2486	0.000	-0.0509	0.000	0.8103	0.000
X_5*X_5	0.0624	0.000	0.0103	0.300	-0.0047	0.744
X_1*X_2	0.0131	0.058	0.0718	0.000	-0.4719	0.000
X_1*X_3	-0.2631	0.000	-0.1418	0.000	0.5006	0.000
X_1*X_4	-0.0844	0.000	-0.06187	0.001	0.2481	0.000
X_1*X_5	-0.1019	0.000	0.04688	0.004	-0.5306	0.000
X_2*X_3	0.0997	0.000	0.07687	0.000	-0.3881	0.000
X_2*X_4	0.1581	0.000	0.08438	0.000	-0.2706	0.000
X_2*X_5	-0.4369	0.000	-0.06188	0.001	-0.4244	0.000
X_3*X_4	-0.1906	0.000	0.07313	0.000	-0.9306	0.000
X_3*X_5	0.1969	0.000	0.10938	0.000	-0.4119	0.000
X_4*X_5	0.0831	0.000	-0.09062	0.000	0.7906	0.000

6.4 OPTIMIZATION OF IMPELLER DESIGN PARAMETERS

The objective of the pump impeller design is to maximize the total head and pump efficiency and to minimize power consumption. These responses are interrelated to each other and the best combinations of geometrical values are determined using the response surface methodology. Response surface methodology is used to identify the input parameters combinations to optimize the response variables. Total head and pump efficiency limits are selected between 30.53 m to 34.53 m and 60.67% to 68.66%, whereas power input limits are selected between 8.34 kW to 9.98 kW for setting optimum point. The optimum setting of impeller parameters for the responses is shown in Figure 6.5. From the RSM analysis, the optimum set parameters of the impeller are outer diameter (X_1) = 180 mm, inlet blade angle (X_2) = 18^o, outlet blade angle (X_3) = 22^o, number of blades (X_4) = 8 and blade thickness (X_5) = 6 mm, and the corresponding performance values are total head (H) = 36.12 m, input power (P) = 8.34 kW and pump efficiency (η) = 77.89%.

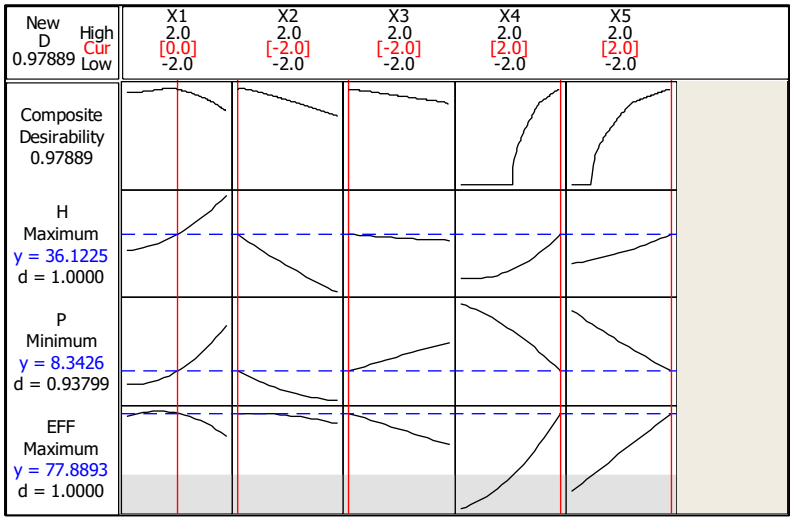

Figure 6.5 RSM optimizer plot

6.4.1 Experimental Study of the Optimum Impeller

The impeller for the optimized parameters from RSM optimizer is fabricated. Performance test on the impeller is conducted as per ISO 9906: 2012 standard. The experimental performance characteristic curves are shown in Figure 6.8. The pump performance values are presented in Table 6.7. From the performance curves, the actual pump total head (H) = 36.8 m, input power (P) = 9.81 kW and pump efficiency (η) = 70.5 % are obtained corresponding to the guaranteed duty point.

Table 6.7 Experimental results of the optimized impeller

Q x 10^{-3}, m^3/s	H, m	P, kW	η, %
22.10	9.75	9.52	27.74
21.95	12.42	9.58	34.87
21.82	21.34	10.05	56.78
21.75	26.40	11.65	60.40
20.45	30.56	11.32	67.66
17.25	35.62	10.40	72.40
15.25	36.83	9.81	70.16
11.25	38.25	9.01	59.58
5.40	39.85	6.56	40.20
0.00	41.65	4.69	0.00

6.4.2 Comparison of the Experimental and Numerical Performance of the Optimized Impeller

Optimization of centrifugal pump impeller is done using various design parameters. Number of blades in centrifugal pump impeller is an

important parameter in pump design. From the output of the optimization, the optimized impeller with higher number of blades shows increased in head and efficiency than the existing base model. The Figure 6.6 and Figure 6.7 show the comparative numerical study results of the base model and the optimized model. The pressure contour comparison figure shows that pressure increase with increase in number of blades which in turn increase the head.

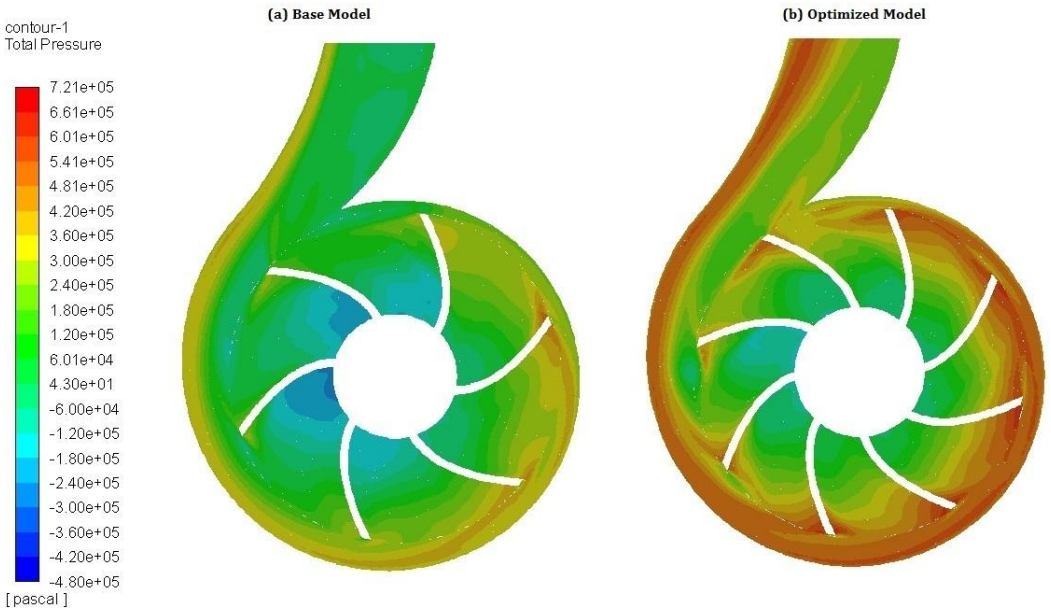

Figure 6.6 Total pressure contour comparisons

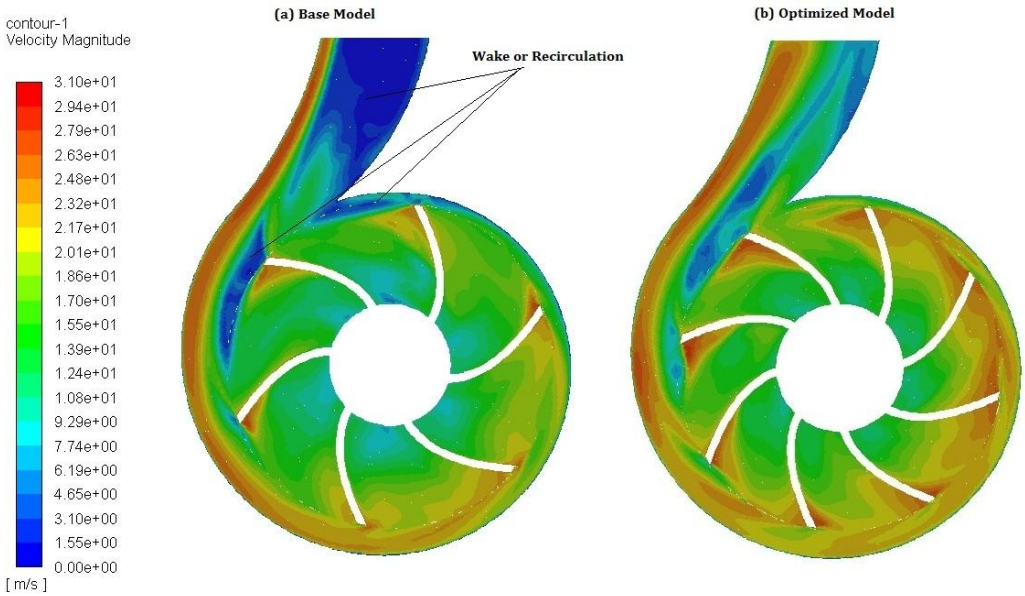

Figure 6.7 Velocity contour comparisons

Table 6.8 Numerical results of the optimized impeller

$Q \times 10^{-3}$, m^3/s	H, m	P, kW	η, %
22.10	10.05	9.20	29.59
22.00	12.92	9.25	37.66
21.80	22.00	9.85	59.67
21.70	26.91	11.38	62.88
20.40	31.25	11.02	70.89
17.10	36.23	9.98	75.54
15.10	38.10	9.82	71.58
11.20	39.50	8.85	61.74
5.40	40.94	6.20	42.66

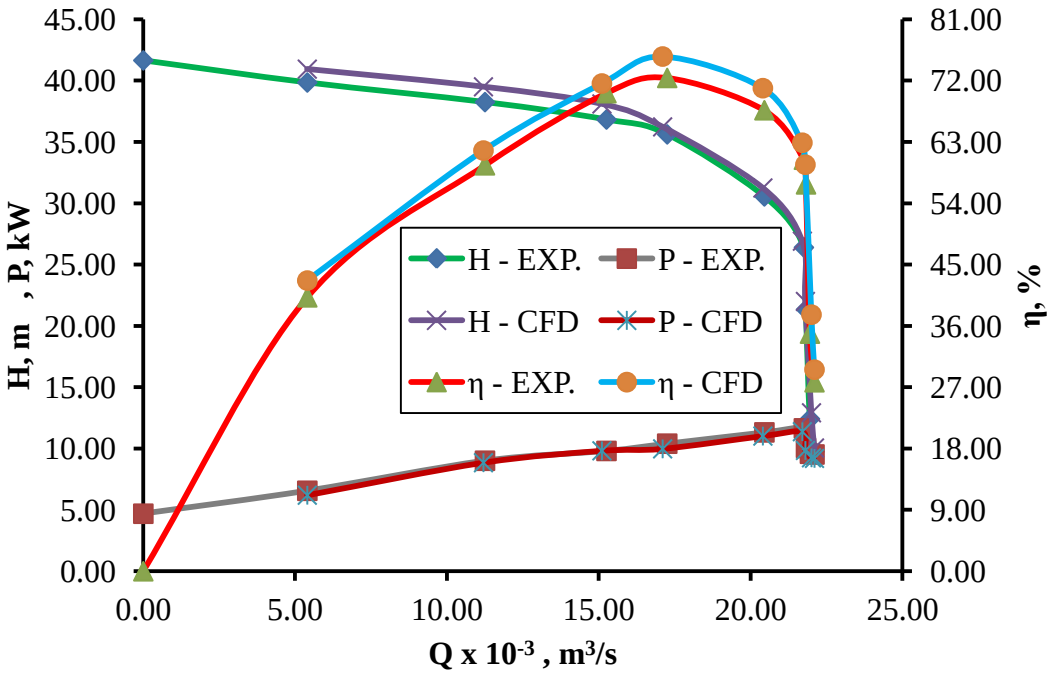

Figure 6.8 Experimental and numerical performance curves of the optimized impeller

The optimized model shows uniform pressure distribution within the impeller blades. The velocity contour comparison figure shows the velocity field inside the pump. The numerical studies clearly shows that lot of wake forms at exit of the volute in the base model compared with the optimized model. Because of the presence of wake, the performance of the pump is reduced. The optimized model with eight impeller blades shows less recirculation and wake in the volute exit.

6.5 CONCLUSION

Optimization of the impeller design parameters is performed using the DOE. The response surface methodology is used to develop the second order mathematical models for the responses and the models are validated statistically. The optimum impeller parameters are found from the RSM optimizer. The efficiency of the optimized impeller has improved by 4.5%

CHAPTER 7

RESULT AND DISCUSSION

7.1 STUDY THE DIRECT EFFECT OF IMPELLER DESIGN PARAMETERS ON THE RESPONSES

Statistically validated mathematical model discussed in earlier chapter 6 are used to study the direct effects of individual impeller design parameter on the responses. This study is performed by changing a design parameter at a time on the response functions, plotting the trend curves and observing the changes on the relevant trend curves.

7.1.1 Direct Effects of Impeller Outer Diameter on the Responses

Figure 7.1 shows the direct effects of impeller outer diameter on the head, power and efficiency. The responses head and power have positive relationships with the outer diameter. When the outer diameter increases, the head and power input values also increase. Also the response efficiency has a positive relationship between -2 to 0 and negative relationship between 0 to +2. The outer diameter has an important parameter and has more influence on the responses head, power and efficiency.

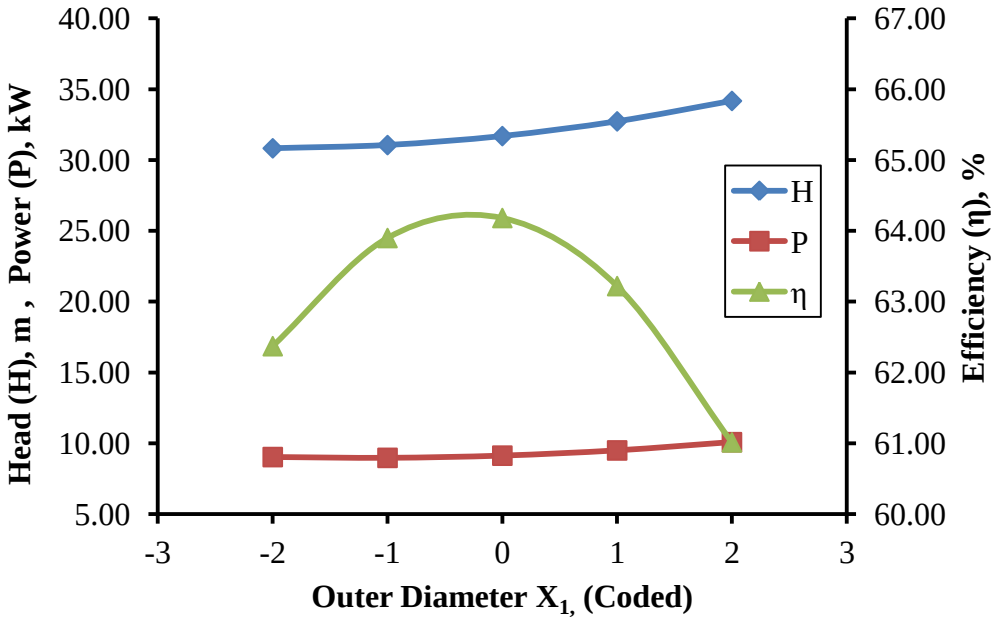

Figure 7.1 Direct effects of outer diameter on head, power and efficiency

7.1.2 Direct Effects of Inlet Blade Angle on the Responses

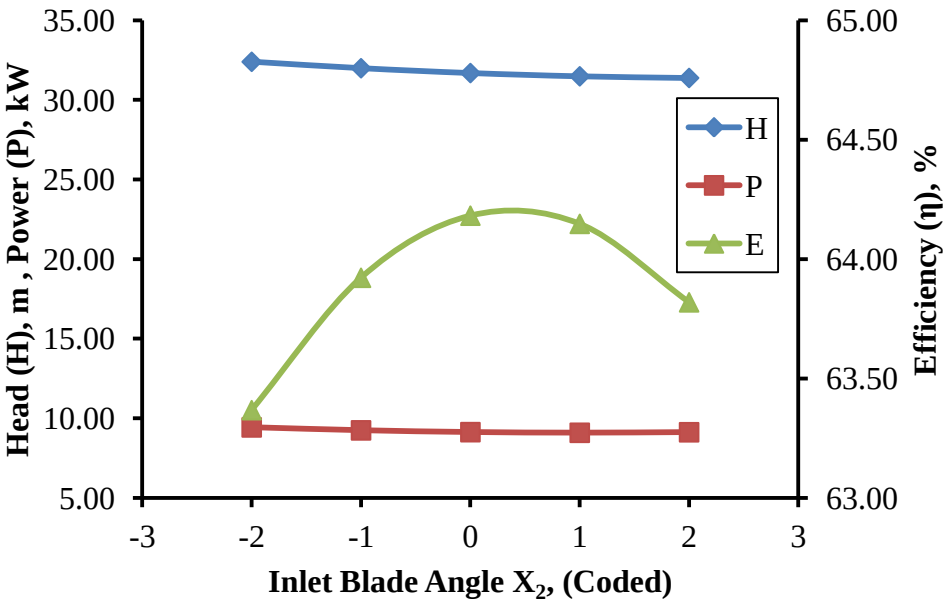

Figure 7.2 Direct effects of inlet blade angle on head, power and efficiency

Figure 7.2 presents the direct effects of the inlet blade angle on the response functions. The responses head and power have a negative relationship when the inlet blade angle increases from -2 to +2. The inlet blade angle has a positive relationship on the response efficiency between the ranges from -2 to 0 and has the opposing relationship between 0 to +2.

7.1.3 Direct Effects of Outlet Blade Angle on the Responses

Figure 7.3 shows the direct effect of outlet blade angle on the response functions head, power and efficiency. The total head and efficiency of the pump have increased with increase in impeller outlet angle. The outlet blade angle has a positive relationship with the head and efficiency characteristics in the range from -2 to +2 and has a negative relationship on power input between the range from -2 to +2. It means, the power input is decrease when the outlet blade angle is increase.

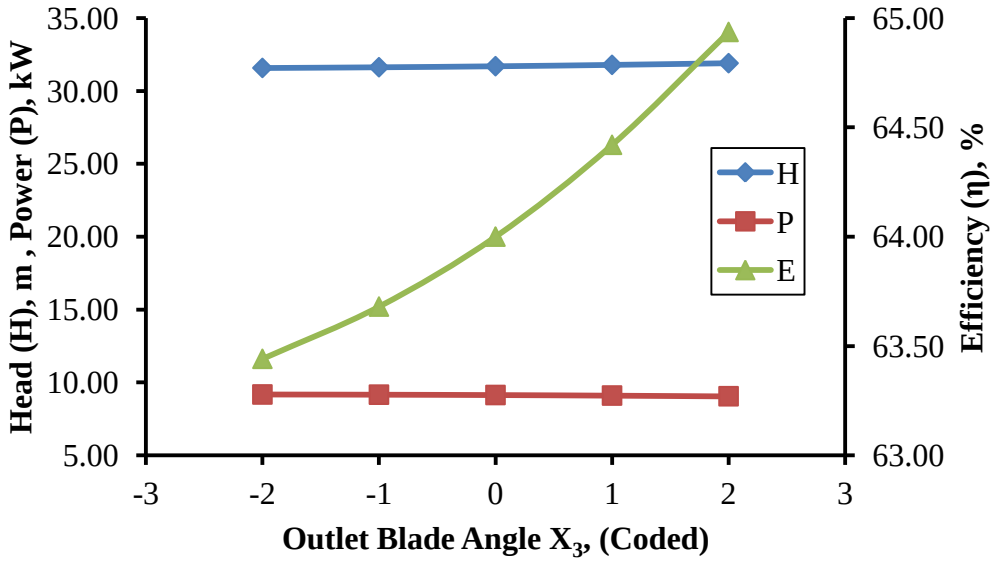

Figure 7.3 Direct effects of outlet blade angle on head, power and efficiency

7.1.4 Direct Effects of Number of Blades on the Responses

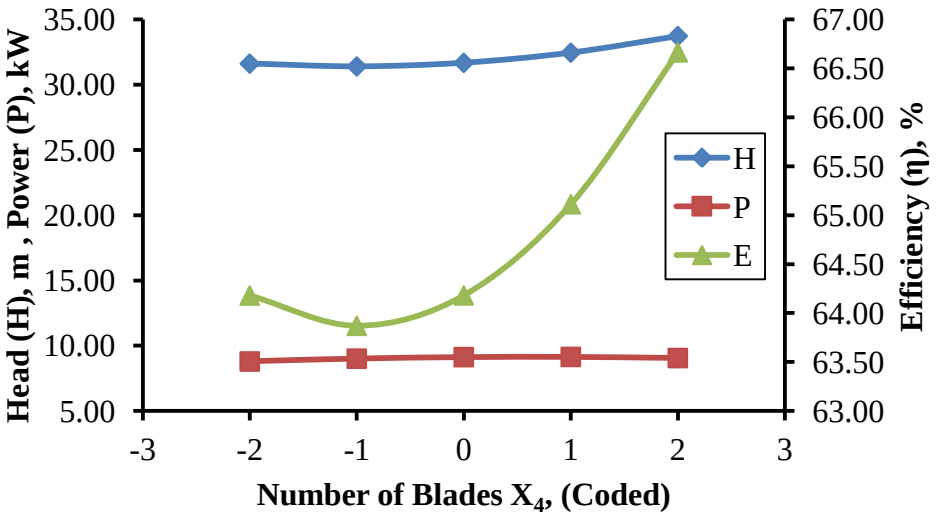

Figure 7.4 Direct effects of a number of blades on head, power and efficiency

Figure 7.4 presents the direct effects of number of blades on the performance characteristics head, power and efficiency. The pump performances head and efficiency values decrease with increase in number of blades in the range from -2 to -1 and increase continuously with increase in number of blades in the range from -1 to +2. The power consumption of the pump has marginally increased with the increase in number of blades and it has a positive relationship between the ranges from -2 to +2.

7.1.5 Direct Effects of Blade Thickness on the Responses

Figure 7.5 shows that the pump characteristics head and power decreases marginally with an increase in blade thickness. When the blade thickness is increases, the flow area decreases and so the pump input is decreases. Because of the decreasing power input, the efficiency of the pump is increasing. The blade thickness has a positive relationship on the response efficiency between the ranges from -2 to +2.

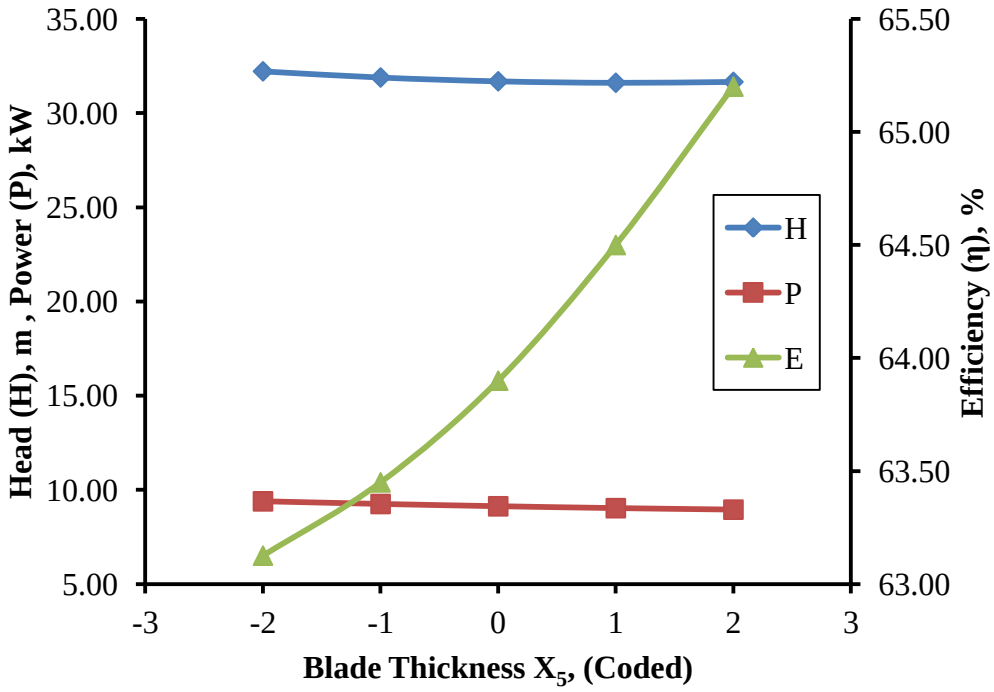

Figure 7.5 Direct effects of blade thickness on head, power and efficiency

7.2 SENSITIVITY ANALYSIS FOR RANKING OF IMPELLER DESIGN PARAMETERS

As discussed in earlier section 7.1, various impeller design parameters are greatly affect the pump performance. However, very few studies have investigated about more than one parameter and each parameter has its own influence. To overcome these issues, ranking the influence of each parameter is carried out using sensitivity analysis and experimental investigation of each varying parameter is not only time-consuming but also expensive.

The reduced models for all responses are used to perform the sensitivity analysis. The reduced mathematical models with significant coefficients are partially differentiated with the impeller design parameters

such as outer diameter (X_1), inlet blade angle (X_2), outlet blade angle (X_3), a number of blades(X_4) and blade thickness(X_5). There are 15 sensitivity equations derived and the pump performance is analyzed for significant impeller geometrical parameters. For instance, the sensitivity of X_1 is analyzed against varying of any one of the parameters such as X_1, X_2, X_3, X_4 or X_5. Similarly, the sensitivity of each design parameters is analyzed against by varying any one of the five parameters. However, the results are shown only for the combination which has some noticeable influence on the response parameters.

7.2.1 Sensitivity of Outer Diameter on the Responses

The impact of outer diameter on three critical output parameters: head, power input and efficiency are investigated using sensitivity analysis. The mathematical equations derived for outer diameter on three parameters are provided in Equations (7.1) to (7.3). The results are depicted in Figure 7.6. A significant change in sensitivity of outer diameter is observed only for varying the dimensions of the outer diameter.

$$\frac{\partial H}{\partial X_1} = 0.83625 + 0.39416\, X_1 - 0.26313\, X_3 - 0.08437\, X_4 - 0.10187\, X_5 \tag{7.1}$$

$$\frac{\partial P}{\partial X_1} = 0.2629 + 0.2125\, X_1 + 0.0719\, X_2 - 0.1419\, X_3 - 0.0619\, X_4 + 0.0469\, X_5 \tag{7.2}$$

$$\frac{\partial \eta}{\partial X_1} = -0.3396 - 1.2438\, X_1 - 0.4719\, X_2 + 0.5006\, X_3 + 0.2481\, X_4 - 0.5306\, X_5 \tag{7.3}$$

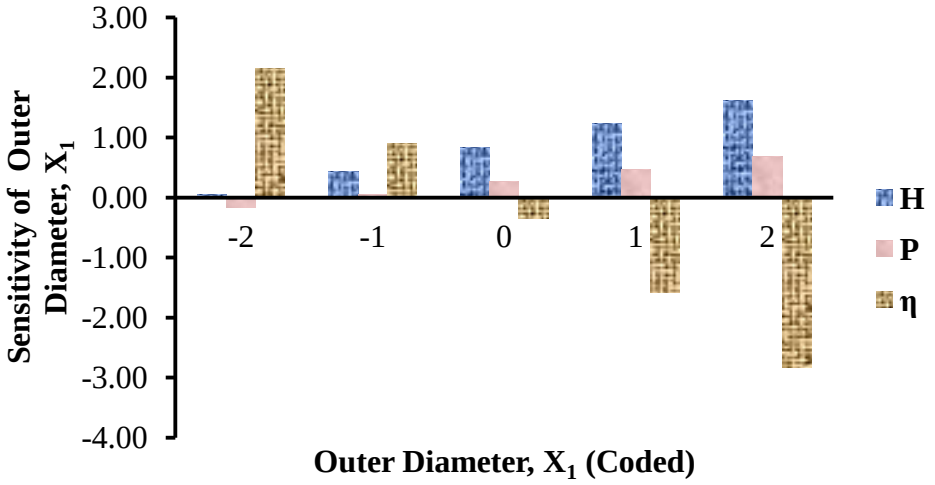

Figure 7.6 Sensitivity of the outer diameter (X_1) on the responses

The results suggest that the efficiency has positive sensitivity for lower DOE levels with a decreasing trend for increasing the DOE levels and has a transition from positive to negative sensitivity when the DOE level is 0. This is due to the increasing trend of head which results in increase in power consumption and subsequent reduction in efficiency. The efficiency has a strong influence on modified outer diameter followed by head and power input.

7.2.2 Sensitivity of Inlet Blade Angle on the Responses

In a similar way to the outer diameter, equations are derived by partially differentiating the second order equations arrived by conducting DOE which is presented in Equations (7.4) to (7.6). The sensitivity of X_2 has an only noticeable change against only for the change in dimension of X_2 and other dimensional parameters had negligible impact. The result of the sensitivity analysis is shown in Figure 7.7. Although the changes in inlet blade angle have marginal influence on all the three output responses, the efficiency has shown some noticeable change in sensitivity.

$$\frac{\partial H}{\partial X_2} = -0.25375 + 0.08916\,X_2 + 0.09937\,X_3 + 0.1583\,X_4 - 0.43688\,X_5 \quad (7.4)$$

$$\frac{\partial P}{\partial X_2} = -0.0763 + 0.0725\,X_2 + 0.0719\,X_1 + 0.0769\,X_3 + 0.0844\,X_4 - 0.0619\,X_5 \quad (7.5)$$

$$\frac{\partial \eta}{\partial X_2} = 0.1129 - 0.2938\,X_2 - 0.4719\,X_1 - 0.3881\,X_3 - 0.2706\,X_4 - 0.4244\,X_5 \quad (7.6)$$

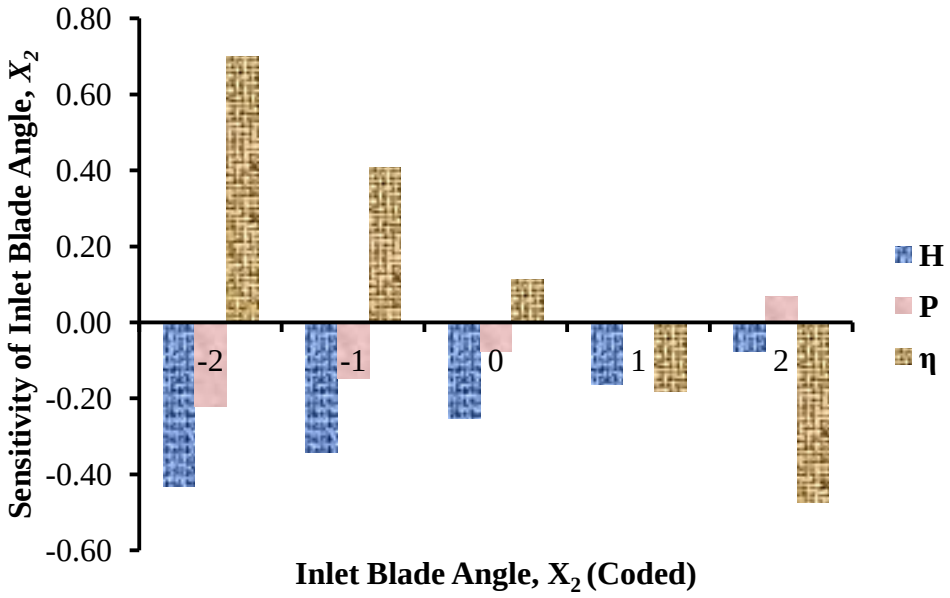

Figure 7.7 Sensitivity of the inlet blade angle (X_2) on the responses

7.2.3 Sensitivity of Outlet Blade Angle on the Responses

The sensitivity equations of outlet blade angle of the impeller on the responses are presented in the Equations (7.7) to (7.9). Unlike X_1 and X_2, the sensitivity of X_3 is significant for the change in dimension of blade thickness (X_5) only.

$$\frac{\partial H}{\partial X_3} = 0.08125 - 0.26313\,X_1 + 0.09937\,X_2 - 0.19063\,X_4 + 0.19687\,X_5 \quad (7.7)$$

$$\frac{\partial P}{\partial X_3} = -0.0304 - 0.1419\,X_1 + 0.0769\,X_2 + 0.0731\,X_4 + 0.1094\,X_5 \quad (7.8)$$

$$\frac{\partial \eta}{\partial X_3} = 0.3737 + 0.5006\,X_1 - 0.3881\,X_2 - 0.9306\,X_4 - 0.4119\,X_5 \quad (7.9)$$

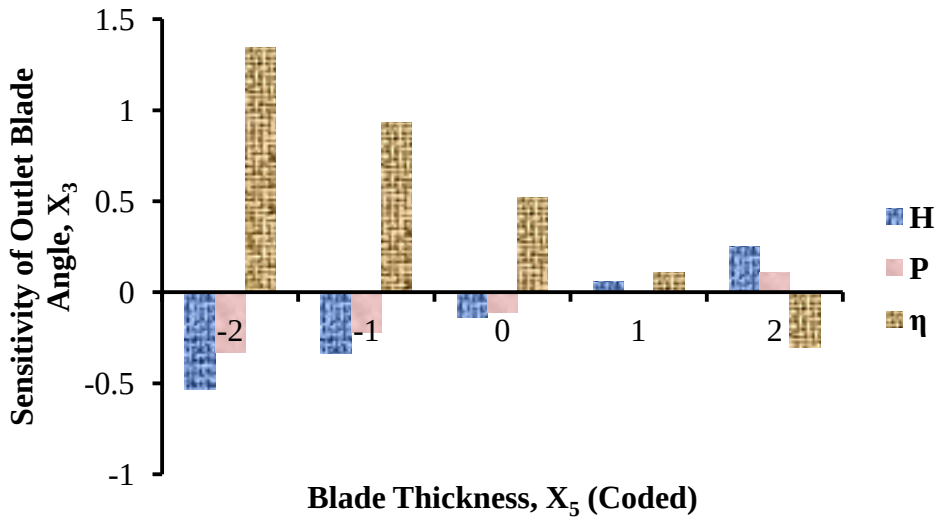

Figure 7.8 Sensitivity of the outlet blade angle (X_3) on the responses

Figure 7.8 shows the sensitivity of outlet blade angle of the impeller on the responses total head, input power and pump efficiency. From the figure, it is found that the pump efficiency decreases with increase in outlet blade angle. The outlet blade angle has positive sensitivity when the level is at -2 and negative sensitivity when the level is at +2. It is also found that the total head and power input increases with increases in outlet blade angle.

7.2.4 Sensitivity of Number of Blades on the Responses

The sensitivity equations of a number of blades of the impeller on the responses are presented in the Equations (7.10) to (7.12). The sensitivity of the number of blades is significant only for increasing the number of blades due to the reduction in the flow passage, which subsequently reduces the power consumption and results in improved efficiency.

$$\frac{\partial H}{\partial X_4} = 0.52875 + 0.48666\,X_4 - 0.08437\,X_1 + 0.15816\,X_2 - 0.19063\,X_3 + 0.08312\,X_5 \quad (7.10)$$

$$\frac{\partial P}{\partial X_4} = 0.0663 - 0.1025\,X_4 - 0.0619\,X_1 + 0.0844\,X_2 + 0.0731\,X_3 - 0.0906\,X_5 \quad (7.11)$$

$$\frac{\partial \eta}{\partial X_4} = 0.6212 + 1.6212\,X_4 + 0.2481\,X_1 - 0.2706\,X_2 - 0.9306\,X_3 + 0.7906\,X_5 \quad (7.12)$$

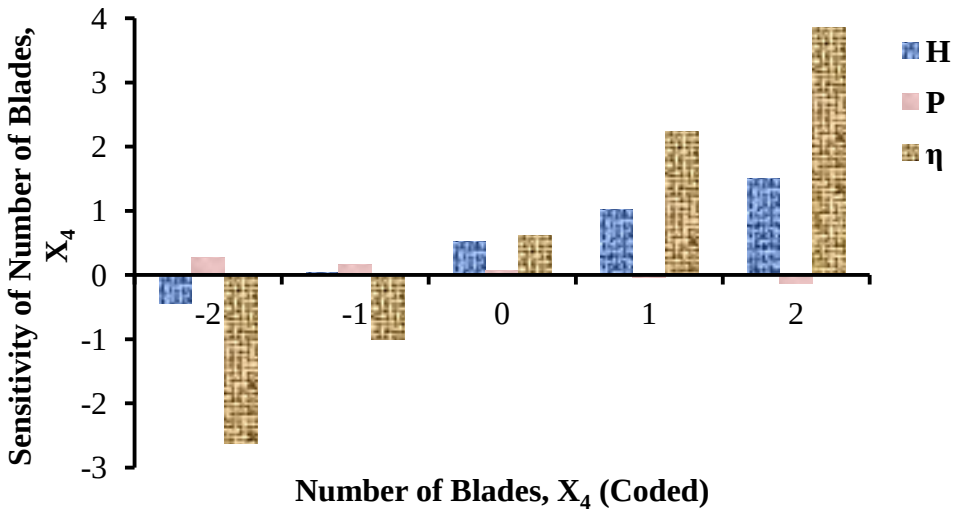

Figure 7.9 Sensitivity of the number of blades (X_4) on the responses

Figure 7.9 shows the sensitivity of a number of blades of the impeller on the responses total head, input power and pump efficiency. From the figure, it is observed that the pump total head and pump efficiency values increase with the increase in number of blades. The sensitivity of a number of blades is negative when the level has -2 and is positive, when the level has +2. The sensitivity of a number of blades on input power is minimum for all levels.

7.2.5 Sensitivity of Blade Thickness on the Responses

The sensitivity equations of blades thickness of the impeller on the responses are presented in the Equations (7.13) to (7.15). The sensitivity of

blade thickness has significantly influenced by increasing the number of blades. This may be due to the further reduction in the flow passage which results in reduced power consumption and improved efficiency similar to the sensitivity of X_4.

$$\frac{\partial H}{\partial X_5} = -0.14042 + 0.11416\,X_5 - 0.10187\,X_1 - 0.43688\,X_2 + 0.19687\,X_3 + 0.08312\,X_4 \quad (7.13)$$

$$\frac{\partial P}{\partial X_5} = -0.1104 + 0.0469\,X_1 - 0.0619\,X_2 + 0.1094\,X_3 - 0.0906\,X_4 \quad (7.14)$$

$$\frac{\partial \eta}{\partial X_5} = 0.5187 - 0.5306\,X_1 - 0.4244\,X_2 - 0.4119\,X_3 + 0.7906\,X_4 \quad (7.15)$$

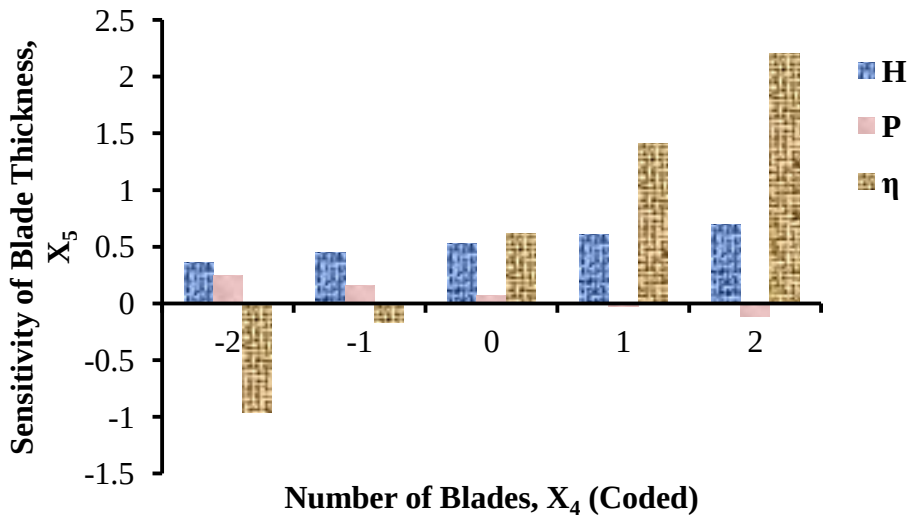

Figure 7.10 Sensitivity of the blade thickness (X_5) on the responses

Figure 7.10 shows the sensitivity of the blade thickness of the impeller on the responses total head, input power and pump efficiency. From the figure, it is observed that the total head is significantly increased with increase in blade thickness of the impeller. Due to an increase in blade thickness, the discharge rate decreases simultaneously the input power also decrease, therefore, the pump efficiency is increases. The sensitivity of blade thickness is positive at level +2 and negative sensitivity at level -2.

7.3 OPTIMIZATION OF IMPELLER DESIGN PARAMETERS USING GENETIC ALGORITHM (GA)

7.3.1 Introduction

The optimum set points of the impeller geometrical parameters can be found by using the various traditional, non-traditional and advanced hybrid optimization techniques. The profile of the centrifugal pump impeller is complex and its relationship between the input and the output characteristics is also too complex. Hence the selection of optimum geometrical set point is a complicated process. The objective of maximizing the head and efficiency and minimizing the power consumption can be achieved by optimizing the various impeller design parameters through the multi-objective genetic algorithm.

Using the multi-objective optimization, a group of optimal points is found instead of a single optimum point for all the functions. The Pareto front provides the decision makers to decide the combination that satisfies the required conditions.

7.3.2 Selection of GA Parameters and Formulation of the Multi-objective Function

The Genetic Algorithm is developed using the principles of Darwin's evolutionary theory. The pump output characteristics are interrelated with each impeller design parameters where, a number of multiple points are derived instead of a single point. The minimization of the objective functions provides a number of optimal solutions. The non-dominated optimal points from the multi-objectives are said to form the Pareto front.

MATLAB®R2017a is used to simulate the multi-objective function *gamultiobj*. Following a set of function values of GA operators are selected during the optimization of impeller geometrical parameters and response functions.

Population type = double vector

Population size = 100

Creation function = constraint dependent

Initial range = [-10; 10]

Selection function= tournament

Tournament size = 2

Crossover fraction = 0.8

Mutation function = Constraint dependent

Crossover function = intermediate

Crossover function ratio = 1.0

Migration direction = forward

Migration fraction = 0.2

Migration interval = 20

Distance measure function = @distance crowding

Pareto front population fraction = 0.35

Stopping Criteria:

Generations = 1000

Time limit = $\propto$

Fitness limit = $-\propto$

Stall generation = 100

Stall time limit = $\propto$

Function tolerance = 1 x 10^{-4}

Optimization of Response Variables Using GA

A single objective function is formulated by combining the other functions for the optimization process which is present in the Equation (7.16).

$$F\{x\} = \left[F_1\{x\}, F_2\{x\}.....F_n\{x\}\right] \tag{7.16}$$

Where, $F\{x\}$ - primary objective function and

$F_1\{X\}, F_2\{x\}.....F_n\{x\}$ is the secondary objective function of the response variables

Equation (7.17) presents the multi-objective function of the given problem formulated by using the objective functions f (1) and f (2). The objective functions f (1) and f (2) represent the responses head and efficiency respectively.

$$function\ f = mymultifn(x)$$

$$f(1) = (-1)*(31.6926 + 0.8363X_1 - 0.2538X_2 + 0.0813X_3 + 0.5287X_4 - 0.1404X_5 + 0.2024X_1^2 + 0.0499X_2^2 + 0.0111X_3^2 + 0.2486X_4^2 + 0.0624X_5^2 + 0.0131X_1X_2 - 0.2631X_1X_3 - 0.0844X_1X_4 - 0.01019X_1X_5 + 0.0994X_2X_3 + 0.1581X_2X_4 - 0.4369X_2X_5 - 0.1906X_3X_4 + 0.1969X_3X_5 + 0.0831X_4X_5)$$

$$f(2) = (-1)*(64.1822 - 0.3396X_1 + 0.1129X_2 + 0.3738X_3 + 0.6212X_4 + 0.5187X_5 - 0.6222X_1^2 - 0.1472X_2^2 + 0.0016X_3^2 + 0.8103X_4^2 - 0.0047X_5^2 - 0.4719X_1X_2 + 0.5006X_1X_3 + 0.2481X_1X_4 - 0.5306X_1X_5 - 0.3881X_2X_3 - 0.2706X_2X_4 - 0.4244X_2X_5 - 0.9306X_3X_4 - 0.4119X_3X_5 + 0.7906X_4X_5)$$

(7.17)

The Pareto optimal set points generated for the responses head and efficiency are shown in Figure 7.11. The corresponding impeller design parameters in coded and actual form along with the response functions values are presented in Table 7.1. The non-dominated set points for the response head varies between 33 to 39 m, and at the same time, the efficiency values vary in the range between 73 to 78.5%. The responses head and efficiency are sensitive to the design parameters outer diameter and inlet blade angle.

Table 7.1 Pareto optimum set points for the head and efficiency

Impeller Design Parameters										Responses	
Outer Diameter,(X_1)		Inlet Blade Angle,(X_2)		Outlet Blade Angle,(X_3)		Number of Blades,(X_4)		Blade Thickness,(X_5)			
Coded	Actual (mm)	Coded	Actual (^{o})	Coded	Actual (^{o})	Coded	Actual	Coded	Actual (mm)	Head (H), m	Efficiency (η), %
2.0000	184.0	-1.9866	18.0	-1.9832	22.0	1.9999	8	1.9932	6.0	38.83	73.44
-0.8582	178.3	-1.3766	19.2	-1.9845	22.0	1.9994	8	1.9976	6.0	34.70	78.46
-0.9075	178.2	-0.7098	20.6	-1.9921	22.0	1.9994	8	1.9986	6.0	33.92	78.64
-0.8345	178.3	-0.8137	20.4	-1.9892	22.0	1.9994	8	1.9979	6.0	34.08	78.58
0.0475	180.1	-1.9544	18.1	-1.9864	22.0	1.9997	8	1.9947	6.0	36.11	77.80
0.5979	181.2	-1.9554	18.1	-1.9812	22.0	1.9995	8	1.9898	6.0	36.70	77.02
-0.7926	178.4	-1.1837	19.6	-1.9880	22.0	1.9993	8	1.9974	6.0	34.52	78.50
1.7871	183.6	-1.9241	18.2	-1.9879	22.0	1.9998	8	1.9946	6.0	38.39	74.10
-0.6384	178.7	-1.8748	18.3	-1.9874	22.0	1.9995	8	1.9965	6.0	35.43	78.25
1.2985	182.6	-1.9860	18.0	-1.9841	22.0	1.9998	8	1.9935	6.0	37.69	75.55
0.4495	180.9	-1.8818	18.2	-1.9645	22.1	1.9995	8	1.9943	6.0	36.44	77.24
0.7178	181.4	-1.9350	18.1	-1.9831	22.0	1.9985	8	1.9911	6.0	36.83	76.80
1.0402	182.1	-1.9653	18.1	-1.9833	22.0	1.9997	8	1.9975	6.0	37.29	76.17
-0.6412	178.7	-1.6944	18.6	-1.9872	22.0	1.9994	8	1.9974	6.0	35.22	78.31
1.9448	183.9	-1.9725	18.1	-1.9819	22.0	1.9996	8	1.9932	6.0	38.71	73.61
0.7588	181.5	-1.9785	18.0	-1.9846	22.0	1.9995	8	1.9944	6.0	36.93	76.75
0.8433	181.7	-1.9705	18.1	-1.9818	22.0	1.9992	8	1.9933	6.0	37.03	76.58
1.3592	182.7	-1.9503	18.1	-1.9826	22.0	1.9997	8	1.9937	6.0	37.73	75.37
-0.6937	178.6	-1.3624	19.3	-1.9837	22.0	1.9995	8	1.9891	6.0	34.79	78.38
0.3495	180.7	-1.9256	18.1	-1.9762	22.0	1.9989	8	1.9922	6.0	36.38	77.40
1.2360	182.5	-1.9860	18.0	-1.9841	22.0	1.9998	8	1.9935	6.0	37.59	75.70
1.1898	182.4	-1.9542	18.1	-1.9818	22.0	1.9997	8	1.9918	6.0	37.49	75.79
-0.8226	178.4	-1.0597	19.9	-1.9886	22.0	1.9994	8	1.9965	6.0	34.36	78.53
-0.0607	179.9	-1.8493	18.3	-1.9821	22.0	1.9994	8	1.9932	6.0	35.88	77.90
-0.5227	179.0	-1.8999	18.2	-1.9819	22.0	1.9995	8	1.9926	6.0	35.55	78.19
1.8195	183.6	-1.9811	18.0	-1.9834	22.0	1.9998	8	1.9933	6.0	38.51	74.03
1.9323	183.9	-1.9661	18.1	-1.9821	22.0	1.9997	8	1.9936	6.0	38.68	73.65
2.0000	184.0	-1.9866	18.0	-1.9832	22.0	1.9999	8	1.9932	6.0	38.83	73.44
1.5009	183.0	-1.9336	18.1	-1.9845	22.0	1.9996	8	1.9932	6.0	37.93	74.96
1.6365	183.3	-1.9770	18.0	-1.9832	22.0	1.9997	8	1.9918	6.0	38.20	74.59
1.8647	183.7	-1.9802	18.0	-1.9839	22.0	1.9997	8	1.9934	6.0	38.59	73.88
1.6730	183.3	-1.9603	18.1	-1.9787	22.0	1.9991	8	1.9920	6.0	38.24	74.46
-0.6844	178.6	-1.5048	19.0	-1.9851	22.0	1.9994	8	1.9975	6.0	34.96	78.38
0.9565	181.9	-1.9281	18.1	-1.9803	22.0	1.9995	8	1.9912	6.0	37.13	76.32
1.5286	183.1	-1.9859	18.0	-1.9836	22.0	1.9995	8	1.9935	6.0	38.04	74.92

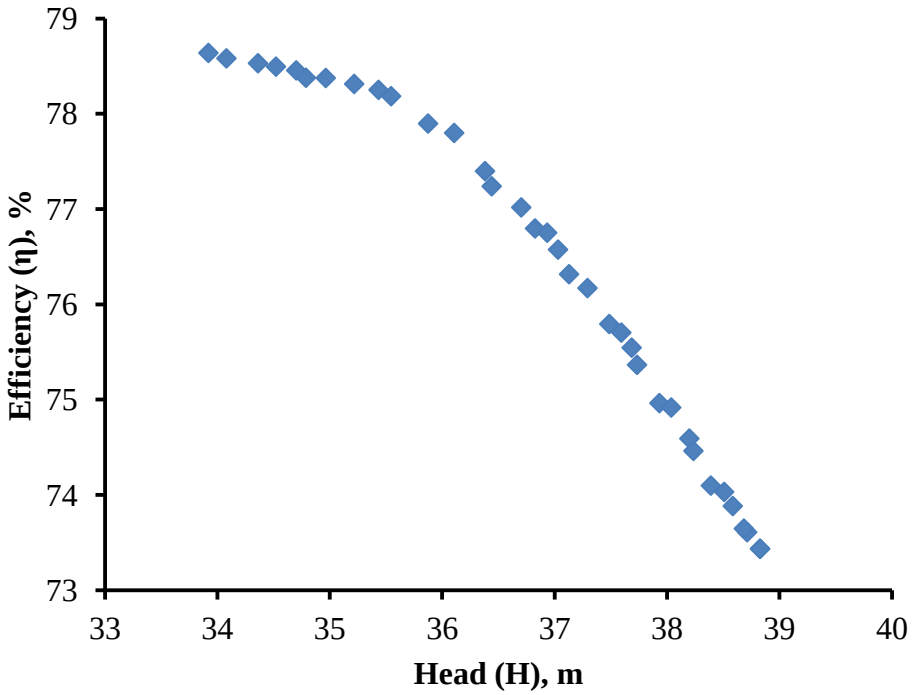

Figure 7.11 The non-dominant set points of the response variables head and efficiency

Equation (7.18) presents the multi-objective function of the given problem formulated by using the objective functions f (1) and f (2). The objective functions f (1) and f (2) are represents the responses head and power respectively.

$$function\ \ f = mymultifn(x)$$

$$f(1) = (-1)*(31.6926 + 0.8363X_1 - 0.2538X_2 + 0.0813X_3 + 0.5287X_4 - 0.1404X_5$$
$$+0.2024X_1^2 + 0.0499X_2^2 + 0.0111X_3^2 + 0.2486X_4^2 + 0.0624X_5^2 + 0.0131X_1X_2$$
$$-0.2631X_1X_3 - 0.0844X_1X_4 - 0.01019X_1X_5 + 0.0994X_2X_3 + 0.1581X_2X_4$$
$$-0.4369X_2X_5 - 0.1906X_3X_4 + 0.1969X_3X_5 + 0.0831X_4X_5)$$

$$f(2) = 9.13216 + 0.26292X_1 - 0.07625X_2 - 0.03042X_3 + 0.06625X_4 - 0.11042X_5 + 0.10659X_1^2 + 0.03659X_2^2 - 0.00591X_3^2 - 0.05091X_4^2 + 0.01034X_5^2 + 0.07187X_1X_2 - 0.14187X_1X_3 - 0.06187X_1X_4 + 0.04688X_1X_5 + 0.07687X_2X_3 + 0.08438X_2X_4 - 0.06188X_2X_5 + 0.07313X_3X_4 + 0.10938X_3X_5 - 0.09062X_4X_5 \quad (7.18)$$

The Pareto optimal set points generated for the responses head and power is shown in Figure 7.12. The corresponding impeller design parameters in coded and actual form along with the response functions values are presented in Table 7.2. The non-dominated set points for the response head varies between 31 to 39 m, and at the same time, the power input values vary in the range between 6.5 to 10 kW. The responses head and power input are sensitive to the design parameters outer diameter, inlet blade angle, and outlet blade angle and blade thickness.

Table 7.2 Pareto optimum set points for the head and power

Impeller Design Parameters										Responses	
Outer Diameter,(X_1)		Inlet Blade Angle,(X_2)		Outlet Blade Angle,(X_3)		Number of Blades,(X_4)		Blade Thickness,(X_5)		Head(H), m	Power(P), kW
Coded	Actual	Coded	Actual	Coded	Actual	Coded	Actual	Coded	Actual		
-1.8623	176.3	1.4047	24.8	-1.9987	22.0	1.9626	8	1.9981	6.0	31.32	6.87
-1.8630	176.3	1.4063	24.8	-1.9983	22.0	1.9622	8	2.0000	6.0	31.31	6.87
-1.7297	176.5	0.5922	23.2	-1.9957	22.0	1.9801	8	1.9755	6.0	32.16	7.10
-1.5079	177.0	-0.2176	21.6	-1.9753	22.0	1.9695	8	1.9672	6.0	33.04	7.40
1.8645	183.7	-1.9851	18.0	-1.9862	22.0	1.9901	8	1.9479	5.9	38.55	9.42
1.4277	182.9	-1.9576	18.1	-1.9777	22.0	1.9926	8	1.9699	6.0	37.82	9.10
0.5637	181.1	-1.9347	18.1	-1.9752	22.0	1.9949	8	1.9692	6.0	36.61	8.58
0.7134	181.4	-1.6484	18.7	-1.9854	22.0	1.9963	8	1.9706	6.0	36.47	8.58
-0.8599	178.3	-0.5338	20.9	-1.9892	22.0	1.9886	8	1.9854	6.0	33.74	7.62
0.8239	181.6	-1.8057	18.4	-1.9748	22.1	1.9949	8	1.9700	6.0	36.79	8.69
1.5672	183.1	-1.7941	18.4	-1.9780	22.0	1.9916	8	1.9472	5.9	37.83	9.17
-1.3946	177.2	0.3112	22.6	-1.9841	22.0	1.9657	8	1.9644	6.0	32.54	7.27
-1.7208	176.6	0.9800	24.0	-1.9976	22.0	1.9689	8	1.9691	6.0	31.77	7.01
-0.6659	178.7	-1.7336	18.5	-1.9780	22.0	1.9921	8	1.9545	6.0	35.20	8.07
0.9338	181.9	-1.8730	18.3	-1.9780	22.0	1.9961	8	1.9348	5.9	36.99	8.77
0.4224	180.8	-1.8495	18.3	-1.9735	22.1	1.9968	8	1.9354	5.9	36.33	8.50
-1.5832	176.8	-0.0653	21.9	-1.9829	22.0	1.9839	8	1.9694	6.0	32.88	7.33
1.2724	182.5	-1.8134	18.4	-1.9846	22.0	1.9945	8	1.9737	6.0	37.42	8.96
1.7717	183.5	-1.9695	18.1	-1.9843	22.0	1.9978	8	1.9426	5.9	38.38	9.35
-1.5113	177.0	-0.5843	20.8	-1.9920	22.0	1.9743	8	1.9622	6.0	33.43	7.51
-1.1657	177.7	-1.4445	19.1	-1.9889	22.0	1.9778	8	1.9903	6.0	34.56	7.85
0.8017	181.6	-1.9078	18.2	-1.9783	22.0	1.9949	8	1.9609	6.0	36.87	8.70
-0.8119	178.4	-1.5154	19.0	-1.9826	22.0	1.9918	8	1.9593	6.0	34.85	7.96
-0.1724	179.7	-1.8508	18.3	-1.9785	22.0	1.9952	8	1.9674	6.0	35.75	8.25
-0.2811	179.4	-1.7874	18.4	-1.9770	22.0	1.9946	8	1.9585	6.0	35.57	8.20
1.3248	182.6	-1.9844	18.0	-1.9811	22.0	1.9949	8	1.9428	5.9	37.68	9.04
0.0921	180.2	-1.8838	18.2	-1.9829	22.0	1.9910	8	1.9597	6.0	36.03	8.36
-1.8537	176.3	1.1388	24.3	-1.9958	22.0	1.9621	8	1.9981	6.0	31.56	6.93
-1.0375	177.9	-0.8462	20.3	-1.9900	22.0	1.9764	8	1.9753	6.0	33.94	7.68
-0.7785	178.4	-0.9990	20.0	-1.9960	22.0	1.9880	8	1.9802	6.0	34.29	7.78
-1.5242	177.0	0.5221	23.0	-1.9808	22.0	1.9800	8	1.9761	6.0	32.31	7.17
1.6613	183.3	-1.9305	18.1	-1.9809	22.0	1.9964	8	1.9439	5.9	38.15	9.26
1.9639	183.9	-1.9862	18.0	-1.9837	22.0	1.9981	8	1.9276	5.9	38.73	9.50
1.9999	184.0	-1.9935	18.0	-1.9847	22.0	1.9982	8	1.9265	5.9	38.80	9.53
-1.5010	177.0	-0.7181	20.6	-1.9771	22.0	1.9792	8	1.9762	6.0	33.59	7.55

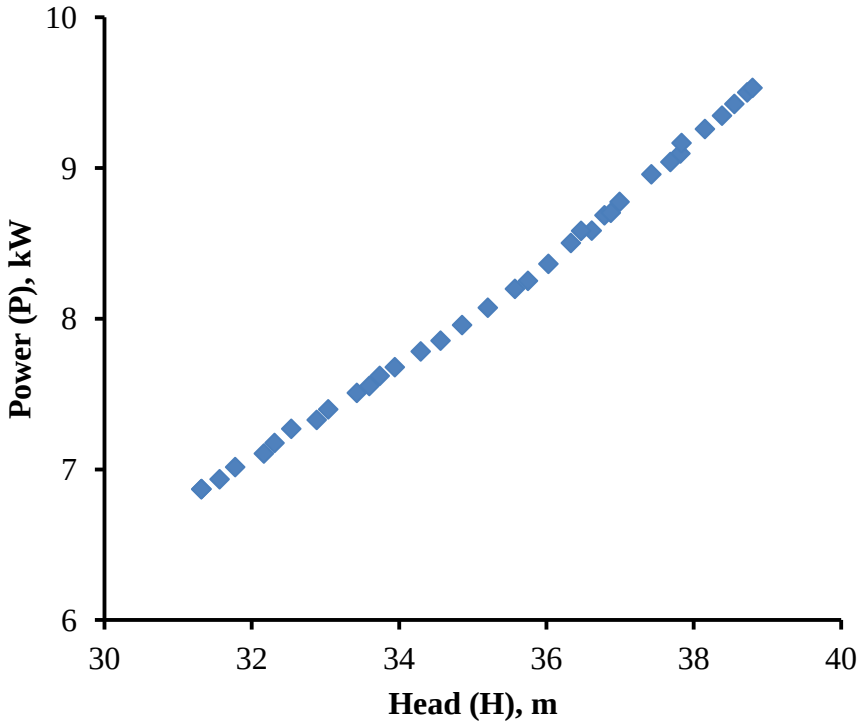

Figure 7.12 The non-dominant set points of the response variables head and power

7.4 SUMMARY

The direct effects of the impeller design parameters on response are discussed. The outer diameters have more influence on head and efficiency values. Inlet blade angle has a negative relationship on responses head and power and has a positive relationship on efficiency. The outlet blade angle and number of the blade have a positive relationship on efficiency and head. The sensitivity analysis provides the ranking of impeller parameters on responses, and the Pareto fronts provide many optimal solutions instead of single solution.

CHAPTER 8

PERFORMANCE ASSESSMENT OF THE EFFECTS OF SURFACE COATING ON CENTRIFUGAL PUMPS

8.1 INTRODUCTION

The centrifugal pump has hydraulic loss and friction loss due to the surface roughness, and it is necessary to study the effect of surface roughness on the pump performance characteristics. The surface roughness is the critical factor which controls the magnitude of friction and hydraulic loss. As the surface roughness increases, the resistance of the flow increases. In laminar flow condition, there is no effect on the flow resistance. The surface roughness on the flow passages has a significant impact on turbulent flow condition. Applying the polymer coating has enhanced the efficiency of the pump.

In this chapter how the efficiency of a centrifugal pump is improved by the application of the surface coating to the pump impeller and volute casing is discussed. A machined impeller and volute flow passage, the surfaces are generally rough. The rough surface increases friction losses and hence increases the input power, and due to increasing the power input the efficiency of the pump is reduced. Surface coating on the flow passage of the impeller and diffuser improves the surface finish of walls which reduces the friction loss. Finally, the pump efficiency can be improved.

8.2 STUDY THE EFFECT OF SURFACE ROUGHNESS ON PUMP COMPONENTS

The process of surface coating is divided into three stages. In the first stage, six Model Centrifugal Pumps (MCP) are assembled with same designed configurations, and a performance test is conducted on these pumps. The Design specification of the model centrifugal pump is presented in Table 8.1. The MCP is selected from M/s. Coimbatore Engineering Corporation (CEC) which is one of the leading pump manufacturers in Coimbatore.

Table 8.1 Specification of model centrifugal pump

Parameters	Value	Unit	Nomenclature
Discharge at the duty point	0.015	m^3/s	Q
Total head at the duty point	32	m	H
Speed of pump	2900	rpm	N
Specific speed	100	rpm	$N_s = N.Q^{1/2}/H^{3/4}$
The inner diameter of the impeller	75	mm	D_1
Width of the impeller at the inlet	18	mm	B_1
Outer diameter of the impeller	180	mm	D_2
Width of the impeller at the outlet	11.5	mm	B_2
Blade thickness	4	mm	t
Number of blades	6	--	--
Volute inlet mean diameter	75	mm	D_3
Volute mean diameter at the outlet	65	mm	D_4
Prime mover rating	7.5	kW	P
Best efficiency point	66	%	BEP
Surface roughness value of Impeller and volute casing (before coating)	4.39	μm	R_a
Pump efficiency	--	%	η

In the second stage, these six pumps are disassembled, and the coating is applied to the impeller and volute casing. Out of the six set of impeller and casing, three sets are coated with the epoxy coating material, and another three sets are coated with polyurethane coating material of different coating thickness. In the third stage, surface roughness and coating thickness values of the coated impeller and volute casing are measured, and the pump performance study is done experimentally and numerically for different surface roughness values. Since the cost of the cast iron materials is comparatively lesser than the cost of the steel or phosphor bronze material, the cast iron material is commonly used and preferred for casting impeller and volute casing by the pump manufacturers.

8.2.1 Measurement of Surface Roughness

The surface roughness value of impeller and volute casing is measured using Mitutoyo make surface roughness tester (Model: ST-210). The measurement of surface roughness on the uncoated impeller and volute casing are taken from three different locations of the flow passages. The roughness values obtained from the various locations are almost uniform. Finally, the average value is taken for further analysis and is presented in Table 8.2. Figure 8.1 shows the surface roughness measurement on SG 210 grade cast iron impeller for the analysis under uncoated condition.

Figure 8.1 Mitutoyo surface roughness tester

Table 8.2 Roughness values before coating

Descriptions	Surface Roughness Values, µm			Average Roughness Value, µm
	Trails			
	1	2	3	
Impeller No. 1	4.38	4.39	4.37	4.38
Impeller No. 2	4.39	4.41	4.42	4.41
Impeller No. 3	4.38	4.39	4.39	4.39
Impeller No. 4	4.39	4.38	4.38	4.38
Impeller No. 5	4.39	4.38	4.39	4.39
Impeller No. 6	4.40	4.38	4.38	4.39
Volute Casing No.1	4.39	4.38	4.39	4.39
Volute Casing No.2	4.39	4.38	4.37	4.38
Volute Casing No.3	4.39	4.38	4.37	4.38
Volute Casing No.4	4.38	4.37	4.39	4.38
Volute Casing No.5	4.39	4.38	4.39	4.39
Volute Casing No.6	4.38	4.39	4.39	4.39
Average Value				4.39

8.3 EXPERIMENTAL PERFORMANCE OF THE EXISTING MODEL CENTRIFUGAL PUMP

The performance testing is done on the six sets of the pump before applying the coating on the impeller and casing. The same prime mover (three phase AC induction motor) is used for testing six sets of pump configurations. The testing setup for testing MCP is fabricated as per ISO 9906:2012 standard and is shown in Figure 3.5 (a) and (b).The performance values are presented in Table 8.3 and the corresponding performance curves are shown in Figure 8.2. The variability in the results of the six uncoated pumps is negligible and hence a test result of the one pump is presented.

Table 8.3 Experimental performance values of the model pump without coating (R_a = 4.39 µm)

Q x 10^{-3}, m^3/s	H, m	P, kW	η, %
22.06	11.19	9.39	32.24
21.93	16.63	10.22	43.74
21.53	21.56	10.96	51.92
21.21	26.44	11.36	60.49
19.73	30.93	11.34	65.95
16.51	35.23	10.62	67.10
13.63	37.57	9.92	63.23
9.83	39.82	8.82	54.39
6.50	40.95	7.81	41.76
0.00	41.26	5.72	0.00

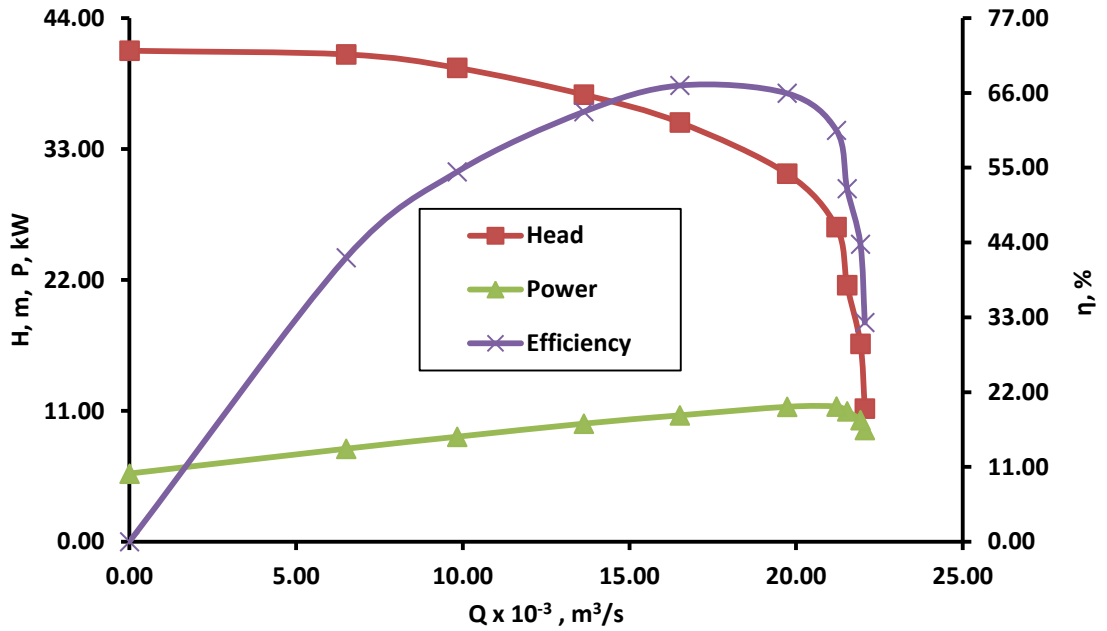

Figure 8.2 Experimental performance curves of the existing pump with surface roughness value R_a = 4.39 µm

8.4 IMPROVING SURFACE FINISH OF THE IMPELLER AND VOLUTE CASING

Two types of coating materials are identified for the coating process, 1) Epoxy material and 2) Polyurethane materials. These two materials are applied by means of hand brushing on the flow passages of the impeller and volute casings. The pumps selected for this analysis are coded as sample No.1 to 6. Out of these six pumps, first three pumps are coated with epoxy coating materials and the remaining three pumps are coated with the polyurethane materials. Each material is applied as a single layer, double layer, and three-layer coating to study the effects of different coating materials with different coating thickness and various surface finishes. The Sample 1 and 4 are coated as single layer, samples 2 and 5 are coated as two layers and sample 3 and 6 are coated as three layers for improving surface finish and its values are measured and tabulated.

8.5 EPOXY COATING

Epoxy is a polymer material which is mixed with a hardener in the ratio of 3:1 and retains at the room temperature for 15 minutes for maturation. It provides good abrasive and corrosion resistance and surface finish to the pump components. The different properties of the epoxy material are given in Table 8.4.

Table 8.4 Physical properties of the epoxy material

(Source: Dolphin Geomembranes, Coimbatore)

Properties		Values
Density, kg/m^3	Resin(Part -A)	1220
	Hardener (Part - B)	960
Viscosity at 23^oC, Ns/m^2	Resin(Part -A)	0.8
	Hardener (Part -B)	0.4
Mixing ratio(by Volume)		3:1
Thermal Conductivity, W/mK		0.28
Shore Hardness at 23^oC		D55 / A90
Cure Time at 23^oC, Hrs		24
The coefficient of thermal expansion, ppm /°C		80 to 100
Tensile Strength, N/mm^2		6.4
Tearing Strength, N/mm^2		24

The mixture is applied on the flow passages of the pump components after which it is allowed to cure for 24 hrs in room conditions. After curing, the thickness of coating and surface finish values are measured at different places and its values are given in Table 8.5. The same procedure is

repeated for samples 2 and 3. Figure 8.3 shows the epoxy material used for different coating thickness.

8.5.1 Measurement of Coating Thickness

The coating thickness value of impeller and volute casing is measured using Times Group make surface coating thickness gauge (Model: TT-210) and it is shown in Figure 8.4. The measurement of coating thickness on the coated impeller and volute casing are taken from three different locations of the flow passages. The coating thickness values obtained from the various locations are almost uniform and hence, the average value is taken for further analysis which is presented in Table 8.5 and 8.7.

Figure 8.3 Epoxy coated impeller and volute casing with different coating thickness and surface finish

Figure 8.4 Coating thickness gauge

Table 8.5 Roughness values after coating (epoxy material coating)

Descriptions	Surface Roughness Value, µm			Average Value, µm	Surface Coating Thickness, µm			Average Value, µm
	Trails				Trails			
	1	2	3		1	2	3	
Impeller No. 1	1.53	1.53	1.52	1.53	61.2	61.3	61.2	61.2
Impeller No. 2	1.23	1.22	1.23	1.23	121	122	120	121
Impeller No. 3	0.78	0.79	0.78	0.78	172	171	172	172
Volute Casing No.1	1.54	1.53	1.52	1.53	61.3	61.2	61.1	61.2
Volute Casing No.2	1.23	1.22	1.23	1.23	121	121	121	121
Volute Casing No.3	0.79	0.78	0.77	0.78	171	172	172	172

8.5.2 Polyurethane Coating

Polyurethane (PU) is a polymer material which is applied on the exterior and interior surfaces of the impeller and volute casing. PU provides

an excellent durability with high-quality gloss and color retention. The properties of the PU material are given in Table 8.6.

Table 8.6 Physical properties of polyurethane material

(Source: Dolphin Geomembranes, Coimbatore)

Properties		Values
Density, kg/m^3	Resin(Part – A)	1010
	Hardener (Part – B)	1060
Viscosity at 23^{o}C, Ns/m^2	Resin(Part – A)	1.7
	Hardener (Part – B)	0.5
Mixing ratio(by Volume)		2.25:1
Thermal Conductivity, W/mK		0.20
Shore Hardness at 23^{o}C		D64 / A95
Cure Time at 23^{o}C, Hrs		20
The coefficient of thermal expansion, ppm /°C		90 to 120
Tensile Strength, N/mm^2		7.6
Tearing Strength, N/mm^2		30

Before coating, the PU material is mixed with a hardener in the ratio of 2.25:1 and allowed to mature in room temperature for 15 minutes. Then the mixture is applied on the surface of the sample No.4 by brushing and then allowed to cool in a room temperature for 20 hrs. A similar procedure is followed for the sample No. 5 and 6. Sample 5 is coated two times and sample 6 is coated three times with the mixture. Figure 8.5 shows the PU coated components.

Figure 8.5 Polyurethane coated impeller and volute casing with different coating thickness and surface finish

The coating thickness (δ) and the corresponding surface roughness (R_a) values are measured in all samples from the various locations of the impeller and casing which are given in Table 8.6.

Table 8.7 Roughness values after coating (polyurethane material coating)

Sample Descriptions	Surface Roughness Value, µm			Average Value, µm	Surface Coating Thickness, µm			Average Value, µm
	Trails				Trails			
	1	2	3		1	2	3	
Impeller No. 4	0.31	0.3	0.29	0.30	34.4	34.5	34.4	34.4
Impeller No. 5	0.14	0.14	0.14	0.14	71.5	71.6	71.4	71.5
Impeller No. 6	0.12	0.11	0.11	0.11	128	128	127	128
Volute Casing No.4	0.31	0.30	0.30	0.30	34.4	34.4	34.4	34.4
Volute Casing No.5	0.14	0.15	0.13	0.14	71.6	71.5	71.5	71.5
Volute Casing No.6	0.11	0.11	0.11	0.11	128	128	128	128

8.6 EXPERIMENTAL PERFORMANCE OF SURFACE COATED PUMPS

8.6.1 Epoxy Coating Pump

The performance testing of epoxy coated pumps (Sample No: 1, 2 and 3) is tested using the same test setup shown in Figure 3.5(a) and (b) for the entire operating range of the pumps and its performance values are calculated. Tables 8.8(a), 8.8(b) and 8.8(c) gives the details of experimentally measured pump performance of the epoxy coated pumps with coating thicknesses of δ = 61.2,121 and 171 µm and its corresponding surface roughness values are R_a = 1.53, 1.22 and 0.78 µm respectively. The performance curves of the epoxy coated pumps and uncoated pump are shown in Figure 8.6. The details of the effect of surface roughness and epoxy

coating materials on the performance in the operating region of the pumps are presented in Figure 8.7 (a) to (c).

Table 8.8 (a) Experimental performance values of model pump with epoxy coating (R_a = 1.53 µm & δ = 61.2 µm)

Q x 10^{-3}, m^3/s	H, m	P, kW	η, %
22.07	11.20	9.24	32.68
21.92	16.61	10.05	44.34
21.70	21.57	10.80	53.03
21.29	26.64	11.34	61.35
19.75	31.00	11.23	66.75
16.52	35.27	10.49	67.91
13.66	37.77	9.85	64.26
9.89	40.34	8.84	55.29
6.50	40.96	7.66	42.52
0.00	41.31	5.58	0.00

Table 8.8 (b) Experimental performance values of model pump with epoxy coating (R_a = 1.22 µm & δ = 121 µm)

Q x 10^{-3}, m^3/s	H, m	P, kW	η, %
22.02	11.14	9.08	33.18
21.84	16.49	9.85	44.94
21.64	21.46	10.63	53.73
21.13	26.25	11.00	62.04
19.70	30.86	11.06	67.43
16.50	35.16	10.35	68.85
13.65	37.71	9.73	64.89
9.83	39.79	8.57	56.01
6.50	40.90	7.56	43.18
0.00	41.23	5.47	0.00

Table 8.8 (c) Experimental performance values of model pump with epoxy coating (R_a = 0.78 µm & δ = 172 µm)

Q x 10^{-3}, m^3/s	H, m	P, kW	η, %
22.07	11.20	9.09	33.55
21.89	16.56	9.85	45.37
21.65	21.48	10.58	54.16
21.14	26.28	10.96	62.50
19.68	30.79	10.96	68.48
16.47	35.06	10.25	69.19
13.65	37.71	9.67	65.70
9.83	39.84	8.53	56.48
6.52	41.16	7.75	43.59
0.00	41.33	5.43	0.00

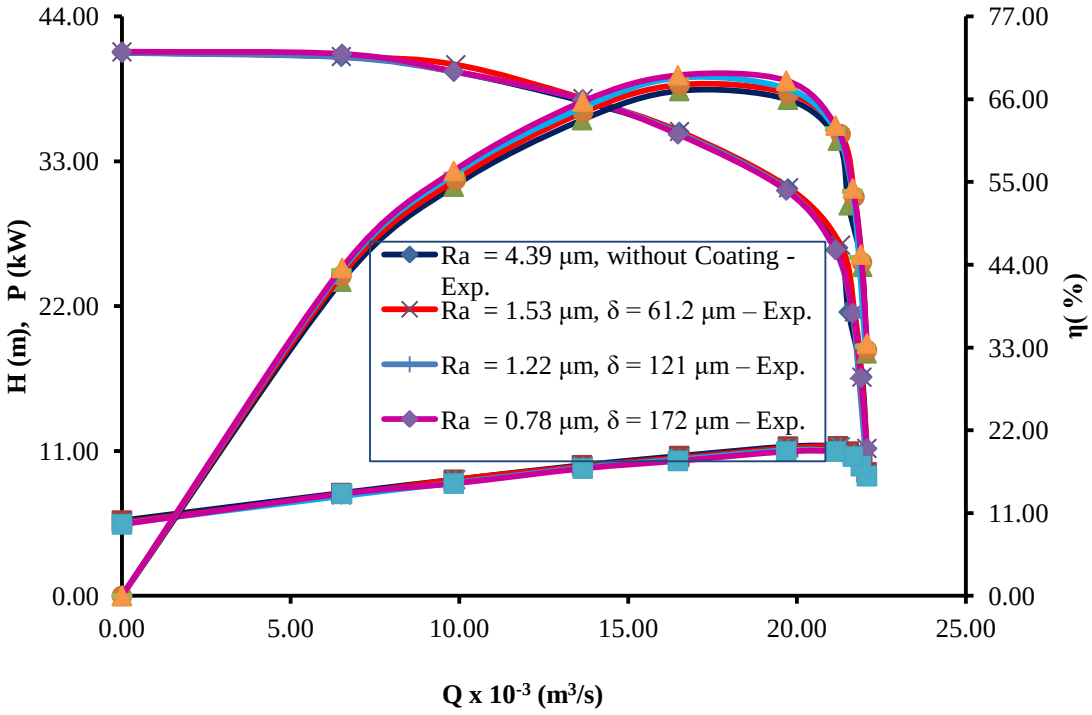

Figure 8.6 Experimental performance curves of an uncoated and epoxy coated pump

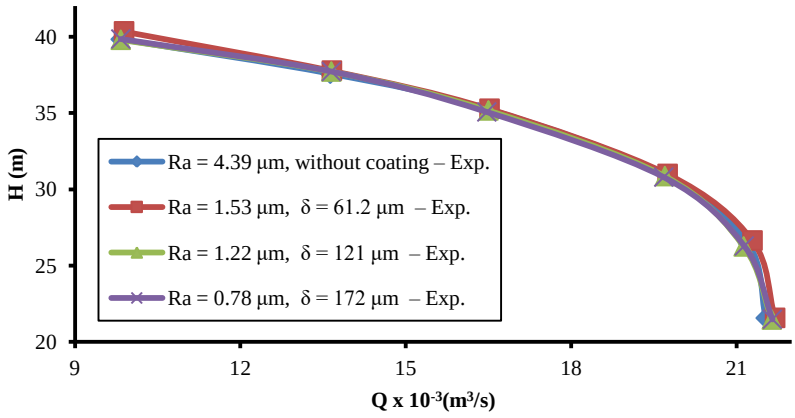

Figure 8.7 (a) Q – H Curve in the operating region (epoxy coated)

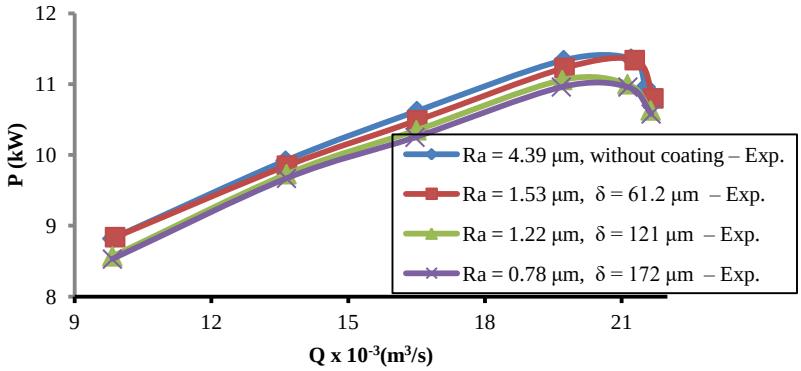

Figure 8.7 (b) Q – P Curve in the operating region (epoxy coated)

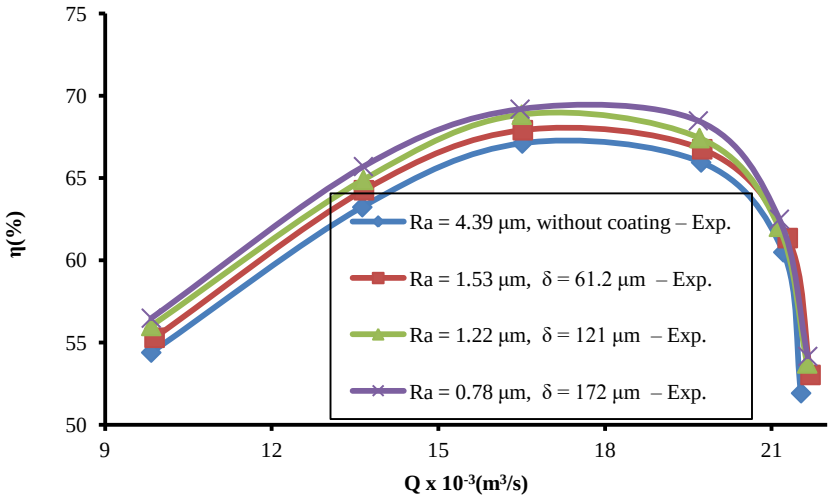

Figure 8.7 (c) Q – η Curve in the operating region (epoxy coated)

8.6.2 Polyurethane Coating Pump

The performance testing of the polyurethane coated pumps (Sample No: 4, 5 and 6) are tested using the same test setup shown in Figure 3.5 (a) and (b) for the entire operating range of the pumps and its performance values are calculated. Tables 8.9(a), 8.9(b) and 8.9(c) give the details of experimentally measured pump performance of the epoxy coated pumps with coating thicknesses of δ = 34.4,71.5 and 128 µm and its corresponding surface roughness values are R_a = 0.30, 0.14 and 0.11 µm respectively. The performance curves of the polyurethane coated pumps and

uncoated pump are shown in Figure 8.8. The details of the effect of surface roughness and polyurethane coating materials on the performance in the operating region of the pumps are presented in Figure 8.9 (a) to (c).

Table 8.9 (a) Experimental performance of model pump with polyurethane coating (R_a = 0.30 µm & δ = 34.4 µm)

Q x 10^{-3}, m^3/s	H, m	P, kW	η, %
22.01	11.14	8.99	33.44
21.88	16.55	9.82	45.24
21.63	21.46	10.55	53.83
21.15	26.30	10.95	62.17
19.70	30.83	10.96	68.00
16.49	35.14	10.26	69.22
13.63	37.59	9.60	65.22
9.84	39.89	8.52	56.50
6.50	40.95	7.49	43.56
0.00	41.28	5.40	0.00

Table 8.9 (b) Experimental performance of model pump with polyurethane coating (R_a = 0.14 µm & δ = 71.5 µm)

Q x 10^{-3}, m^3/s	H, m	P, kW	η, %
22.03	11.14	8.89	34.00
21.90	16.57	9.73	45.86
21.63	21.84	10.46	54.62
21.16	26.30	10.84	63.11
19.72	30.87	10.87	68.87
16.51	35.17	10.17	70.12
13.65	37.55	9.48	66.34
9.84	39.83	8.39	57.38
6.51	40.90	7.37	44.33
0.00	41.24	5.29	0.00

Table 8.9 (c) Experimental performance of model pump with polyurethane coating (R_a = 0.11 µm & δ = 128 µm)

Q x 10^{-3}, m^3/s	H, m	P, kW	η, %
22.02	11.16	8.67	34.91
21.89	16.59	9.51	47.09
21.61	21.48	10.22	55.98
21.16	26.34	10.63	64.53
19.69	30.84	10.62	70.62
16.48	35.11	9.90	71.89
13.63	37.54	9.24	68.11
9.82	39.79	8.14	59.06
6.49	40.90	7.13	45.65
0.00	41.31	5.06	0.00

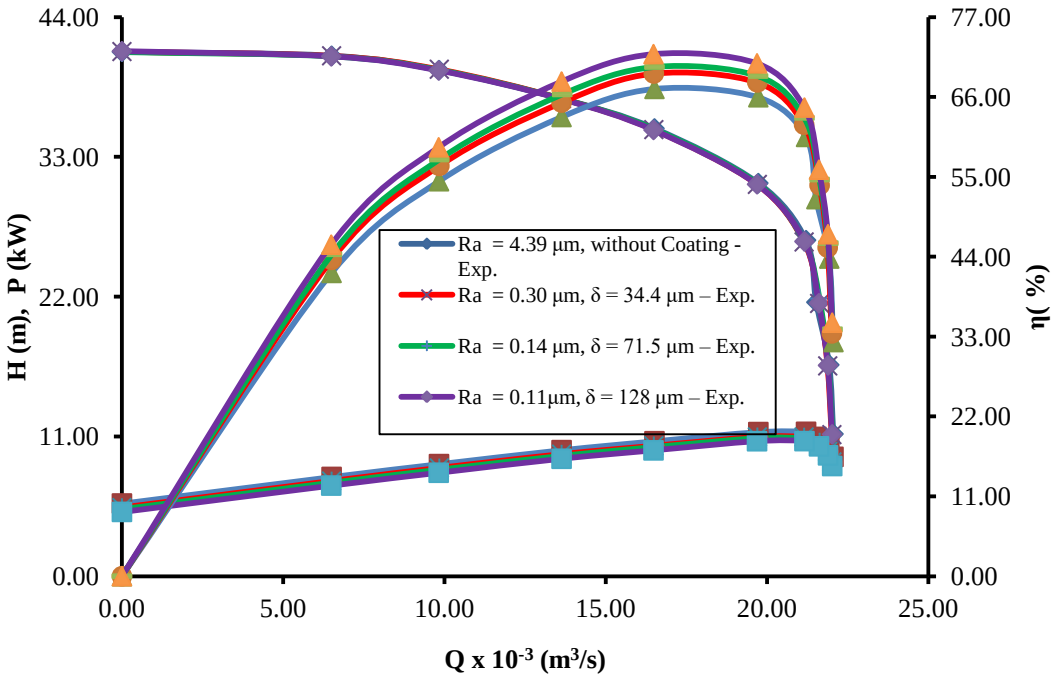

Figure 8.8 Experimental performance curves of an uncoated and polyurethane coated pump

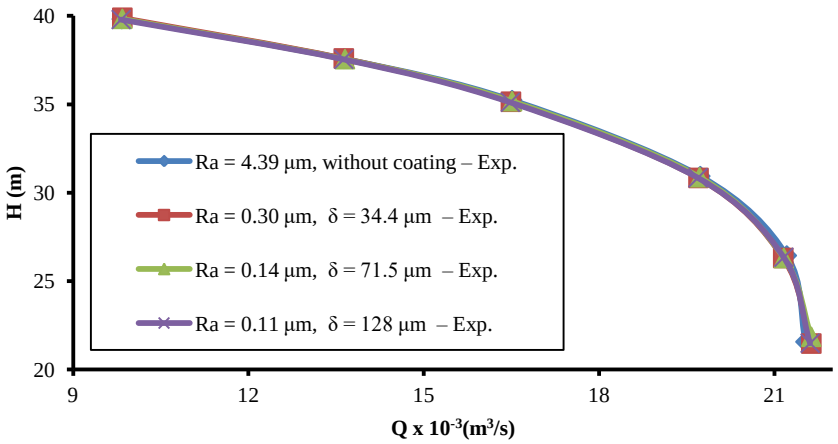

Figure 8.9 (a) Q – H Curve in the operating region (polyurethane coated)

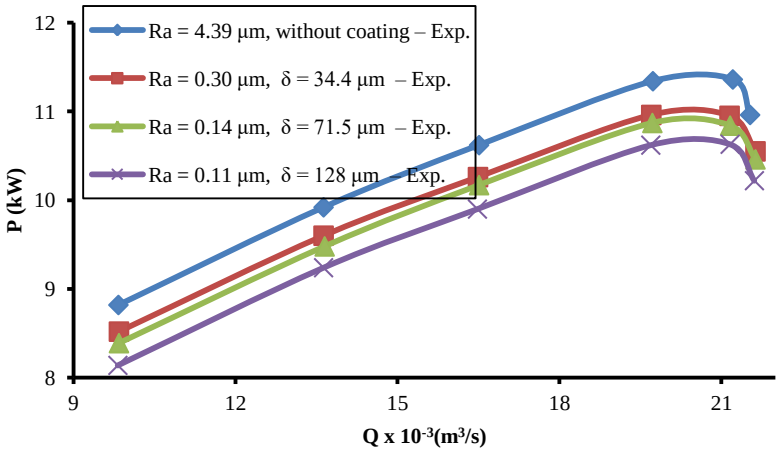

Figure 8.9 (b) Q – P Curve in the operating region (polyurethane coated)

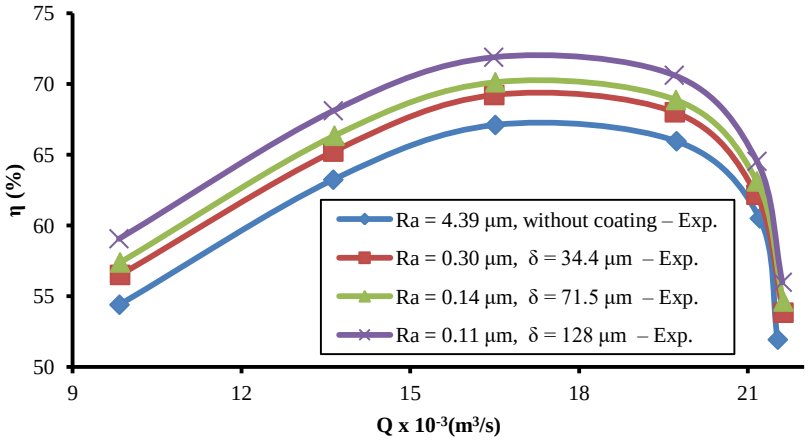

Figure 8.9 (c) Q – η Curve in the operating region (polyurethane coated)

8.7 NUMERICAL ANALYSIS OF SURFACE COATED PUMPS

The numerical simulation of MCP is done based on the solutions of the governing equations of fluid dynamics. The governing equations selected are the conservation of mass and momentum equations. The fluid domain of the MCP shown in Figure 8.10 is modeled using 3D CAD software and it is discretized with unstructured tetrahedral mesh. The unsteady RANS model is used to simulate the unsteady flow in the pump. In order to capture the wall roughness and skin friction effect, k-ω SST turbulence model is used

(Murugesan & Rudramoorthy 2016) To specify the relative motion between the impeller and volute casing, a mesh interface is provided and mesh motion is selected for the transient simulation. The condition of the inlet boundary and outlet boundary are selected, pressure as the inlet and mass flow rate as the outlet. Mesh motion with 2900 rpm is applied to the impeller cell zone condition. Table 8.10 shows the detailed boundary conditions of the numerical simulation. Based on the number of blades in the impeller and speed of rotation, the time step for the transient simulation is set as 0.00345s. The unsteady simulation is computed for 10 impeller rotations to achieve solution convergence.

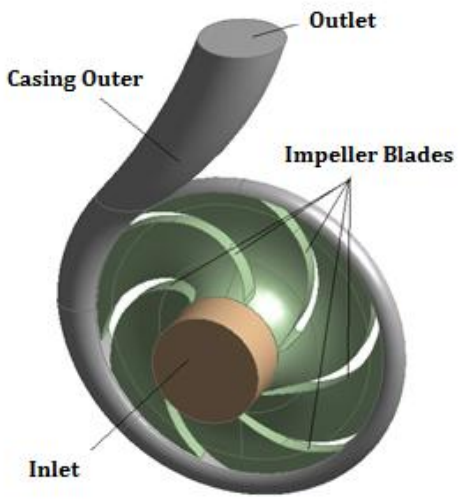

Figure 8.10 Computational fluid domain of MCP

Table 8.10 Boundary conditions for CFD analysis

Analysis type	Unsteady-State Incompressible
Fluid	Water
CFD Model	k – ω SST Model
Turbulence Intensity	5% (medium intensity)
Inlet	Total Pressure(10^5 Pa)
Outlet	Mass flow rate
Rotational Speed	2900 rpm
Convergence criteria	10^{-4}
Mass Imbalance	10^{-2}

8.7.1 Mesh Dependency Study

The accuracy of the numerical results is entirely based on the mesh size and the selected turbulence model. The entire flow domain is discretized from the coarse mesh of size 3.5 to fine mesh of size 1.0 and the number of a mesh in the flow domain is between 0.136 and 5.64 million. Mesh dependency test for the total head of the pump is performed for each mesh size and mesh numbers for the duty point mass flow rate. From the analysis, an optimum mesh size of 1.5 and mesh number 1.69 million is selected for further analysis. For the better quality of mesh, skewness of mesh is also considered (ANSYS CFX Theory Guide, 2013). The average mesh skewness is maintained as 0.21. The details of mesh and mesh dependency tests are presented in Table 8.11 and Figure 8.11 respectively. In order to capture the wall roughness effect, a boundary layer mesh is created over the impeller blades and volute surface. Mesh inflation of maximum 5 layers with a smooth transition and uniform growth rate is selected for the boundary layer mesh.

Figure 8.12 shows the unstructured mesh of the flow domain and a close-up view near to impeller blade with boundary layer mesh.

Table 8.11 Computation mesh details

Mesh Size	No of Mesh (x 10^5)	Total Head, m
3.5	1.36	18.72
3.0	2.18	24.56
2.5	3.72	27.01
2.0	7.18	28.34
1.5	16.90	33.09
1.0	56.40	33.12

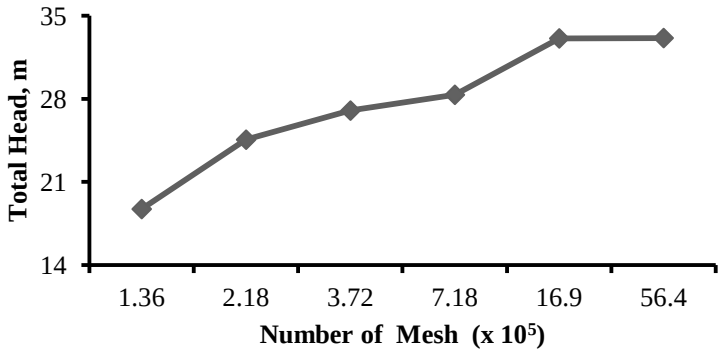

Figure 8. 11 Mesh dependency test

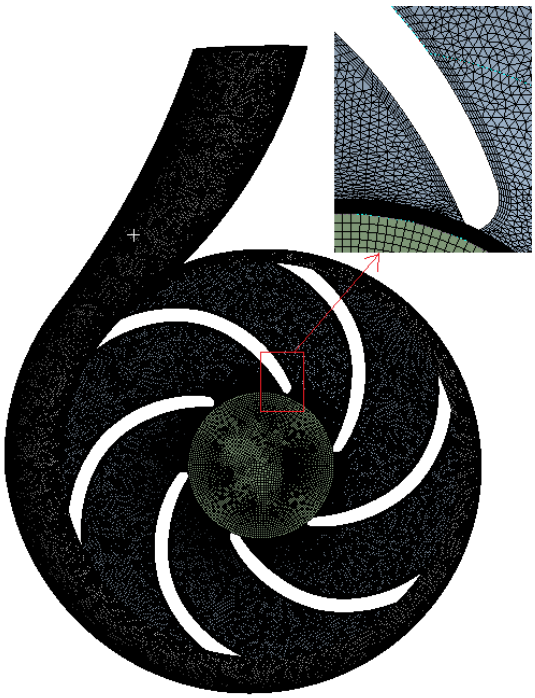

Figure 8.12 Meshed flow volume with a close-up view of the blade

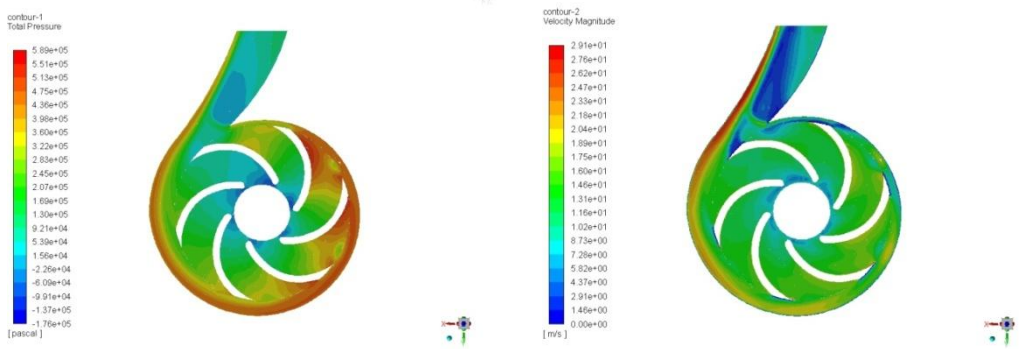

Figure 8.13 Pressure (Pa) and Velocity Distribution (m/s) of the uncoated pump (R_a = 4.39 µm)

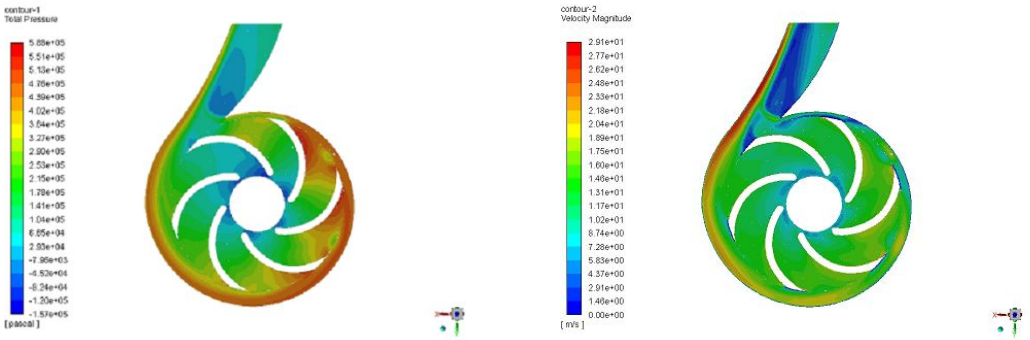

Figure 8.14 Pressure (Pa) and Velocity Distribution (m/s) of the polyurethane coated pump (R_a = 0.11µm)

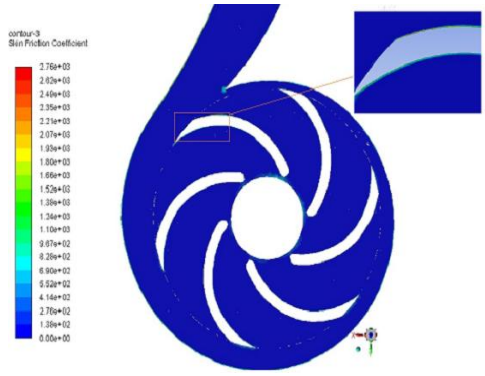

Figure 8.15 Effect of Skin Friction (uncoated)

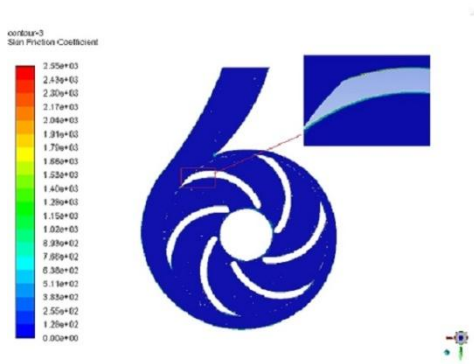

Figure 8.16 Effect of Skin Friction (coated)

8.7.2 Numerical Performance of a Coated Pump

The numerical performance values of an MCP are measured by simulating three sets of the pump. In which, one set is uncoated and the other two are coated with epoxy and polyurethane coatings. The simulations are performed for all mass flow rates. Figure 8.13 and 8.14 show the pressure and velocity distributions of the uncoated pump and coated pump with polyurethane coating.

Table 8.12 (a) Numerical performance of a model pump without coating

Q x 10^{-3}, m^3/s	H, m	P, kW	η, %
22	11.73	7.23	34.99
21	23.01	9.67	48.99
20	27.52	9.46	57.04
18	32.11	8.62	65.74
17	33.41	8.22	67.74
15	35.62	7.75	67.59
11	38.63	7.12	58.51
7	40.52	6.19	44.92
5	40.83	5.42	36.93

Table 8.12 (b) Numerical performance values of model pump with epoxy coating (R_a = 0.78 µm & δ = 172 µm)

Q x 10^{-3}, m^3/s	H, m	P, kW	η, %
22	11.78	7.02	36.19
21	23.02	9.41	50.37
20	27.56	9.21	58.67
18	32.21	8.39	67.75
17	33.42	8.01	69.54
15	35.75	7.52	69.91
11	38.64	6.92	60.22
7	40.53	6.03	46.13
5	40.86	5.29	37.86

Table 8.12 (c) Numerical performance values of model pump with polyurethane coating (R_a = 0.11 µm & δ = 128 µm)

Q x 10^{-3}, m^3/s	H, m	P, kW	η, %
22	11.84	6.72	38.00
21	23.12	9.02	52.77
20	27.59	8.86	61.06
18	32.3	8.08	70.54
17	33.43	7.72	72.17
15	35.79	7.27	72.40
11	38.69	6.61	63.12
7	40.56	5.81	47.91
5	40.92	5.08	39.49

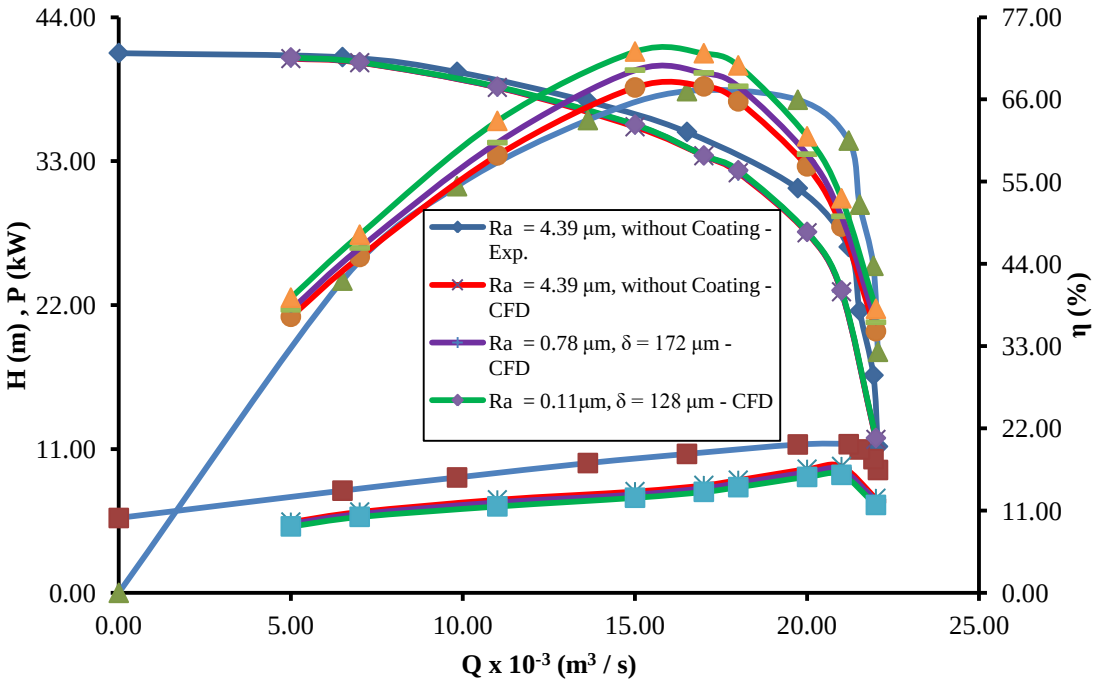

Figure 8.17 Numerical and experimental performance curves of an uncoated and coated pump

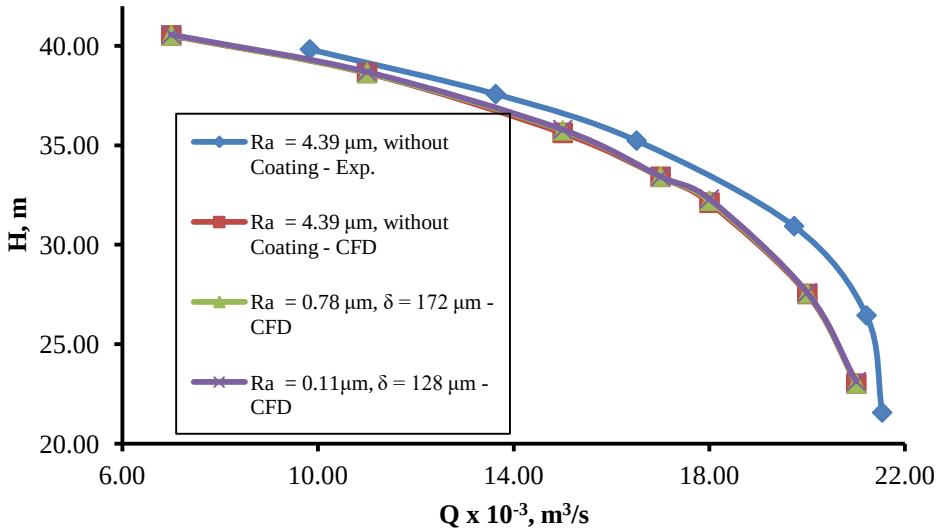

Figure 8.18 (a) Q – H Curve in the operating region (numerical performance)

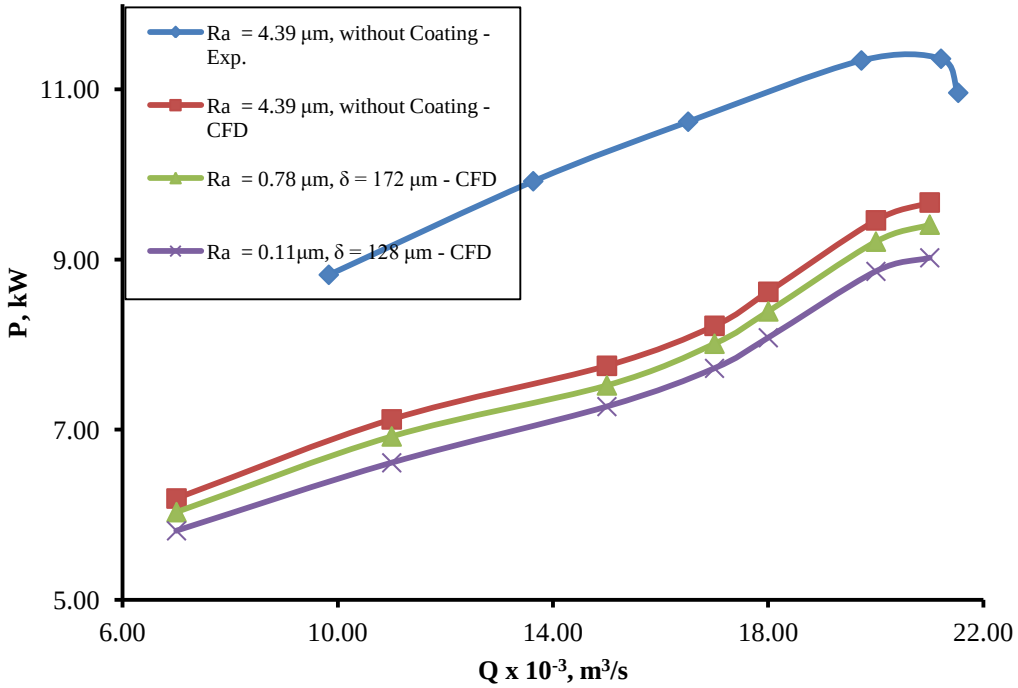

Figure 8.18 (b) Q – P Curve in the operating region (numerical performance)

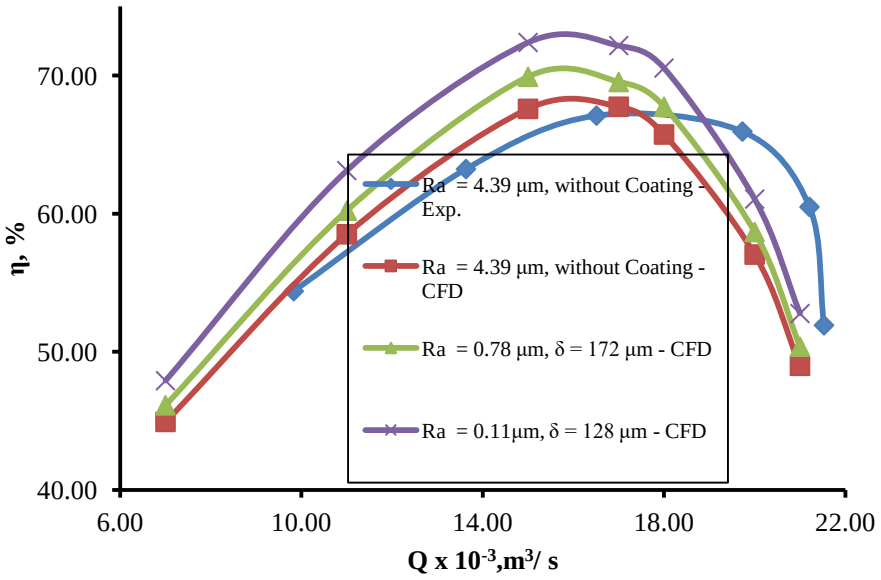

Figure 8.18 (c) Q – η Curve in the operating region (numerical performance)

The wall shear stress is based on the fluid properties of density and viscosity and physical properties such as cross-section and surface roughness. Also the ratio of wall shear stress and reference dynamic pressure gives the non-dimensional parameter called skin friction coefficient. The skin friction coefficient increases with an increase in wall roughness and in wall shear stress. Figure 8.15 and Figure 8.16 show the effects of skin friction coefficient over the impeller blades of the uncoated pump (R_a = 4.39 µm) and polyurethane coated pump (R_a = 0.11 µm) and its value is decreased from 0.027 to 0.023. The Tables 8.12 (a), (b) and (c) presents the performance values of uncoated and coated pumps with epoxy and polyurethane coatings respectively and the numerical results are compared with the experimental results. Figure 8.17 shows the numerical and experimental performance curves of uncoated and coated pumps. The exploded view of the performance curves in the operating head range is shown in Figure 8.18 (a) to (c) which show the effects of surface coating on the pump performances.

8.8 COST ANALYSIS OF THE COATED PUMPS

Cost analysis is performed for the application of a surface coating of the MCP. For cost analysis, Payback Period (PBP) and Net Present Value (NPV) are used. The PB is a simple and common method used to estimate the period in years to recover the initial investment for the coating process. Equation (8.1) is used to calculate the PBP.

$$PBP = \frac{C_i}{C_e} \tag{8.1}$$

Where, C_i - initial cost invested for the coating process and C_e - expected cost recovered per year

The NPV method is used for estimating the net present value of the money invested in a long-term process. It helps the manufacturer and user to know how much cost is saved by using the application of the coating process. The Equation (8.2) is used to calculate the NPV.

$$NPV = C_s . \frac{\left[(1+i)^n - 1\right]}{(1+i)^n . i} \tag{8.2}$$

Where, C_s - Annual cost saving, i - annual interest rate and n - Number of years

In this analysis, the cost of electricity for water distribution applications was taken as 0.109 USD/kWh in Tamil Nadu, India. The initial investment cost of epoxy and polyurethane coating was approximately 375 and 625 USD for the flow passages of the MCP including the cost of material and labour. Operating time of the pump is assumed as 20 hours per day for the estimation of the electric power consumption and saving.

8.9 RESULTS AND DISCUSSION

8.9.1 Comparisons of Experimental Test Results

Table 8.3 presents the experimental test results of MCP before coating and Tables 8.8 (a) to (c) and Tables 8.9 (a) to (c) present the performance values of pumps with epoxy and polyurethane coating with different coating thickness and surface roughness values and the corresponding performance curves are shown in Figure 8.6 and Figure 8.7. The enlarged view of the performance curves in the operating range of the pumps is also presented in the Figure 8.7 (a) to (c) and Figure 8.9 (a) to (c). From the performance curves, it is found that the pump total head and discharge rate are not improved significantly. The power input and pump efficiency are improved by applying coating materials to the flow passages of the impeller and volute casing. While comparing the power input and efficiency of the coated against the uncoated pump components, the input power is decreased and efficiency is increased. At the duty point, the power input of the coated pumps are decreased by 0.12, 0.25 and 0.35 kW and efficiency values are increased by 0.8, 1.6 and 2.2 % by applying an epoxy coating on the pump components. Power input values of the coated pumps are decreased by 0.35, 0.47 and 0.75 kW and efficiency values are increased by 2.1, 3.05 and 4.75 % by applying the polyurethane coating. For the entire flow range, the power input 0.13 to 0.38 kW is reduced by applying the epoxy coating and 0.36 to 0.74 kW is reduced when using a polyurethane coating.

At the pump duty point, the efficiency of the uncoated pump is 65.7 %, whereas the epoxy coated pump is 67.9 % and polyurethane coated pump is 70.45 %. It is shown that the efficiency of the pump is improved by applying a polyurethane coating with minimum coating thickness. At the duty point, considering the good surface finish of the pump components, electricity

is saved by the MCP with epoxy and polyurethane coating at the rate of 0.35 kW and 0.75 kW respectively. Using the Equation (8.1), annual cost saving is calculated as 275, and 585 USD and PBP is found as 0.73 and 0.94 years. The NPV is calculated at the annual interest rate of 10% with 5 years life of the coating materials (recommended by the coating materials supplier) using Equation (8.2), are 1043 and 2218 USD. This is really higher than the initial investment of 375 and 625 USD.

8.9.2 Comparisons of Results of Numerical Simulation

Tables 8.12(a) to (c) presents the numerical performance of uncoated and coated pumps and the corresponding performance curves are shown in Figure 8.17. From the Figure 8.17, it is observed that the difference in numerical performance and experimental performance values are within the acceptable limit (Nataraj & Singh 2014). The differences in corresponding performance value at the duty point are 2.7 % variation on the total head and 2.9 % on pump efficiency. While comparing the numerical performance values of the coated pump with uncoated pumps, there is no significant change in head and discharge values. Significant changes are found in the input power and pump efficiency values. At the duty point conditions, the input power is reduced in the range of 0.23 to 0.48 kW and the efficiency was increased in the range of 2.32 to 4.81 %. The above result shows that the application of the surface coating on the pump components has improved the surface finish and finally improves the overall performance characteristics of the pump.

8.10 CONCLUSION

From the experimental and numerical analysis of surface coating on the pump components, it is concluded that the efficiency of the pump is

improved by 2.2% and 4.75% when the epoxy and polyurethane coating materials is used and the corresponding power input is reduced by 0.35 kW and 0.75 kW respectively. There is no significant variation found in the flow rate and head of the pump. Remarkable energy and cost saving are achieved by using coating materials on the pump components which improve the life of the centrifugal pump.

CHAPTER 9

CONCLUSIONS AND SCOPE OF FUTURE WORK

9.1 INTRODUCTION

The objective of this research work is to improve the performance of centrifugal pump commonly used in agricultural, wastewater treatment plant and water supply and distribution system. Improving the efficiency of the centrifugal pump is a mandatory requirement of the pump manufacturers based on the requirements of Bureau of Indian Standard (BIS) for maintaining the BIS certifications, Bureau of Energy efficiency (BEE) for star labelling product scheme, Hydraulic Institute (HI) and Euro Pump Standards for maintaining global marketing. In contrast to the existing studies, from literature survey which considered only two or three impeller design parameters for studying the performance of the centrifugal pumps. But in this study, five parameters are considered for design optimization to improve the performance of the pump.

9.2 THESIS CONTRIBUTION

Detailed literature study is carried out regarding the influence of impeller design parameters , experimental study, numerical models used for CFD analysis, types of grids for meshing the computational domain of the pump, CFD tools, optimization techniques for maximizing or minimizing the single or multi-objective functions, effects of surface roughness and Reynolds number.

- Experimental study of the selected pump is conducted and it efficiency is found to be 65.6%. The current efficiency level is

less than the minimum efficiency required by the pump standard (IS 9079: 2002).

- Uncertainty in measurement for performance characteristics of flow rate, head, power and efficiency are estimated and the expanded uncertainty at the 95% confidence level are found to be ±1.51%, ±2.85%, 1.87% and ±3.02 respectively.
- An impeller is developed based on the turbo machinery theory for the duty point flow rate, head and speed of rotation and its efficiency at the duty point is measured as 66% and it is exactly corresponding to the efficiency required by the pump standard.
- The numerical performance of the developed impeller has been carried out and its results are compared with the experimental results and the deviation is found to be 2 to 5% for the entire operating conditions of the pump.
- Further, pump efficiency can be improved by optimization of geometrical parameters of the pump. Since the impeller is the main component of the centrifugal pump, optimization of the impeller design parameters are carried out.
- Five geometrical parameters of the impeller are selected and design optimization is carried out by design of experiments. Second order mathematical models for the pump output parameters of head, power input and efficiency are developed.
- The developed mathematical models are validated using F-test, R^2 – values and model adequacy test. All models are found satisfied at the 95% confidence level.

- The R^2- values of the predicted and actual values of the all responses are above 90% and hence the developed model has good prediction capability.
- The optimum impeller parameters are found from the RSM optimizer. The performance for the optimum impeller design parameters are evaluated by experimental and numerical analysis. The efficiency of the optimum impeller is improved by 4.5%.
- The direct effects of impeller design parameter are studied. It is found that the outer diameter, inlet blade angle and number of blades have positive relationship with the head and efficiency.
- Sensitivity analysis performed on the reduced model helps to identify the effects of impeller geometry parameters on the responses. Increase in impeller outer diameter is more effect on the total head (H) input power (P) and pump efficiency.
- The sensitivity of inlet and outlet blade angles and the number of blades on the impeller have more influence on the total head when compared to the other impeller parameters.
- The pump efficiency is observed that maximum positive and negative sensitivity with the number of blades on the impeller when the levels are -2 and +2 respectively and it was found that the influence of a number of blades is more on the total head.
- Impeller blade thickness is also strongly influenced by the pump efficiency and total head and it has minimum influence

on input power. The sensitivity analysis helps the pump manufacturers to design and manufacture the energy efficient pumps.

- Genetic Algorithm is used for performing the multi-objective optimization. The Pareto front provides the multiple optimum solutions for the responses. These results provide to the manufacturer to select many number design points instead of a single point.
- The surface coating on the pump components improves the pump performances significantly. Epoxy and Polyurethane materials are applied on the flow passage of the pump components with different coating thicknesses to improve the surface finish of the flow passage.
- Experimental and numerical performances are measured and it is found that there is no significant change flow rate and head values.
- The efficiency of pump is increased by 2.2% and power input is decreased by 0.35 kW when epoxy coating is used.
- The efficiency of pump is increased by 4.75 % and power input is decreased by 0.75 kW when polyurethane coating is used.
- Finally, the cost analysis of the coating process is made and a significant cost is saved using surface coating on the pump components.

9.3 SCOPE FOR THE FUTURE WORK

In future, similar work may be carried out on the centrifugal pump which is used in domestic, oil industries and chemical industries for improving the performance. This will result in more energy saving and cost.

REFERENCES

1. Aldaş, K & Yapıcı, R 2014, 'Investigation of effects of scale and surface roughness on efficiency of water jet pumps using CFD'. Engineering Applications of Computational Fluid Mechanics, vol. 8, no. 1, pp. 14-25.

2. Alemi, H, Nourbakhsh, SA, Raisee, M & Najafi, AF 2015, 'Effects of volute curvature on performance of a low specific-speed centrifugal pump at design and off-design conditions. Journal of Turbomachinery, vol. 137, no. 4, pp. 041009.

3. Allali, A, Belbachir, S, Lousdad, A & Merahi, L 2015, 'Numerical approach based design of centrifugal pump volute'. Mechanics, vol. 21, no. 4, pp. 301-306.

4. ANSYS CFX Theory Guide, ANSYS Inc

5. Asuaje, M, Bakir, F, Kouidri, S, Kenyery, F & Rey, R 2005, 'Numerical modelization of the flow in centrifugal pump: volute influence in velocity and pressure fields'. International journal of rotating machinery, vol. 2005, no. 3, pp. 244-255.

6. Ayad, AF, Abdalla, HM & El-Azm, AA 2015, 'Study of the effect of impeller side clearance on the centrifugal pump performance using CFD'. In ASME 2015 International Mechanical Engineering Congress and Exposition American Society of Mechanical Engineers, pp. V07AT09A037-V07AT09A037.

7. Badhurshah, R & Samad, A 2014, 'Surrogate assisted design optimization of an air turbine'. International Journal of Rotating Machinery.

8. Barrio, R, Parrondo, J & Blanco, E 2010, 'Numerical analysis of the unsteady flow in the near-tongue region in a volute-type centrifugal pump for different operating points'. Computers & Fluids, vol. 39, no. 5, pp. 859-870.

9. Baun, DO & Flack, RD 2003, 'Effects of volute design and number of impeller blades on lateral impeller forces and hydraulic performance'. International Journal of Rotating Machinery, vol. 9, no. 2, pp. 145-152.

10. Behzadmehr, A, Mercadier, Y & Galanis, N 2006, 'Sensitivity analysis of entrance design parameters of a backward-inclined centrifugal fan using DOE method and CFD calculations'. Journal of fluids engineering, vol. 128, no. 3, pp. 446-453.

11. Bellary, SAI & Samad, A 2015, 'Numerical analysis of centrifugal impeller for different viscous liquids'. International Journal of Fluid Machinery and Systems, vol. 8, no. 1, pp. 36-45.

12. Bellary, SAI & Samad, A 2016a, 'Centrifugal impeller blade shape optimization through numerical modeling'. International Journal of Fluid Machinery and Systems, vol. 9, no. 4, pp. 313-324.

13. Bellary, SAI & Samad, A 2016b, 'Pumping crude oil by centrifugal impeller having different blade angles and surface roughness'. Journal of Petroleum Exploration and Production Technology, vol. 6, no. 1, pp. 117-127.

14. Bellary, SAI, Husain, A & Samad, A 2014, 'Effectiveness of meta-models for multi-objective optimization of centrifugal impeller'. Journal of mechanical science and technology, vol. 28, no. 12, pp. 4947-4957.

15. Bing, H, Cao, S, Tan, L & Zhu, B 2013, 'Effects of meridional flow passage shape on hydraulic performance of mixed-flow pump impellers'. Chinese Journal of Mechanical Engineering, vol. 26, no. 3, pp. 469-475.

16. Bonaiuti, D, Zangeneh, M, Aartojarvi, R & Eriksson, J 2010, 'Parametric design of a waterjet pump by means of inverse design, CFD calculations and experimental analyses'. Journal of Fluids Engineering, vol. 132, no. 3, pp. 031104.

17. BS EN ISO 9906 : 2012, Rotodynamic Pumps — Hydraulic Performance Acceptance Tests — Grades 1 and 2

18. Cai, J, Pan, J & Guzzomi, A 2014, 'The flow field in a centrifugal pump with a large tongue gap and back blades'. Journal of Mechanical Science and Technology, vol. 28, no. 11, pp. 4455-4464.

19. Cao, S, Peng, G & Yu, Z 2005, 'Hydrodynamic design of rotodynamic pump impeller for multiphase pumping by combined approach of inverse design and CFD analysis'. Journal of Fluids Engineering, vol. 127, no. 2, pp. 330-338.

20. Chakraborty, S & Pandey, KM 2011, 'Numerical Studies on Effects of Blade Number Variationson Performance of Centrifugal Pumps at 4000 RPM'. International Journal of Engineering and Technology, vol. 3, no. 4, pp. 410.

21. Cheah, KW, Lee, TS & SH, W 2011, 'Numerical study of inlet and impeller flow structures in centrifugal pump at design and off-design points'. International Journal of Fluid Machinery and Systems, vol. 4, no. 1, pp. 25-32.

22. Cheah, KW, Lee, TS & Winoto, SH 2011, 'Unsteady analysis of impeller-volute interaction in centrifugal pump'. International Journal of Fluid Machinery and Systems, vol. 4, no. 3, pp. 349-359.

23. Cheah, KW, Lee, TS, Winoto, SH & Zhao, ZM 2007, 'Numerical flow simulation in a centrifugal pump at design and off-design conditions'. International Journal of Rotating Machinery.

24. Choi, YD, Kurokawa, J & Matsui, J 2006, 'Performance and internal flow characteristics of a very low specific speed centrifugal pump'. Journal of fluids engineering, vol. 128, no. 2, pp. 341-349.

25. Das, LG, Sen, PK, Saha, TK & Chanda, A 2010, 'Performance Prediction of Vertical Submersible Centrifugal Slurry Pump'. International Journal of Fluid Machinery and Systems, vol. 3, no. 2, pp. 181-203.

26. Datta, S, Sahu, RK, Mahapatra, SS, Biswas, A & Majumdar, G 2014, 'Optimisation of percent dilution and HAZ width of submerged arc weldment using Taguchi philosophy coupled with fuzzy inference system'. International Journal of Productivity and Quality Management, vol. 13, no. 4, pp. 430-449.

27. Derakhshan, S, Pourmahdavi, M, Abdolahnejad, E, Reihani, A & Ojaghi, A 2013, 'Numerical shape optimization of a centrifugal pump impeller using artificial bee colony algorithm'. Computers & Fluids, vol. 81, pp. 145-151.

28. Ding, H, Visser, FC, Jiang, Y & Furmanczyk, M 2011, ' Demonstration and validation of a 3D CFD simulation tool predicting pump performance and cavitation for industrial applications'. Journal of fluids engineering, vol. 133, no. 1, pp. 011101.

29. Fan, J, Eves, J, Thompson, HM, Toropov, VV, Kapur, N, Copley, D & Mincher, A 2011. 'Computational fluid dynamic analysis and design optimization of jet pumps'. Computers & Fluids, vol. 46, no. 1, pp. 212-217.

30. Friedrichs, J & Kosyna, G 2002, 'Rotating cavitation in a centrifugal pump impeller of low specific speed'. Journal of fluids Engineering, vol. 124, no. 2, pp. 356-362.

31. Gao, Z, Zhu, W, Lu, L, Deng, J, Zhang, J & Wuang, F 2014, 'Numerical and experimental study of unsteady flow in a large centrifugal pump with stay vanes'. Journal of Fluids Engineering, vol. 136, no. 7, pp. 071101.

32. Gao, Z, Zhu, W, Lu, L, Deng, J, Zhang, J & Wuang, F 2014, 'Numerical and experimental study of unsteady flow in a large centrifugal pump with stay vanes'. Journal of Fluids Engineering, vol. 136, no. 7, pp. 071101.

33. Goto, A & Zangeneh, M 2002, 'Hydrodynamic design of pump diffuser using inverse design method and CFD'. Journal of Fluids Engineering, vol. 124, no. 2, pp. 319-328.

34. Goto, A, Nohmi, M, Sakurai, T & Sogawa, Y 2002. 'Hydrodynamic design system for pumps based on 3-D CAD, CFD, and inverse design method'. Journal of fluids Engineering, vol. 124, no. 2, pp. 329-335.

35. Grapsas, V, Anagnostopoulos, J & Papantonis, D 2010, 'Improved design of a centrifugal pump impeller using CFD and numerical optimisation tools'. International Journal of Advanced Intelligence Paradigms, vol. 2, no. 4, pp. 336-353.

36. Gulich, JF 2003, 'Effect of Reynolds number and surface roughness on the efficiency of centrifugal pumps'. Journal of fluids engineering, vol. 125, no. 4, pp. 670-679.

37. Gundale, VA & Joshi, GR 2013, 'A simplified 3d model approach in constructing the plain vane profile of a radial type submersible pump impeller'. Research Journal of Engineering Sciences, vol. 2, no. 7, pp. 33-37.

38. Heinrich, M & Schwarze, R 2016, 'Genetic algorithm optimization of the volute shape of a centrifugal compressor'. International Journal of Rotating Machinery.

39. Heo, MW, Kim, KY, Kim, JH & Choi, YS 2016, 'High-efficiency design of a mixed-flow pump using a surrogate model'. Journal of Mechanical Science and Technology, vol. 30, no. 2, pp. 541-547.

40. Heo, MW, Ma, SB, Shim, HS & Kim, KY 2016, 'High-efficiency design optimization of a centrifugal pump'. Journal of Mechanical Science and Technology, vol. 30, no. 9, pp. 3917-3927.

41. Husain, A, Sonawat, A, Mohan, S & Samad, A 2016, 'Energy efficient design of a jet pump by ensemble of surrogates and evolutionary approach'. International Journal of Fluid Machinery and Systems, vol. 9, no. 3, pp. 265-276.

42. IS 9079: 2002 Indian Standard - Electric Monoset Pumps for Clear, Cold Water for Agricultural and Water Supply purposes.

43. IS 9694(Part1) 1987, Indian Standard - Code of Practice for the Selection, Installation, Operation and Maintenance of Horizontal Centrifugal Pumps for Agricultural Applications.

44. Jin, HB, Kim, MJ, Son, CH & Chung, WJ 2013, 'Spiral casing of a volute centrifugal pump-effects of the cross sectional shape'. The KSFM Journal of Fluid Machinery, vol. 16, no. 14, pp. 28-34.

45. Jung, UH, Kim, JH, Kim, JH, Park, CH, Jun, SO & Choi, YS 2016, 'Optimum design of diffuser in a small high-speed centrifugal fan using CFD & DOE'. Journal of Mechanical Science and Technology, vol. 30, no. 3, pp. 1171-1184.

46. Kaewnai, S, Chamaoot, M & Wongwises, S 2009, 'Predicting performance of radial flow type impeller of centrifugal pump using CFD'. Journal of mechanical science and technology, vol. 23, no. 6, pp. 1620-1627.

47. Kampolis, IC & Giannakoglou, KC 2008, 'A multilevel approach to single-and multiobjective aerodynamic optimization'. Computer Methods in Applied Mechanics and Engineering, vol. 197, no. 33-40, pp. 2963-2975.

48. Kang, HS & Kim, YJ 2016, 'A Study on the Multi-Objective Optimization of Impeller for High-Power Centrifugal Compressor'. International Journal of Fluid Machinery and Systems, vol. 9, no. 2, pp. 143-149.

49. Kannan, T & Yoganandh, J 2010, 'Effect of process parameters on clad bead geometry and its shape relationships of stainless steel claddings deposited by GMAW'. The International Journal of Advanced Manufacturing Technology, vol. 47, no. 9-12, pp. 1083-1095.

50. Kannan, T & Abraham, CC 2009, 'Effects of gas metal arc welding parameters on weld deposit area of stainless steel claddings'. Journal for Manufacturing Science and Production, vol. 10, no. 2, pp. 123-136.

51. Kelder, JDH, Dijkers, RJH, Van Esch, BPM & Kruyt, NP 2001, 'Experimental and theoretical study of the flow in the volute of a low specific-speed pump'. Fluid Dynamics Research, vol. 28, no. 4, pp. 267.

52. Kim, JH & Kim, KY 2011, 'Optimization of vane diffuser in a mixed-flow pump for high efficiency design'. International Journal of Fluid Machinery and Systems, vol. 4, no. 1, pp. 172-178.

53. Kim, JH & Kim, KY 2012, 'Analysis and optimization of a vaned diffuser in a mixed flow pump to improve hydrodynamic performance'. Journal of Fluids Engineering, vol. 134, no. 7, pp. 071104.

54. Kim, JH, Lee, HC, Kim, JH, Choi, YS, Yoon, JY, Yoo, IS & Choi, WC 2015, 'Improvement of hydrodynamic performance of a multiphase pump using design of experiment techniques'. Journal of Fluids Engineering, vol. 137, no. 8, pp. 081301.

55. Kim, JH, Lee, HC, Kim, JH, Kim, S, Yoon, JY & Choi, YS 2015, 'Design techniques to improve the performance of a centrifugal pump using CFD'. Journal of Mechanical Science and Technology, vol. 29, no. 1, pp. 215-225.

56. Kim, S, Choi, YS, Lee, KY & Yoon, JY 2009, 'Design optimization of centrifugal pump impellers in a fixed meridional geometry using DOE'. International Journal of Fluid Machinery and Systems, vol. 2, no. 2, pp. 172-178.

57. Kim, S, Choi, YS, Lee, KY & Yoon, JY 2009, 'Design optimization of centrifugal pump impellers in a fixed meridional geometry using DOE'. International Journal of Fluid Machinery and Systems, vol. 2, no. 2, pp. 172-178.

58. Kim, S, Lee, KY, Kim, JH, Kim, JH, Jung, UH & Choi, YS 2015, 'High performance hydraulic design techniques of mixed-flow pump impeller and diffuser'. Journal of Mechanical Science and Technology, vol. 29, no. 1, pp. 227-240.

59. Korkmaz, E., Gölcü, M. and Kurbanoğlu, C., 2017. Effects of blade discharge angle, blade number and splitter blade length on deep well pump performance. Journal of Applied Fluid Mechanics, 10(2), pp.529-540.

60. Lei, C, Yiyang, Z, Zhengwei, W, Yexiang, X & Ruixiang, L 2015, 'Effect of axial clearance on the efficiency of a shrouded centrifugal pump'. Journal of Fluids Engineering, vol. 137, no. 7, pp. 071101.

61. Li, WG 2016, 'Effects of viscosity on turbine mode performance and flow of a low specific speed centrifugal pump'. Applied Mathematical Modelling, vol. 40, no. 2, pp. 904-926.

62. Limbach, P & Skoda, R 2017, 'Numerical and Experimental Analysis of Cavitating Flow in a Low Specific Speed Centrifugal Pump With Different Surface Roughness'. Journal of Fluids Engineering, vol. 139, no. 10, pp. 101201.

63. Luo, X, Zhang, Y, Peng, J, Xu, H & Yu, W 2008, 'Impeller inlet geometry effect on performance improvement for centrifugal pumps'. Journal of mechanical science and technology, vol. 22, no. 10, pp. 1971-1976.

64. Menter, FR 1994, 'Two-equation eddy-viscosity turbulence models for engineering applications'. AIAA journal, vol. 32, no. 8, pp. 1598-1605.

65. Mohammadi, N & Fakharzadeh, M 2017, 'Analysis of effect of impeller geometry including blade outlet angle on the performance of multi-pressure pumps: simulation and experiment'. Mechanics, vol. 23, no. 1, pp. 107-119.

66. Montgomery, DC & Runger, GC 2010. Applied statistics and probability for engineers. John Wiley & Sons.

67. Montgomery, DC 2017, Design and analysis of experiments. John wiley & sons.

68. Mortazavi, F, Riasi, A & Nourbakhsh, A 2017, 'Numerical Investigation of Back Vane Design and Its Impact on Pump Performance. Journal of Fluids Engineering, vol. 139, no. 12, pp. 121104.

69. Murugesan, C & Rudramoorthy, R 2016, 'Experimental and Numerical Study of Efficiency Improvement by Surface Coating on the Impellers and Diffusers of Mixed Flow Submersible Borewell Pumps'.

70. Murugesan, C & Rudramoorthy, R 2016, 'Numerical and experimental study of single stage and multistage centrifugal mixed flow submersible borewell pumps'. International Journal of Fluid Machinery and Systems, vol. 9, no. 2, pp. 107-118.

71. Nataraj, M & Arunachalam, VP 2006, 'Optimizing impeller geometry for performance enhancement of a centrifugal pump using the Taguchi quality concept'. Proceedings of the Institution of Mechanical Engineers, Part A: Journal of Power and Energy, vol. 220, no. 7, pp. 765-782.

72. Nataraj, M & Ragoth Singh, R 2014, 'Analyzing pump impeller for performance evaluation using RSM and CFD'. Desalination and Water Treatment, vol. 52, no. 34-36, pp. 6822-6831.

73. Palani, PK & Murugan, N 2006, 'Sensitivity analysis for process parameters in cladding of stainless steel by flux cored arc welding'. Journal of Manufacturing Processes, vol. 8, no. 2, pp. 90-100.

74. Pei, J, Wang, W & Yuan, S 2016, 'Multi-point optimization on meridional shape of a centrifugal pump impeller for performance improvement'. Journal of Mechanical Science and Technology, vol. 30, no. 11, pp. 4949-4960.

75. Pei, J, Wang, W, Yuan, S & Zhang, J 2016, 'Optimization on the impeller of a low-specific-speed centrifugal pump for hydraulic performance improvement'. Chinese Journal of Mechanical Engineering, vol. 29, no. 5, pp. 992-1002.

76. Pei, J, Yin, T, Yuan, S, Wang, W & Wang, J 2017, 'Cavitation optimization for a centrifugal pump impeller by using orthogonal design of experiment'. Chinese Journal of Mechanical Engineering, vol. 30, no. 1, pp. 103-109.

77. Periyanan, PR & Natarajan, U 2013, 'Multiple parameters optimisation in micro-WEDG process. International Journal of Productivity and Quality Management, vol. 11, no. 3, pp. 334-356.

78. Petit, O & Nilsson, H 2013, 'Numerical investigations of unsteady flow in a centrifugal pump with a vaned diffuser'. International Journal of Rotating Machinery.

79. Safikhani, H, Khalkhali, A & Farajpoor, M 2011, 'Pareto based multi-objective optimization of centrifugal pumps using CFD, neural networks and genetic algorithms'. Engineering Applications of Computational Fluid Mechanics, vol. 5, no. 1, pp. 37-48.

80. Sahu, J, Mahapatra, SS & Puhan, D 2013, 'Multi-response optimisation of electrical discharge machining process using combined approach of RSM and FIS'. International Journal of Productivity and Quality Management, vol. 12, no. 2, pp. 185-208.

81. Samad, A & Kim, KY 2009, 'Surrogate based optimization techniques for aerodynamic design of turbomachinery'. International Journal of Fluid Machinery and Systems, vol. 2, no. 2, pp. 179-188.

82. Senthilkumar, B & Kannan, T 2013, 'Sensitivity analysis of flux cored arc welding process variables in super duplex stainless steel claddings'. Procedia Engineering, vol. 64, pp. 1030-1039.

83. Senthilkumar, B, Kannan, T & Arun, KK 2016, 'Development of response-dilution maps for super duplex stainless steel claddings deposited by FCAW'. International Journal of Productivity and Quality Management, vol. 19, no. 2, pp. 242-257.

84. Shi, W, Zhou, L, Lu, W, Pei, B & Lang, T 2013, 'Numerical prediction and performance experiment in a deep-well centrifugal pump with different impeller outlet width'. Chinese Journal of Mechanical Engineering, vol. 26, no. 1, pp. 46-52.

85. Shigemitsu, T, Fukutomi, J & Kaji, K 2011, 'Influence of Blade Outlet Angle and Blade Thickness on Performance and Internal Flow Conditions of Mini Centrifugal Pump'. International Journal of Fluid Machinery and Systems, vol. 4, no. 3, pp. 317-323.

86. Shojaeefard, MH, Tahani, M, Ehghaghi, MB, Fallahian, MA & Beglari, M 2012, 'Numerical study of the effects of some geometric characteristics of a centrifugal pump impeller that pumps a viscous fluid'. Computers & Fluids, vol. 60, pp. 61-70.

87. Singh, RR & Nataraj, M 2014, 'Design and analysis of pump impeller using SWFS'. World Journal of Modelling and Simulation, vol. 10, no. 2, pp. 152-160.

88. Singh, RR, Nataraj, M, Surendar, S & Siva, M 2013, 'Investigation of a centrifugal pump impeller vane profile using CFD'. International Review on Modelling and Simulations, vol. 6, no. 4, pp. 1327-1333.

89. Srinivasan, KM 2008, 'Rotodynamic pumps (centrifugal and axial)'. New Age International.

90. Stepanoff, AJ 1957, 'Centrifugal and axial flow pumps: theory, design, and application'. New York: Wiley.

91. Tan, L, Zhu, B, Cao, S, Bing, H & Wang, Y 2014, 'Influence of blade wrap angle on centrifugal pump performance by numerical and experimental study'. Chinese journal of mechanical engineering, vol. 27, no. 1, pp. 171-177.

92. Tanco, M, Costa, N & Viles, E 2009, 'Experimental design selection: guidelines for practitioners'. International Journal of Productivity and Quality Management, vol. 4, no. 3, pp. 283-302.

93. Wang, W & Wang, Y 2013, 'Analysis of inner flow in low specific speed centrifugal pump based on LES'. Journal of Mechanical Science and Technology, vol. 27, no. 6, pp. 1619-1626.

94. Wang, W, Pei, J, Yuan, S, Zhang, J, Yuan, J & Xu, C 2016, 'Application of different surrogate models on the optimization of centrifugal pump'. Journal of Mechanical Science and Technology, vol. 30, no. 2, pp. 567-574.

95. Weidong, S, Chuan, W, Weigang, L, Ling, Z & Li, Z 2010, 'Optimization design of stainless steel stamping multistage pump based on orthogonal test'. International Journal of Fluid Machinery and Systems, vol. 3, no. 4, pp. 309-314.

96. Wen-Guang, L 2011, 'Blade exit angle effects on performance of a standard industrial centrifugal oil pump'. Journal of applied fluid mechanics, vol. 4, pp. 105-119.

97. Yang, S, Kong, F & Chen, B 2011, 'Research on pump volute design method using CFD'. International Journal of Rotating Machinery.

98. Yang, SS, Kong, FY, Jiang, WM & Qu, XY 2012, 'Effects of impeller trimming influencing pump as turbine'. Computers & Fluids, vol. 67, pp. 72-78.

99. Yang, W & Xiao, R 2014, 'Multiobjective optimization design of a pump–turbine impeller based on an inverse design using a combination optimization strategy'. Journal of Fluids Engineering, vol. 136, no. 1, pp. 014501.

100. Zhang, Lei, Songling Wang, Chenxing Hu & Qian Zhang 2013, 'Multi-objective optimization design and experimental investigation of centrifugal fan performance', Chinese Journal of Mechanical Engineering, vol. 26, no. 6, pp. 1267-1276.

101. Zhou, L, Shi, W & Wu, S 2013, 'Performance optimization in a centrifugal pump impeller by orthogonal experiment and numerical simulation'. Advances in Mechanical Engineering, vol. 5, pp. 385809.

102. Zhou, L, Shi, W, Lu, W, Hu, B & Wu, S 2012, 'Numerical investigations and performance experiments of a deep-well centrifugal pump with different diffusers'. Journal of Fluids Engineering, vol. 134, no. 7, pp. 071102.

103. Zhou, X, Zhang, Y, Ji, Z & Hou, H 2014, 'The optimal hydraulic design of centrifugal impeller using genetic algorithm with BVF'. International Journal of Rotating Machinery.

LIST OF PUBLICATIONS

International Journals

1. **Ulaganathan, K** & Karuppuswamy, P 2018, 'Experimental and Numerical Evaluation and Design Optimization of Centrifugal Pump Impeller Parameters through Response Surface Methodology', Journal of the Balkan Tribological Association, vol. 4, no. 24, pp. 633-653. **Annexure – I, Impact Factor: 0.737.**

2. **Ulaganathan, K** & Karuppuswamy, P 2018, 'Study the effects of surface coating on impeller and volute casing to improve the efficiency of the water pump', Desalination and Water Treatment, vol. 132, pp. 79-88. **Annexure – I, Impact Factor: 1.681.**